Western Norway University of Applied Sciences

BACHELOR'S ASSIGNMENT

Environmental change recorded in sediments of the anoxic Ikjefjord, Western-Norway, over the last 50 years

Candidate No.: 215

Bachelor assignment in Geology

28.05.2018

I confirm that the work is self-prepared and that references/source references to all sources used in the work are provided, cf. Regulation relating to academic studies and examinations at the Western Norway University of Applied Sciences (HVL), § 10.

Environmental change recorded in sediments of the anoxic Ikjefjord, Western-Norway, over the last 50 years

Bachelor Thesis

Candidate No.: 215
28.05.2018

Høgskulen på Vestlandet

van hall larenstein
university of applied sciences

Acknowledgement

This thesis is the final assignment of a bachelor program in environmental sciences at the VHL University of Applied Sciences, campus Leeuwarden. This report is furthermore the final product of two semesters at the Western Norway University of Applied Sciences, campus Sogndal.

I would like to thank Matthias Paetzel, professor at the department of Environment and Natural Sciences at the Western Norway University of Applied Sciences, for the many hours of discussion, and all of the advice during the process of conducting research and writing this bachelor thesis.

My gratitude goes out to Torbjørn Dale for introducing me to the topic of fjord hydrology during the course ‘Fjord Processes’ and all the help with microscopy issues.

Thanks go to Haflidi Haflidason for the guidance and use of equipment at Earth Lab geological laboratories at the Department of Earth Science at the University of Bergen.

I would like to thank my supervisors at the VHL University of Applied Sciences, Erik Leunissen and Leo Bentvelzen, for taking a critical look at the research approach.

X,
Sogndal, 28.05.2018

Abstract

It is the aim of this thesis to reconstruct natural and human-induced environmental change that occurred in the Ikjefjord area during the previous five decades, i.e. 1957-2017, by investigating the geological record of deposited Ikjefjord sediments.

Fieldwork at 29.08.2017 and 18.10.2017 provided two sediment cores and two grab samples from the Outer and Inner Ikjefjord basin. As a radiometric dating of the cores was not available, the sediment cores were dated based on a sand-precipitation relationship (Paetzel & Dale, 2010). The dating indicates linear sedimentation rates of 0.47 cm/year and 0.44 cm/year since 1960.

The overflow event in the Øystrebøelva of 1983 can be observed in both sediment cores in changes of the particulate matter fraction (increasing grainsize and mineral matter; decreasing organic matter). The main changing pattern seems to occur as a result of the securing of the river valley of the Øystrebøelva by elevating the riverbanks after 1983. The value of the magnetic susceptibility is on average 7×10^{-5} before and 70×10^{-5} after the construction in 1983. Silicon versus iron (Si/Fe) has values of 0.025 before and 0.028 after 1983. Potassium versus iron (K/Fe), calcium versus iron (Ca/Fe) and the magnetic coherence versus incoherence ratio show a similar trend. These differences suggest a different source of mineral matter supply after 1983, thus confirming that non-local material was used for elevating the riverbank. The grainsizes and the mineral matter content seem gradually to go back to the conditions before the 1983 event during the later years. The relative amount of terrestrial organic matter (in relation to marine organic matter) is 27% before and 10% after 1983. During the later years, the terrestrial organic matter concentration increases again. This variation can be explained by a temporarily lower abundance of vegetation along the Øystrebøelva after the construction and a successive reestablishment of the plant community.

Ikjefjord surface sediments are polluted with up to 24 µg/kg sediment dry weight of TBT, and values of 140 mg/kg sediment dry weight of zinc. Furthermore, the Ikjefjord sediments are polluted with PAHs Anthracene, Pyrene, Benzo[a]anthracene, Benzo[b]fluoranthene, Benzo[k]fluoranthene, Benzo[a]pyrene, Indeno[1,2,3-cd]pyrene, Dibenzo[a,h]anthracene and Benzo[ghi]perylene. This pollution data of the Ikjefjord provides additional data about the chemical state of the Ikjefjord. The higher sediment pollution than previously anticipated leaves the environmental authorities of the County Governor (Fylkesmannen i Sogn og Fjordane) with a challenge.

Table of contents

1 Introduction 1

1.1 Background 1

1.2 Objectives 2

1.2.1 Objective 1: Is it possible to date the sediments of the Ikjefjord deposited throughout the last 50 years? 2

1.2.2 Objective 2: Does the particulate mineral matter content and the particulate organic particulate matter content of the Ikjefjord sediments vary throughout the last 50 years? 3

1.2.3 Objective 3: Is it possible to relate the particulate matter variations to documented environmental change in the Ikjefjord area? 3

1.2.4 Objective 4: Is there any pollution in the sediment record of the Ikjefjord of the last 50 years? 4

1.2.5 Objective 5: Is it possible to link this pollution to their source? 4

2 Theoretical framework 5

2.1 Particulate matter sources of temperate fjords 5

2.2 Runoff and erosional processes – the Hjulström curve 5

3 Settings 7

3.1 Environmental setting 7

3.1.1 Topography 7

3.1.2 Geology 8

3.1.3 Bathymetry 9

3.1.4 Hydrography 10

3.2 Historical setting 14

3.2.1 Hydroelectric power production by BKK 14

3.2.2 Bridge construction 17

3.2.3 Boat traffic 17

3.2.4 Car traffic 18

3.2.5 Petroleum industry by Statoil in Mongstad 18

3.2.6 Precipitation intensity 1957 – 2017 19

4 Methods 21

4.1 Retrieving the sediment samples 21

4.2 Core description 23

4.3 Dating 24

4.4 Smear slide analyses of particulate matter 26

4.4.1 Smear slide preparation 26

4.4.2 Organic matter determination 27
4.4.3 Mineral matter determination 28
4.5 Geochemical analyses 29
4.5.1 Geochemical analyses with the GEOTEK Multi Sensor Core Logger (MSCL) 29
4.5.2 Geochemical analyses with the ITRAX- multi-functional X-ray core scanner 31
4.6 Pollution analyses 34
4.6.1 Quantitative determination of pollutants 34
4.6.2 Interpreting environmental quality 36
5 Results 37
5.1 Core description 37
5.2 Dating 38
5.3 Smear slide analyses of particulate matter 40
5.3.1 Results sediment core MF2017-1 40
5.3.2 Results sediment core MF2017-2 42
5.4 Geochemical analyses of particulate matter 44
5.5 Pollution analyses 48
6 Discussion 49
6.1 Dating 49
6.2 Comparison of the core records 49
6.3 Relating variation in the particulate mineral and organic matter content to documented environmental change 51
6.4 Pollution 54
7 Conclusion 56
8 Reference list 57
Appendices
Appendix I: Method descriptions
A: Equipment for sediment retrievement
B: Microscope picture and result smear slide analysis
Appendix II: Results smear slide analyses of particulate matter
A: Sediment core MF2017-1
B: Sediment core MF2017-2
Appendix III: Geochemical analyses of particulate matter
A: Magnetic coherence versus incoherence ratio, magnetic susceptibility, gamma density

B: Elemental composition

Appendix IV: Results of pollution analyses

A: Quantitative determinations

B: Quantitative determinations expressed in environmental quality reference classes

List of tables

Table 3.1: Mineral associations in dioritic/granitic gneiss, and migmatite (Nesse, 2012). 8

Table 3.2: Hydrographical characteristics of the Ikjefjord (Norges vassdrags- og energidirektorat, 2018a). 10

Table 4.1: The specifications of meteorological station Lavik, including its location and recordings (Norwegian Meteorological Institute, 2018b). 25

Table 4.2: Udden-Wentworth (1922) scale of grain size distribution and the corresponding units on the microscope-measuring bar. 28

Table 4.3: The standards applied in the quantitative determination of pollutants. 34

Table 4.4: Classification system for water and sediment (Miljødirektoratet, 2016)
AA-QS: Ambient Air Quality Standards. PNEC: Predicted No Effect Concentration. MAC-QS: Maximum Allowable Concentration Quality Standard. PNECacute: Predicted No Effect Concentration with a factor applied to indicate the acute toxicity level. AF^1: Safety factor that takes into account the variation in sensitivity between organisms. 36

Table 5.1: Results of pollution analyses. The concentrations of various pollutants throughout three transects of the Ikjefjord sediment record expressed in environmental quality reference classes. Reference classes III, IV and V indicate pollution with an increasing severity. 48

Appendices

Table Ia: Raw data of the smear slide analysis, i.e. the percentage distribution of mineral matter versus organic matter (in blue), the percentage distribution of terrestrial organic matter versus marine organic matter (in green), and the ratio of mineral grainsizes (in orange), performed on sediment core MF2017-2 segment 24 – 24.5 cm area 3.

Table VIa: Classification system for water and sediment (Miljødirektoratet, 2016) AA-QS: Ambient Air Quality Standards. PNEC: Predicted No Effect Concentration. MAC-QS: Maximum Allowable Concentration Quality Standard. $PNEC_{acute}$: Predicted No Effect Concentration with a factor applied to indicate the acute toxicity level. AF^1: Safety factor that takes into account the variation in sensitivity between organisms.

List of figures

Figure 2.1: The erosion, transportation and deposition of river sediment as a function of flow speed on a logarithmic scale, a simplified illustration reality, modified after Hjulström (1935). Diagram source: (Puşcaş et al., 2010). 6

Figure 3.1: Projection of the 'Ytre Sogn' region, showing the outline of the Outer Sogn region (with a blue line) and the location of the Outer Sogn region (in the red framed inset map).
Modified after Norges vassdrags- og energidirektorat (2018b). 7

Figure 3.2: Projection of the Ikjefjord, showing the outline of the Ikjefjord (blue line) and the location of the Ikjefjord (in the red framed inset map).
Modified after Norges vassdrags- og energidirektorat (2018a). 7

Figure 3.3: Projection of the geology in the Ikjefjord area. Modified after Norges geologiske undersøkelse (2018). 8

Figure 3.4: Bathymetry map of the Inner and Outer Ikjefjord basin, pointing out the sill depths (yellow numbers) and maximum water depths (white numbers) (Paetzel, 2017a). 9

Figure 3.5: Projection of the outlets of rivers Øystrebøelva , Snjogilet and Storelva (indicated with black arrows). Modified after Norges vassdrags- og energidirektorat (2018b). 11

Figure 3.6: Illustration of the waterexhange between fjords and coastal water (Institute of Marine Research, 2014). 13

Figure 3.7: Illustration of the Matre river systems and adjacent river systems in relation to the Ikjefjord. The Matre hydro power plant (red square) and Stølsvatn (striped red square) are indicated. The rivers Storelva (S) and Øystrebøelva (Ø) are indicated with black arrows. Modified after BKK AS (2018). 15

Figure 3.8: Flood protection Øystrebøelva, showing the elevated riverbank on the left (Paetzel, 2017b). 16

Figure 3.9: The Ikjefjordsbrua. former island Storeholmen is indicated in a red striped square (kartverket, 2018). 17

Figure 3.10: Illustration of the Statoil oil refinery in Mongstad in relation to the Ikjefjord. Modified after statoil ASA (2018a). 18

Figure 3.11: Annual precipitation 1957-2017 measured by weather station Lavik (56320), data source: eKlima. 20

Figure 4.1 22
Figure 4.1a: Projection of the sampling locations of the Ikjefjord sediment record (indicated with red dots) and the transect of the Echo-Sounder profile (red line) from the Ikjefjord outlet (A) to the inner sill (B) and the shore (C). The black framed inset map shows the geographical location of the Ikjefjord.

Figure 4.1b**:** Echo-Sounder profile of the Ikjefjord, the Ikjefjord outlet (A), inner sill (B) and the Ikjefjord shore (C) are indicated (Paetzel, 2017a). The sample locations located in the vicinity of the transect are indicated with markings. Figure 4.1c: Overview of the Ikjefjord sediment record, describing sample locations and the retrieved material. Coordinates are provided using World Geodetic System scheme 84.

Figure 4.2: Illustration of the GEOTEK Multi Sensor Core Logger (MSCL) (Department of Earth Science UiB, 2017). 30

Figure 4.3: Illustration of the ITRAX core scanner showing the optical-line camera (A), laser triangulation system (B), motorized XRF Si-drift chamber detector (C), X-ray tube (D), flat-beam X-ray waveguide (E) and the X-ray line camera (F). The horizontal arrow shows the moving direction of the sediment core. 32

Figure 5.1: Description of sediment cores MF2017-1 and MF2017-2, using the Munsell® (1994) colour classification. 37

Figure 5.2: The dating of sediment cores MF2017-1 and MF2017-2 based on the sand-precipitation relationship. Grey translucent bars indicate similar patterns, yellow translucent boxes indicate patterns where the relationship is less visible. Black lines correspond to the indicated decennia. 39

Figure 5.3: Results of smear slide analyses on sediment core MF2017-1, showing the total mineral matter vs organic matter content, the terrestrial organic matter vs marine organic matter content and the cumulative grainsize distribution of sand, silt and clay. The blue, translucent area indicates the position of the marker layer in the sediment. 41

Figure 5.4: Results of smear slide analyses on sediment core MF2017-2, showing the total mineral matter vs organic matter content, the terrestrial organic matter vs marine organic matter content and the cumulative grainsize distribution of sand, silt and clay. The blue, translucent area indicates the position of the marker layer in the sediment. 43

Figure 5.5: Results of geochemical analysis on sediment core MF2017-2 part 1, showing the gamma density, magnetic suceptibility and the magnetic coherence versus incoherence ratio next to an optical image and X-radiograph. The blue, translucent area indicates the position of the marker layer in the sediment after a precise indication by the X-radiograph. 45

Figure 5.6: Results of geochemical analysis on sediment core MF2017-2 part 2, showing the results of a selection of elements next to an optical image and X-radiograph. The results are presented against iron with a moving average of 20 (equal to 1 cm). The blue, translucent area indicates the position of the marker layer in the sediment after a precise indication by the X-radiograph. 47

Figure 6.1: Surface current of the Ikjefjord, indicating sample locations (red dots) and river outlets (orange arrows). Background map: Norges vassdrags- og energidirektorat (2018b). 50

Figure 6.2: Areal pictures of the Øystrebøelva before the elevation of the riverbanks in 1973 (left picture) and after the elevation of the riverbanks in 2016 (right picture) (NorgeiBilder, 2018), red arrows indicate main changes. 51

Figure 6.3: Summary of the results of particulate mineral matter parameters besides the dating. The blue, translucent box indicates the marker layer as shown by the X-radiograph. 52

Figure 6.4: Summary of the results of particulate organic matter parameters besides the dating. The blue, translucent box indicates the marker layer as shown by the X-radiograph. 53

Appendices

Figure Ia: Niemistö (1974) Gravity Corer (Meskanen, 2017).

Figure Ib: Van Veen Grab sampler (Meskanen, 2017).

Figure Ic: Microscope view (bright-field microscopy) of sediment core MF2017-2 segment 24-24.5 cm area 3, showing mineral matter (in the blue square), terrestrial organic matter (in red square) and marine organic matter (in the yellow square).

1 Introduction

1.1 Background

Howe et al. (2010) argue that fjords are appropriate environments for recording climate and environmental change due to overall high and continuous sedimentation. Biological, chemical and physical characteristics of sediments derived from aquatic ecosystems, such as fjords, can function as an indicator of previous environmental conditions (Smol, 1992).

The Ikjefjord is an oxygen-deficient, semi-enclosed fjord located in the municipality of Høyanger, Western Norway. The Ikjefjord is a southward tending tributary fjord of the larger and deeper Sognefjord (Figure 3.2). Starting in de 1950s, several environmental aspects of the Ikjefjord and its surrounding area have changed. The precipitation in the area increased gradually from 2000 mm/year to 2500 mm/year since the late 1950s (Norwegian Meteorological Institute, 2018a). The rivers Øystrebøelva and Storelva are partially redirected from their natural course towards the Ikjefjord to increase the hydropower production by the Matre hydropower plant in Masfjorden, i.e. the adjacent drainage area. The result is a decline in the freshwater supply towards the Ikjefjord after 1971 (Solbakken et al., 2011). The water exchange between the Ikjefjord and the Sognefjord is restricted since the construction of the Ikjefjordsbrua. This bridge connects the west side of the Ikjefjord outlet with the east side and is in use since 1977 (Ese, 2005). Furthermore, there are various potential sources of pollution located in the surrounding area of the Ikjefjord:

a. Boat traffic on the Sognefjord and small boats on the Ikjefjord, are a potential sources of tributyltin (TBT). TBT was mainly used in the shippery, as a compound in antifouling paint, between 1960 and the prohibition of its use in 2003 (The European Maritime Safety Agency, 2017).
b. The oil refinery of Statoil Refining ASA at Mongstad, operational since 1975 (Statoil ASA, 2018b), is a potential source of polycyclic aromatic hydrocarbons (PAHs). Other potential sources include car and boat traffic (Kvernheim et al., 1992).
c. The road surface forms a potential source of copper, zinc, lead and PAHs by the extensive use of spikes on car winter tires (Bækken, 1993).

In spite of this, there is a lack of data on the ecological and chemical state of the Ikjefjord. The Sogn og Fjordane River Basin District states that due to the lack of data, there is a risk that the environmental goals of the EU Water Framework Directive will not be reached before the deadline of 2021 (Norges vassdrags- og energidirektorat, 2018a).

The ambition of this thesis is reconstructing any natural and human-induced environmental change that occurred in the Ikjefjord in the previous five decades (1957-2017) by investigating the particulate mineral and organic matter content of sediments and examining the sediments on pollution. This thesis might provide a scientific basis on the pollution state of the Ikjefjord, and thus indicate whether the regional environmental authorities of the County Governor (Fylkesmannen i Sogn og Fjordane) are facing a challenge.

1.2 Objectives

The geological record of deposited Ikfjord sediments is expected to provide information on the evolution of the Ikjefjord over the last decades, including the documentation of natural and human-induced environmental impact. Based on this expectation, this thesis will answer the following objectives to meet the ambition mentioned above:

Objective 1: Is it possible to date the sediments of the Ikjefjord deposited throughout the last 50 years?

Objective 2: Does the particulate mineral matter content and the particulate organic particulate matter content of the Ikjefjord sediments vary throughout the last 50 years?

Objective 3: Is it possible to relate the particulate matter variations to documented environmental change in the Ikjefjord area?

Objective 4: Is there any pollution in the sediment record of the Ikjefjord of the last 50 years?

Objective 5: Is it possible to link this pollution to their source?

1.2.1 Objective 1: Is it possible to date the sediments of the Ikjefjord deposited throughout the last 50 years?

Standard methods to date marine sediments are radiometric methods, for example Lead-210 (^{210}Pb) and Cesium-137 (^{137}Cs). However, sediments first need to settle over a significant amount of time (~ 1.5 years) after their retrieval, before these methods can be applied. Radiometric dating methods are therefore currently not a possibility. Paetzel & Dale (2010) suggest using sediment-climate relations where radiometric dating methods cannot be applied.

According to Howe et al. (2010), riverine discharge is the main source of sediment supply in temperate non-glaciated fjords with a restricted exchange with coastal water, as is the case in the Ikjefjord. The riverine discharge is connected to the precipitation in the catchment area of a river. The sediment composition thus relates to the regional precipitation. Sediments will be dated by comparing the sand, silt and clay fractions (% of total mineral grains) of particulate matter throughout the sediment

cores with the regional precipitation (cumulative in mm a year). Smear slide analyses will provide the grainsize data. The grainsize versus precipitation dating is a valid first approach to estimate time lines of sedimentation in Western Norwegian fjord sediments (Paetzel & Dale 2010).

1.2.2 Objective 2: Does the particulate mineral matter content and the particulate organic particulate matter content of the Ikjefjord sediments vary throughout the last 50 years?

The particulate matter content in the Ikjefjord sediment record can indicate changes in the environment of the Ikjefjord. As described above, riverine discharge is the main source of sediments in the Ikjefjord. As a consequence, the particulate matter content of sediments should mainly relate to the riverine discharge.

Particulate organic matter originates either from riverine discharge and land runoff (terrestrial organic matter) or from primary production in the photic zone of the waterbody or adjacent waterbodies (marine organic matter) (Howe et al., 2010). Variation in the ratio of terrestrial organic matter versus marine organic matter can indicate changes in the organic matter sources and changes in the transport conditions from their source towards the Ikjefjord (Howe et al.,2010; Syvitski et al 1987). These can be changes in the riverine discharge of freshwater or changes in the water exchange between the Sognefjord and the Ikjefjord. Variation in the relative abundancy of particulate mineral matter can indicate changes in the particulate matter sources of both the particulate mineral and the particulate organic matter, and it might point out changes in the transport conditions. The Hjulström curve describes how the grainsize distribution of riverine discharge relates to the riverine flow speed (Hjulström, 1935).

The particulate matter content of the sediments throughout the sediment record is analyzed by smear slide analyses and geochemical analyses. The smear slide analyses go into the volume ratio of mineral matter versus organic matter, terrestrial organic matter versus marine organic matter and the grainsize distribution. The geochemical analyses go into the gamma density, magnetic susceptibility, elemental composition and the magnetic coherence versus incoherence ratio. In addition, a high-resolution optical image and a high resolution X-radiograph are made. The geochemical analyses provide high resolution data that can help getting a more detailed impression of the changes observed in the sediment record by smear slide analysis.

1.2.3 Objective 3: Is it possible to relate the particulate matter variations to documented environmental change in the Ikjefjord area?

The environmental change can be indicated if variations in the particulate matter content of the sediments throughout the sediment record of the Ikjefjord can be linked to documented changes in the environmental aspects of the Ikjefjord and its surrounding area. The changes in the sediments are linked to the documented changes in the environmental aspects based on a time resolution. The dating of the

sediment record, by the grainsize-climate relation (Chapter 1.2.1), provides a time resolution on the sediment record.

1.2.4 Objective 4: Is there any pollution in the sediment record of the Ikjefjord of the last 50 years?

The sediment record of the Ikjefjord of the last 50 years is analyzed on pollution to find out whether the Ikjefjord has been subjected to pollution. Quantitative determinations for prioritized trace elements (arsenic, lead, cadmium, copper, chromium, mercury, nickel and zinc), polychlorinated biphenyls (PCBs), polycyclic aromatic hydrocarbons (PAHs) and Tributyltin (TBT) will be performed on sediments of the Inner and Outer Ikjefjord. Analyzing these samples allows giving a first impression of the presence of pollution throughout the sediment record. The results of the determinations will be classified according to the environmental quality classes for marine sediments of the Norwegian Environmental Agency to indicate pollution (Miljødirektoratet, 2016).

1.2.5 Objective 5: Is it possible to link this pollution to their source?

The sources of any indicated pollution can be found if the pollution throughout the sediment record of the Ikjefjord can be linked to known potential sources based on the time resolution provided by dating the sediments (objective 1).

2 Theoretical framework

This chapter provides an introduction into two issues that are of relevance for the particulate matter content of the Ikjefjord sediments. The particulate matter sources of temperate fjords and the runoff of particulate matter by riverine discharge are discussed.

2.1 Particulate matter sources of temperate fjords

Riverine discharge is the main source of sediment supply in temperate non-glaciated fjords with a restricted exchange of coastal water (Howe et al., 2010). Riverine discharge supplies fjords with particulate mineral matter and particulate terrestrial organic matter.

A second sediment source of temperate fjords is the particulate marine organic matter production in the photic zone of the fjord itself (Howe et al., 2010). The production of marine organic matter in a fjord depends mainly on the light conditions and on the nutrient supply towards the fjord. Light conditions depend on season and water turbidity. The nutrient supply towards a fjord is determined by the quantity of riverine and marine nutrient supply and the extent of transportation towards the fjord. The quantity of marine nutrient supply is related to the coastal upwelling of nutrient rich water layers (Inall & Gillebrand, 2010).

A third sediment source is marine organic matter production in the photic zone of adjacent waterbodies (Howe et al., 2010). In the case of the Ikjefjord this could for example be marine organic matter production in the Sognefjord, the North Sea or the Norwegian Sea.

2.2 Runoff and erosional processes – the Hjulström curve

The Hjulström curve (Figure 2.1) describes the erosion, transportation and deposition of river sediment as a function of flow speed in cm s^{-1} (Hjulström, 1935). The flow speed required to erode, transport and deposit a mineral is related to the grain size of the mineral material.

The upper curve (Figure 2.1) describes the erosion of grainsizes as a function of flow speed. The curve indicates that the erosion of clay particles (< 0.004 mm on the Udden-Wentworth Scale) requires a larger flow speed than the erosion of silt (0.004-0.062 mm) and sand particles (0.062-2 mm). This trend can be explained by the strong cohesive characteristics of clay caused by their enhanced surface area and electrical charges, compared to silt and sand. The flow speed required for erosion starts to increase again within the sand fraction. Pebbles (2 – 64 mm), cobbles (64-128 mm) and boulders (128 mm>) require an increasing flow speed for erosion.

The lower curve describes the maximum flow speed at which deposition takes place. The curve shows that the maximum flow speed at which deposition takes place increases with increasing grain size. Consequently, smaller particles are, once eroded, in suspension under a larger variety of flow speed conditions.

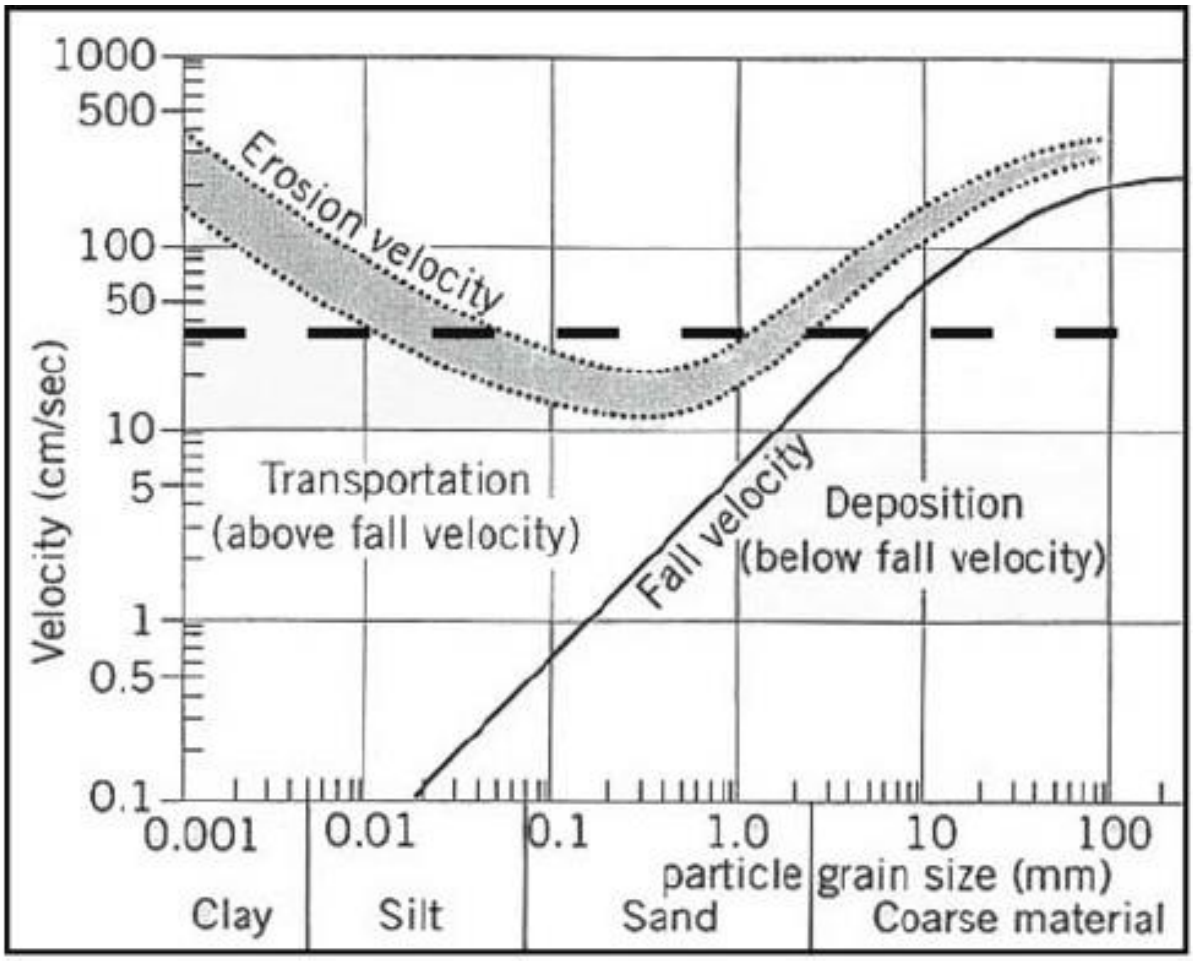

Figure 2.1: The erosion, transportation and deposition of river sediment as a function of flow speed on a logarithmic scale, a simplified illustration reality, modified after Hjulström (1935). Diagram source: (Puşcaş et al., 2010).

3 Settings

This chapter describes the Ikjefjord and provides an overview of the history of the Ikjefjord area. The topography, geology, bathymetry and hydrography are described.

3.1 Environmental setting

3.1.1 Topography

The Ikjefjord is a 5km long, south eastward tending tributary fjord of the Sognefjord, located in the municipality of Høyanger in Sogn og Fjordane county, Western Norway (Figure 3.2).

The Sognefjord connects the coastal zone 'Nordsjøen Nord' (North Sea North) with the Norwegian inland (Norges vassdrags- og energidirektorat, 2018b). The Sognefjord is subdivided into the regions Indre (i.e. Inner) Sogn and Ytre (i.e. Outer) Sogn, the latter illustrated in Figure 3.1 (Vannportalen, 2015a). The Ikjefjord is located at the southern site of the Outer Sogn region, as outlined in Figure 3.2.

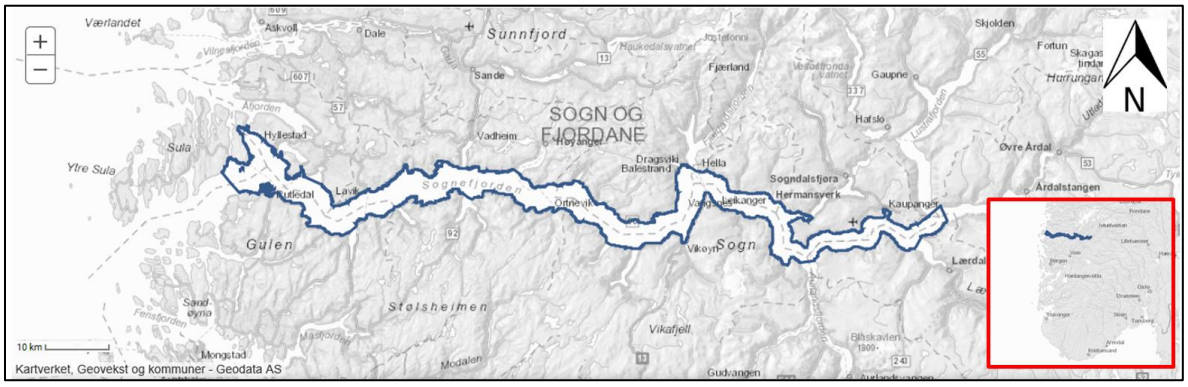

Figure 3.1: Projection of the 'Ytre Sogn' region, showing the outline of the Outer Sogn region (with a blue line) and the location of the Outer Sogn region (in the red framed inset map). Modified after Norges vassdrags- og energidirektorat (2018b).

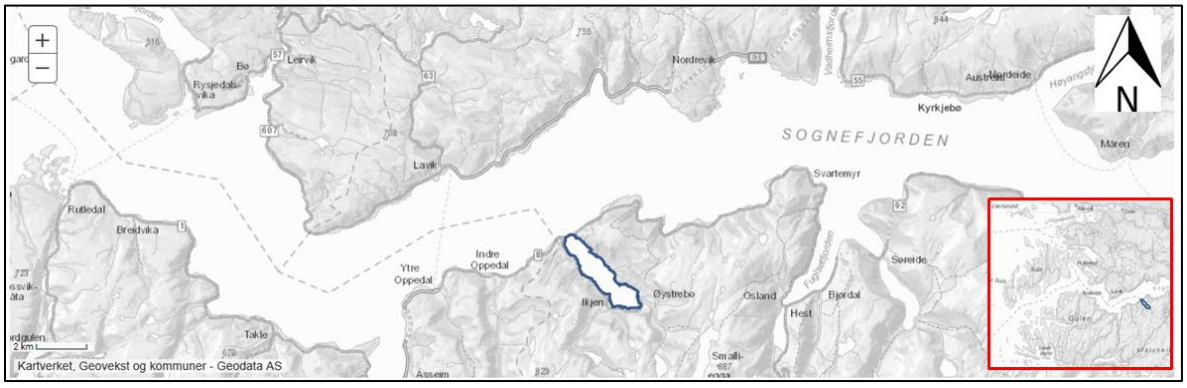

Figure 3.2: Projection of the Ikjefjord, showing the outline of the Ikjefjord (blue line) and the location of the Ikjefjord (in the red framed inset map). Modified after Norges vassdrags- og energidirektorat (2018a).

3.1.2 Geology

The main rock types in the region of the Ikjefjord are mylonite, phyllonite; mangerite to gabbro, gneiss and amphibolite; metasandstone, slate; dioritic to granitic gneiss, migmatite and Augen gneiss, granite, folliated gneiss (Figure 3.3).

The drainage area of the Ikjefjord consist of dioritic to granitic gneiss, and migmatite as the dominating rock type. Common mineral associations in dioritic to granitic gneiss, and migmatite rocks are described in Table 3.1.

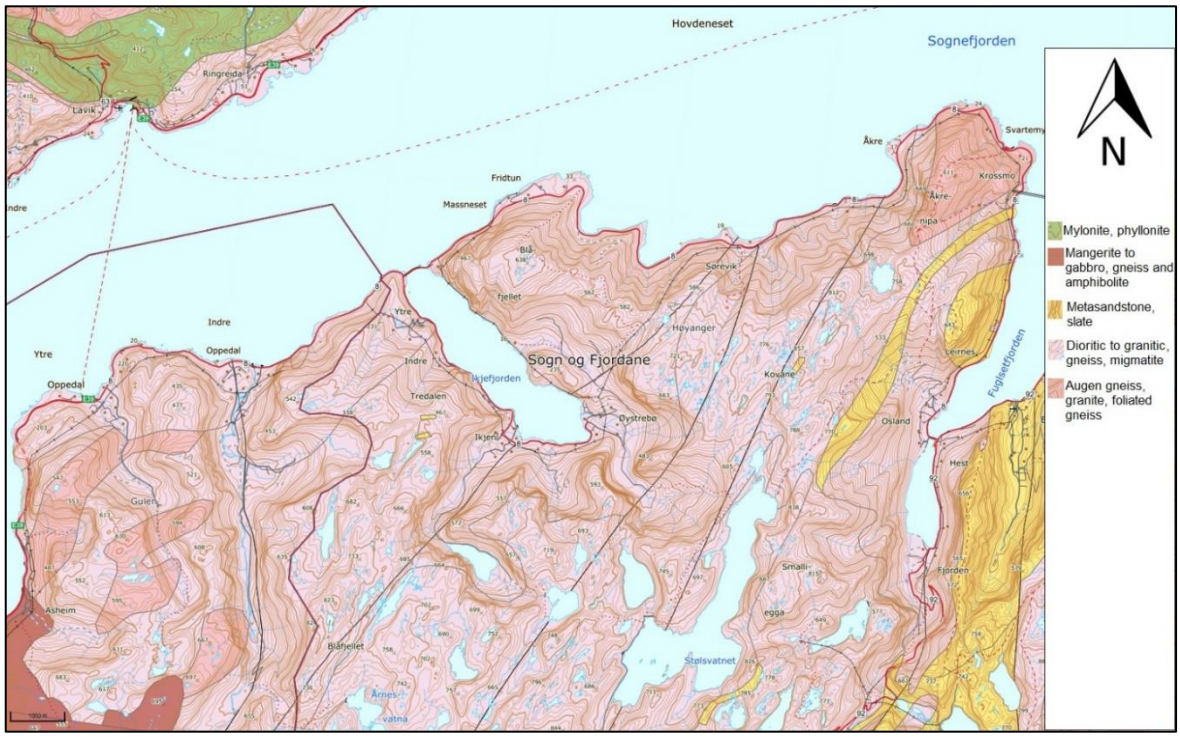

Figure 3.3: Projection of the geology in the Ikjefjord area. Modified after Norges geologiske undersøkelse (2018).

Table 3.1: Mineral associations in dioritic/granitic gneiss, and migmatite (Nesse, 2012).

Mineral name	Mineral formula
Quartz	SiO_2
Plagioclase	$NaAlSi_3O_8$, $CaAl_2Si_2O_8$
Potassium feldspar	$KAlSi_3O_8$
Biotite	$K(Mg,Fe)_3(AlSi_3O_{10})(F,OH)_2$
Orthopyroxene	$(Mg,Fe,Mn)Si_2O_6$
Cordierite	$(Mg,Fe)_2Al_4Si_5O_{18}$
Hornblende (amphibole)	$(Na,K)_{0\text{-}1}Ca_2(Mg, Fe, Al)_5 (Al, Si)_8O_{22}(OH)_2$

3.1.3 Bathymetry

The maximum water depth of the Ikjefjord is ca. 90m in the Inner Ikjefjord basin and ca. 113m and 120m in the Outer Ikjefjord basin (Figure 3.4). A 53m deep sill divides the Inner and the Outer Ikjefjord basin. A sill with a depth of 16m forms the natural border between the Outer Ikjefjord basin and the Sognefjord.

The bathymetry data is gathered with a Lowrance HDS-5 mobile echo sounder (Paetzel, 2017a). Figure 3.4 illustrates the bathymetry of the Ikjefjord by using a 50 m and a 100 m depth line and the maximum sill and water depth. Figure 4.1a illustrates the bathymetry of a cross section of the Ikjefjord.

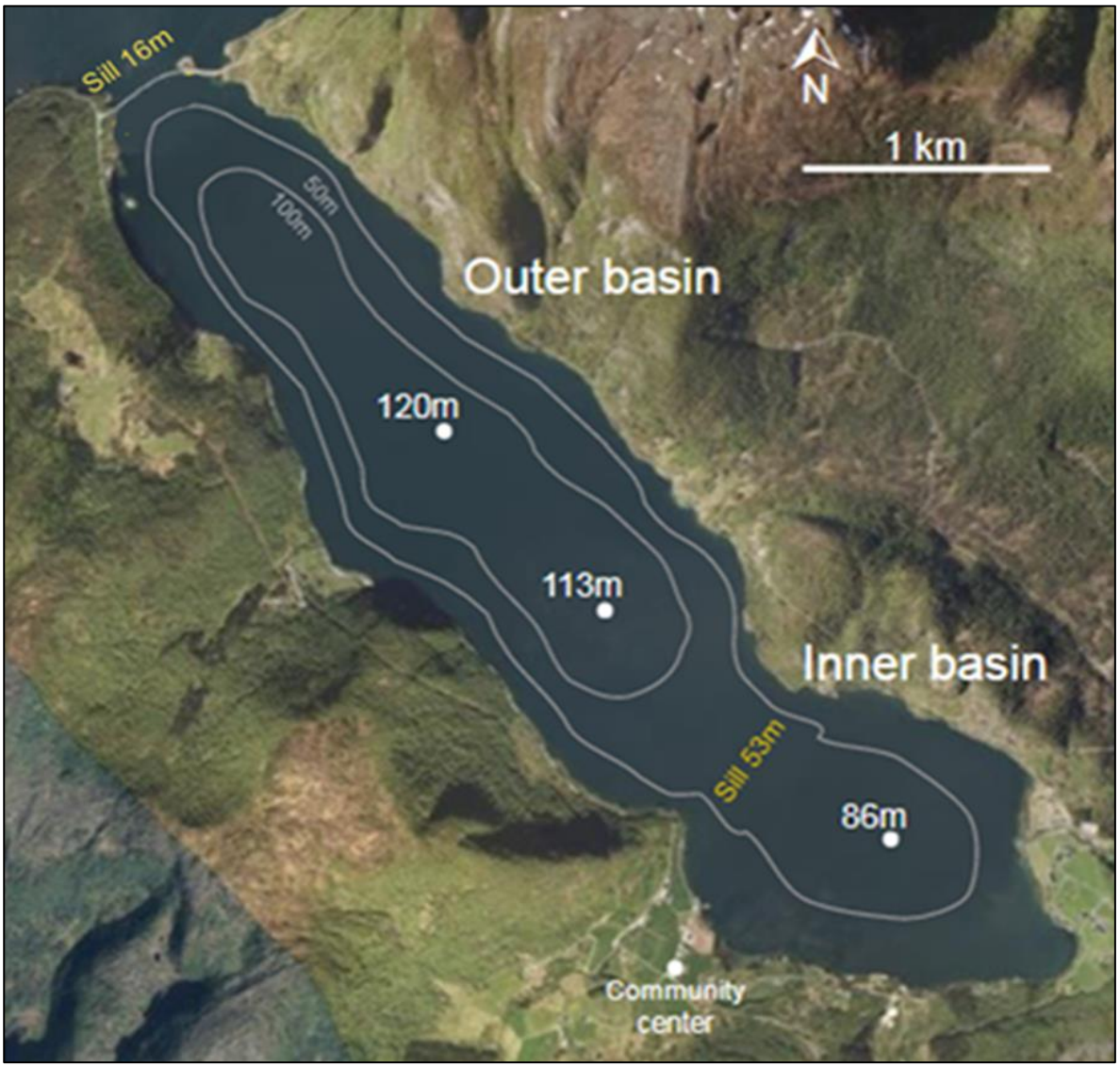

Figure 3.4: Bathymetry map of the Inner and Outer Ikjefjord basin, pointing out the sill depths (yellow numbers) and maximum water depths (white numbers) (Paetzel, 2017a).

3.1.4 Hydrography

Riverine freshwater supply and the water exchange processes between the Ikjefjord and the Sognefjord form the basis of the Ikjefjord hydrography. The narrow outlet of the Ikjefjord and a sill restrict the water exchange between the Ikjefjord and the Sognefjord. These topographical constraints largely influence the hydrography of the Ikjefjord.

The Ikjefjord is mesohaline and has a stratified water column. The fjord has a basin water retention time of several months up to years and is oxygen-defIcient (Norges vassdrags- og energidirektorat, 2018a). Table 3.2 provides an overview of these and other characteristics. The Sogn og Fjordane River Basin District assumes that the ecological state of the Ikjefjord is good (Norges vassdrags- og energidirektorat, 2018a). This assumption is based on the historic evolution of the area rather than ecological analyses. The chemical state of the Ikjefjord is unknown. Due to the lack of data, the Sogn of Fjordane River Basin District concludes that there is a risk that environmental goals of the Water Framework Directive will not be reached before 2021 (Norges vassdrags- og energidirektorat, 2018a).

Table 3.2: Hydrographical characteristics of the Ikjefjord (Norges vassdrags- og energidirektorat, 2018a).

Characteristic	Description
Water type	Oxygen-deficient fjord
Area km^2	4
Basin water retention time	Long (months/years)
Salinity	Mesohaline (5-18)
Wave exposure	Protected
Tidal difference	Small (< 1m)
Mixing in water column	Partially layered
Flow rate	Weak (< 1 knot)

Freshwater supply

Rivers Øystrebøelva, Snjogilet and Storelva supply the Inner basin of the Ikjefjord with freshwater. Figure 3.5 illustrates the freshwater supply by riverine discharge**.** The riverine discharge causes a density stratification throughout the water column of the Ikjefjord during the summer, with freshwater and brackish water on top and denser intermediate and bottom waters below (Dale 2017, *personal communication)*. The rivers Øystrebøelva and the Storelva are regulated since 1971 (Solbakken et al, 2011). Since then, their freshwater discharge depends on the hydropower production by the Matre hydropowerplant in Masfjorden (BKK, 2018).

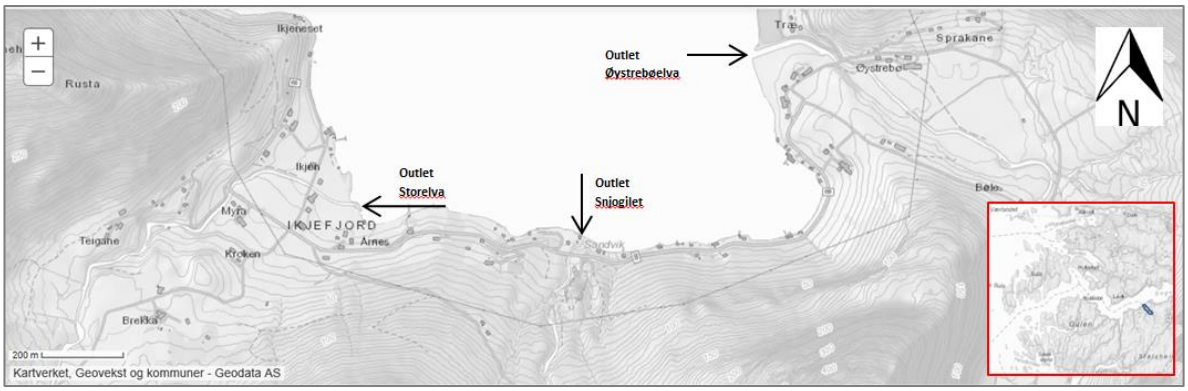

Figure 3.5: Projection of the outlets of rivers Øystrebøelva , Snjogilet and Storelva (indicated with black arrows). Modified after Norges vassdrags- og energidirektorat (2018b).

Current system

The Coriolis force deflects wind driven ocean currents towards the right in the northern hemisphere. As a result, surface water is deflected at an angle 45° to the right of the wind direction (Ekman, 1905). The bulk water mass is deflected at an angle of 90° to the right of the wind direction. The consequence is a counter-clockwise current in the Sognefjord and the Ikjefjord.

Water exchange with the Sognefjord

The water exchange between the Ikjefjord and the Sognefjord is driven by differences in the density stratification between the water column of the ikjefjord and the water column of the Sognefjord. This type of water exchange is referred to as baroclinic exchange (Inall & Gillebrand, 2010). The water exchange between the Ikjefjord and the Sognefjord consists of several separate exchange processes. These processes are estuarine circulation, deep water renewal and possible intermediate water exchange. Figure 3.6 illustrates the processes of estuarine circulation, deep water renewal and intermediate water exchange between fjords and coastal water.

Estuarine circulation is a water exchange process that takes place between the upper part of the water column of the Ikjefjord and the upper part of the water column of the Sognefjord. In general, the surface water layer of a fjord consists of fresh water originating from riverine discharge. The average flow direction of the surface water layer in fjords is away from the location of riverine discharge towards the fjord outlet.

Mixing occurs between the fresh surface water layer and the underlying water, making the fresh water layer more saline. The fresh surface water layer is replaced by deeper and more saline ocean water. This process is referred to as estuarine circulation (Inall & Gillebrand, 2010).

The intermediate water layer is the water layer between the outflowing water layer of estuarine circulation, i.e. the freshwater and brackish water layer, and the fjord bottom water. A fjord only has an intermediate water layer when the sill depth, i.e. the distance between the water surface and the sill, is larger than the depth of the freshwater and brackish water layer of the estuarine circulation (Inall & Gillebrand, 2010). The depth of the sill between the Ikjefjord and the Sognefjord is 16m. During May to October 2017, the freshwater and brackish water layer varied between 1m and 7m thickness (Dale 2017, *personal communication),* suggesting intermediate water exchange takes place between the Sognefjord and the Ikjefjord at least periodically. The strength of intermediate water exchange in most southern Norwegian fjords depends on the stratification of the intermediate water layer of coastal water. The stratification of the intermediate water layer of coastal waters and fjords depends on wind-driven coastal upwelling and downwelling (Inall & Gillebrand, 2010).

Fjord water located below sill depth is in general not connected to the adjacent (coastal) water at the same depth on the other side of the sill. This is caused by the generally strong stratification towards the deep water layers on both sides of the sill. Deep basin water is therefore overall isolated (Inall & Gillebrand, 2010). Water from below sill depth in the adjacent water body can be transported across the sill towards the deep basin of the fjord when a pressure difference is created based on differences in sea surface height. This could be created by wind amongst others. The name of this process of water transport is aspiration. The transported water finds its way to densities equal to its own on the fjordside of the sill. It forces isolated deep basin water up in the water column. If the density of the foreign water is higher than the density throughout the water column of the fjord, all deep water is transferred upwards. This replacement of deep water is referred to as deep-water renewal (Inall & Gillebrand, 2010). The density throughout the water column of the adjacent water is influenced by the tides. In general, the density of water decreases from ocean to coast. At strong tides, such as spring tide, denser water is brought towards the coast. As a result, the density of the water located below sill depth in the waterbody adjacent to the fjord is higher. High tides therefore have the potential of causing basin water renewal. Furthermore, deep-water renewal is influenced by the density throughout the water column of the fjord. When the density throughout the water column of a fjord is lower, less dense foreign water are required to replace the deep basin water. The density throughout the water column of a fjord depends on the amount of freshwater transported towards the fjord since the previous deep water renewal and is therefore also related to the time since the previous deep water renewal event (Inall & Gillebrand, 2010). The basin water retention time of the Ikjefjord is described as months up to years (Norges vassdrags- og energidirektorat, 2018a). As a result, the level of dissolved oxygen in the deep basin water of the Ikjefjord is low and the nutrient content is most likely high. The Ikjefjord has been characterized as an oxygen-deficient fjord based on its basin water retention time,

wave exposure, tidal difference, mixing in the water column and flow rate (Vannportalen, 2015b).

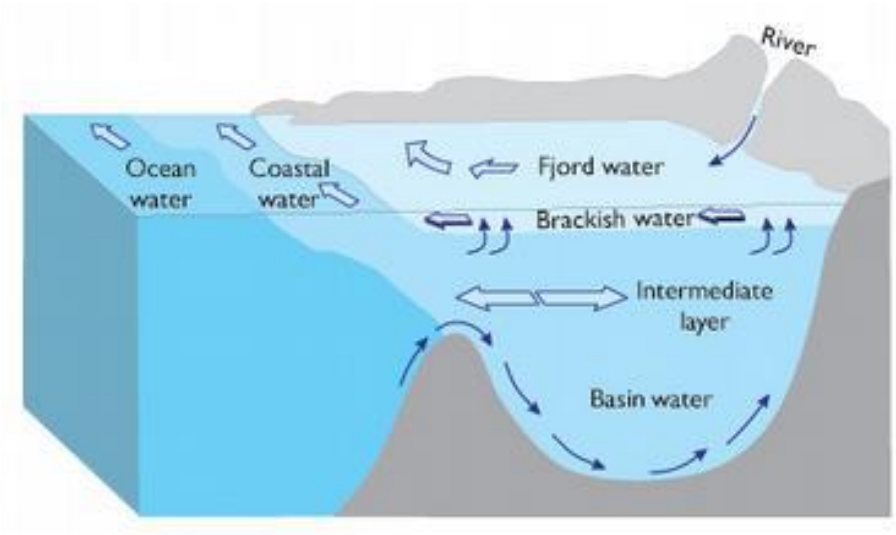

Figure 3.6: Illustration of the waterexhange between fjords and coastal water (Institute of Marine Research, 2014).

3.2 Historical setting

This paragraph describes the history of the Ikjefjord area over the last 60 years. Only those activities, events and changes are described that could have left traces in the sediments of the Ikjefjord deposited over the last 50 years.

3.2.1 Hydroelectric power production by BKK

The Matre hydropower plant in the municipality of Masfjorden located to south of the Ikjefjord (Figure 3.7), produces hydroelectric power since the early 1960s. In 1971, alterations were made in the flow direction of rivers Øystrebøelva and Storelva to increase the hydropower production. Dams and tunnels were built to partly redirect the rivers Øystrebøelva and Storelva from their natural course towards the Ikjefjord (Figure 3.7). As a result, the catchment area of the Øystrebøelva decreased to 40% of its natural size since 1971. Furthermore, the water regulation causes periods of low water levels in the Øystrebøelva. The catchment area of the Storelva decreased to 60% of its natural size since 1971 (Solbakken et al., 2011). The alterations in the river system have caused a decline in the riverine discharge of freshwater into the Ikjefjord (Massnes 2017, *Personal communication*).

The overflow event of 1983

In 1983, an overflow event occurred that is related to the hydroelectric power production by the Matre hydropower plant. The regulated lake Stølsvatnet, part of the Matre river systems, was filled up with water. A dam breach then caused a large volume of water to flow down the watercourse of the Øystrebøelva, towards the Ikjefjord. According to Massnes, this event coloured the Ikjefjord white for several days (Massnes 2017, *Personal communication*). The BKK Power Company had the control over the Øystrebøelva back in one to two days (Massnes 2017, *Personal communication*).

Flood protection

High water levels during the 1983 overflow event reached grazing areas for cattle, located close to the Øystrebøelva. The owners complained to power company BKK. The power company responded with construction a flood protection, i.e. elevating the riverbanks, along the riverbed to protect both the grazing areas and local roads shortly after. **Figure 3.8** illustrates the elevated riverbanks. Non-local material was most likely used to elevate the riverbanks (Massnes 2017, *Personal communication*).

Overflow events in 2008 – 2017

Four overflow events occurred of the Stølsvatnet in period 2008 – 2017. Overflow events occurred in autumn 2011, autumn 2012 (two events) and winter 2015 (BKK AS, 2017). The overflow event of winter 2015 was most severe. These events might have had the same effect as the 1983 overflow event are recorded by the BKK; however, they were not described as having a major impact on the Ikjefjord compared to the 1983 event.

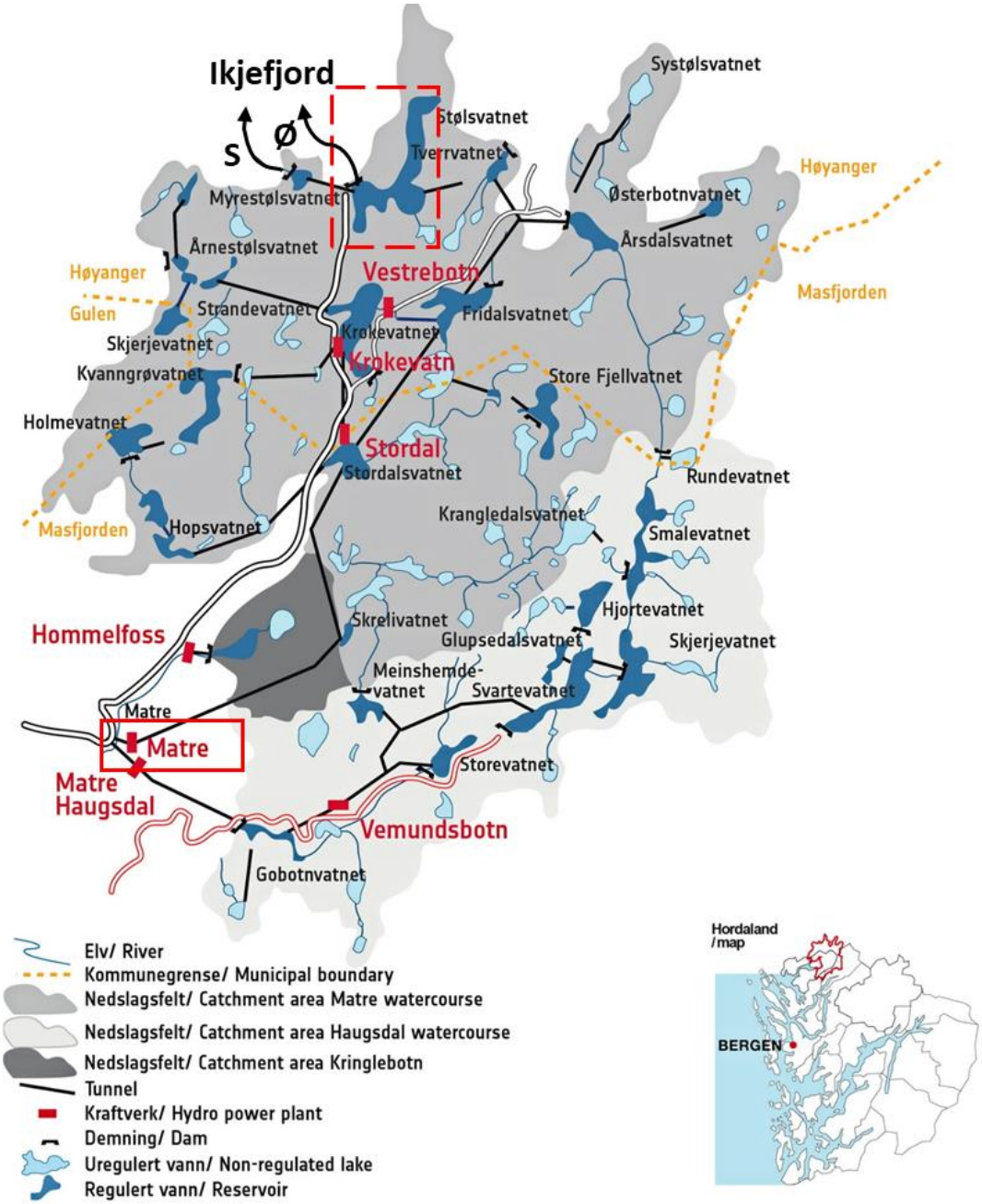

Figure 3.7: Illustration of the Matre river systems and adjacent river systems in relation to the Ikjefjord. The Matre hydro power plant (red square) and Stølsvatn (striped red square) are indicated. The rivers Storelva (S) and Øystrebøelva (Ø) are indicated with black arrows. Modified after BKK AS (2018).

Figure 3.8: Flood protection Øystrebøelva, showing the elevated riverbank on the left (Paetzel, 2017b).

3.2.2 Bridge construction

The Ikjefjordsbrua, located at the border of the Ikjefjord with the Sognefjord (Figure 3.9), was constructed during period 1973-1977 (Ese, 2005). The bridge pillars restrict the water exchange between the Sognefjord and the Ikjefjord. A sill was created that connects the island Storeholmen with the eastern site of the Ikjefjord (Figure 3.9). The sill construction has narrowed the outlet of the Ikjefjord, forming a topographical constraint.

Figure 3.9: The Ikjefjordsbrua. former island Storeholmen is indicated in a red striped square (kartverket, 2018).

3.2.3 Boat traffic

The Sognefjord is a waterway that is intensively used by cruise ships and ferries amongst others. The boat traffic on the Sognefjord and small boats on the Ikjefjord might have polluted the Ikjefjord with tributyltinoxide (TBT) from the 1960s up to 2008.

Since the 1960s TBT was used in coatings on boats to prevent aquatic organisms to attach to the boats. Later research showed a negative impact of TBT in antifouling paint on the aquatic environment. At the AFS Convention of the International Maritime Organisation in 2001, legislation was formed to ban the use of TBT in anti-fouling paints. It no longer allowed to apply TBT on ships since June 2003. Ships with an anti-fouling layer that contains accessible TBT are banned from the waters of all member states of the United Nations since January 2008 (The European Maritime Safety Agency, 2017).

Furthermore, boat traffic forms a potential source of PAHs by the treatment of ships with coal tar and incomplete combustion of fossil fuels (Kvernheim et al., 1992).

3.2.4 Car traffic

The main road in Western-Norway, i.e. the E39, has a distance of approximately 4km to the Ikjefjord. Car traffic on the main road and local roads is a potential source of PAHs by the incomplete combustion of fossil fuels (Kvernheim et al., 1992). Furthermore, the road surface forms a potential source of PAHs, and copper, zinc and lead (Bækken, 1993). Bækken (1993) states that the extensive use of spikes on car winter tires damages the Norwegian road surface considerable and argues that the released road dust forms a potential source of various environmental hazardous compounds.

3.2.5 Petroleum industry by Statoil in Mongstad

The Statoil oil refinery at Mongstad, located approximately 72km to the South-West of the Ikjefjord in Nord-Hordaland County, went into operation in 1975 (Statoil ASA, 2018b). Since 1975 the facility has expanded. Nowadays the refinery has a capacity of close to 12 million tonnes of crude oil per year. A large part of the produced oil is transported from the terminal in Mongstad (Statoil ASA, 2018b).

Since incomplete combustion of fossil fuels is the main source of PAHs in marine environments, the oil refinery at Mongstad forms a potential source of PAHs by exhaust gases (Kvernheim et al., 1992). Exhaust gases from the petroleum industry in Mongstad, possible containing polycyclic aromatic hydrocarbons (PAHs), can travel towards the Ikjefjord with a southwestern wind (Figure 3.10), prevailing during the winter period, i.e. October to March.

Figure 3.10: Illustration of the Statoil oil refinery in Mongstad in relation to the Ikjefjord. Modified after statoil ASA (2018a).

3.2.6 Precipitation intensity 1957 – 2017

The annual precipitation in Norway increased with approximately 20% between 1900 and 2012 (Norwegian Ministry of Climate and Environment, 2014). Local precipitation data shows a clear trend of increased precipitation throughout the last 50 years (period 1957-2017). Precipitation data from weather station Lavik, i.e. station number 56320 of the Norwegian Meteorological Institute, shows a gradual increase of about 500 mm of annual precipitation between 1957 and 2017 (Figure 3.11). Weather station Lavik is located 5km north of the Ikjefjord at an elevation of 31m (Norwegian Meteorological Institute, 2018b).

The flood of 2003

A road located close to the Ikjefjord was flooded in 2003. The flood was the result of an increase in the size of the river Snjogilet. The probable cause for this event was an indicated elevation in local precipitation (Massnes 2017, *Personal communication*). This event might have caused an increased transport of particulate matter towards the Ikjefjord.

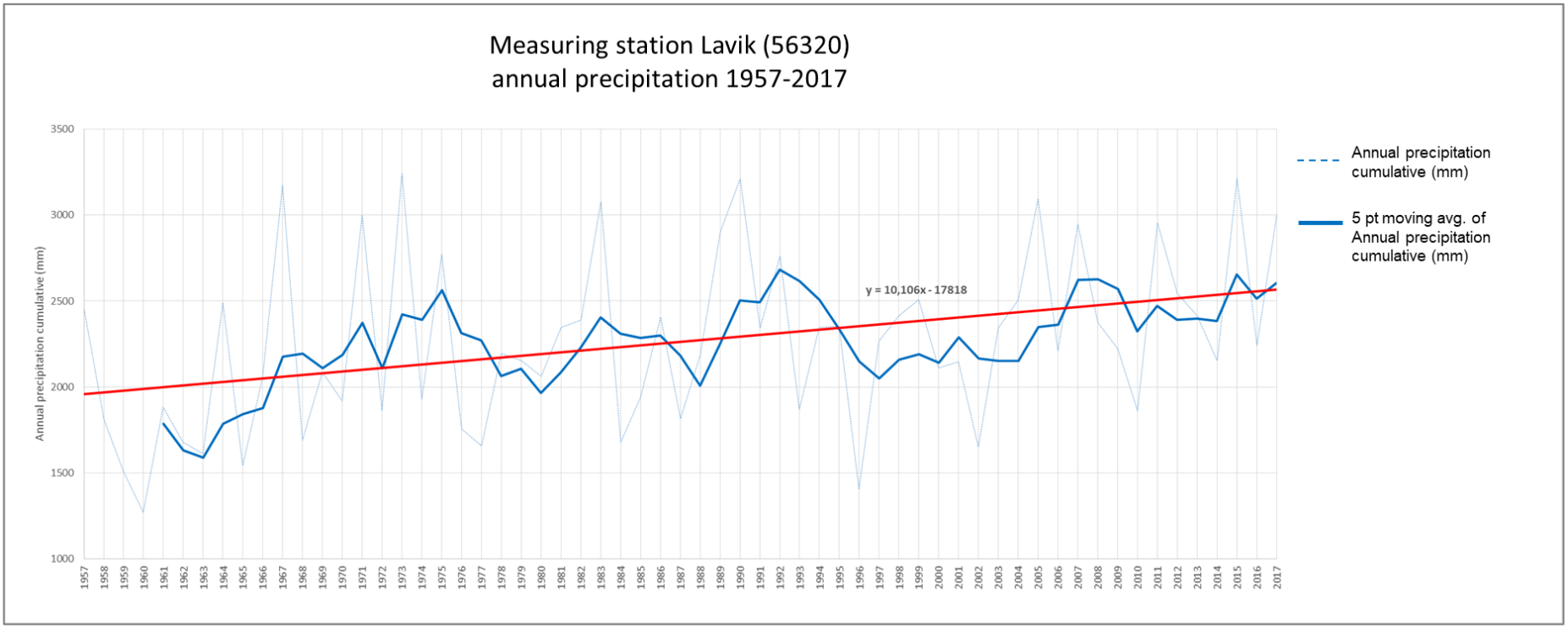

Figure 3.11: Annual precipitation 1957-2017 measured by weather station Lavik (56320), data source: eKlima.

4 Methods

This chapter describes the used methods of sediment retrieving, core description, dating, smear slide analyses, geochemical analyses and pollution analyses.

4.1 Retrieving the sediment samples

Figure 4.1c summarizes the sediment material gathered from the Inner and Outer Ikjefjord locations. The sediment record of the Ikjefjord consists of two sediment cores and two grab samples.

Sediment cores MF2017-1 and MF2017-2 were taken with a modified Niemistö (1974) Gravity Corer (Appendix I Figure a) with 60cm long and 6.8cm diameter plastic pipes in the Inner Ikjefjord basin in August 2017. The Niemistö (1974) Gravity Corer allows retrieving soft sediments with intact sediment-water interfaces and intact stratigraphy (Niemistö, 1974). This ensures that the year of retrieval corresponds to the year of the deposition of the sediment surface (if not eroded), and that the sediment core has a consistent time resolution.

In addition, a Van Veen (1933) Grab (Appendix I Figure b) was used to retrieve a 20cm x 20cm surface area and 20 cm deep sediment block from the sediment surface of location MF2017-2 in the Inner Ikjefjord (Van Veen, 1933). In contrast to the Niemistö (1974) Gravity Corer, this method retrieves a sufficient amount of sediment material, which is necessary for the analysis of pollutants. On the other hand, the Van Veen Grab does not sample the sediment-water interface, and does not allow storage of the sample with intact stratigraphy. Van Veen Grab samples are thus only used for pollution analyses.

It was not possible to locate decent sampling locations for the Niemistö (1974) Gravity Corer in the Outer Ikjefjord due to the lack of an echo sounder during the sampling cruise in August 2017.

Echo-sounder profiles across the Ikjefjord (Figure 4.1b) were taken on a second sampling cruise in October 2017. Based on that profile, an additional Van Veen Grab sediment sample was retrieved at location MF2017-3 in the Outer Ikjefjord. The boat was not equipped to use the Niemistö (1974) Gravity Corer. Figure 4.1a and Figure 4.1c show the sampling locations. Having a sediment record that consists of sediments from the Inner and the Outer Ikjefjord basin allows the indication of basinwide environmental change.

The plastic pipes of the Niemistö (1974) sediment gravity cores MF2017-1 and MF2017-2 were horizontally stored in a cool storage room (~4 °C) upon arrival at the Western Norway University of Applied Sciences, Campus Sogndal, until opening. The sediment cores were exposed to temperatures of 10-15 °C during the transport towards Campus Sogndal.

Acid cleaned and sterilized glass jars were filled with sediment from the sediment surface at 0-2 cm and 10-12 cm of the Van Veen grab sample at location MF2017-2 (Inner Ikjefjord) and with sediment of the Van Veen grab sample at location MF2017-

3 (Outer Ikjefjorde). The glass jars were cooled to ~ 4 °C immediately, and frozen upon arrival at Campus Sogndal circa 3 hours later. The glass jars were sent to the laboratory of Eurofins Environment Testing Norway AS for pollution analyses.

1a

1b

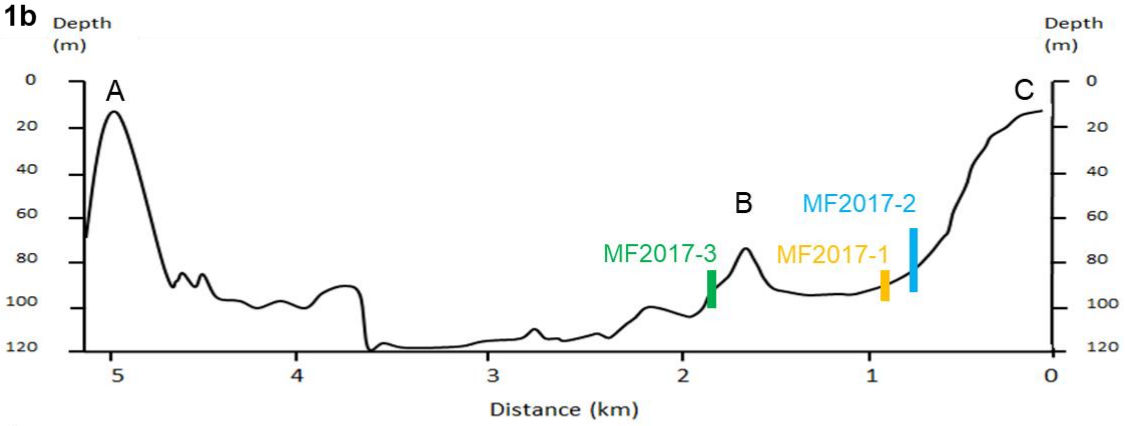

1c

Station	Type of record	Coordinates (WGS 84)	Basin	water depth	Penetration depth
MF2017-1	Niemistö core	61°03,780' 05°39,930'	Inner basin	86.0 m	31.5 cm
MF2017-2	Niemistö core Van Veen grab	61°03,700' 05°39,995'	Inner basin	82.0 m	32.0 cm 20.0 cm
MF2017-3	Van Veen grab	61°04,045' 05°39,590'	Outer basin	88.4 m	10.0 cm

Figure 4.1a: Projection of the sampling locations of the Ikjefjord sediment record (indicated with red dots) and the transect of the Echo-Sounder profile (red line) from the Ikjefjord outlet (A) to the inner sill (B) and the shore (C). The black framed inset map shows the geographical location of the Ikjefjord.
Figure 4.1b: Echo-Sounder profile of the Ikjefjord, the Ikjefjord outlet (A), inner sill (B) and the Ikjefjord shore (C) are indicated (Paetzel, 2017a). The sample locations located in the vicinity of the transect are indicated with markings.
Figure 4.1c: Overview of the Ikjefjord sediment record, describing sample locations and the retrieved material. Coordinates are provided using World Geodetic System scheme 84.

4.2 Core description

The lithology of a sediment core gives a first impression of the properties and quality of the sediment core. The lithology of sediment cores MF2017-1 and MF2017-2 has been inspected visually according to variations in colour, structure and texture. The cores were photographed upon opening.

Munsell® (1994) soil color charts provided a colour classification of the cores. The visual inspection noted the occurrence of sediment structures, i.e. lamination, disturbed layers, visual grain size variation, and gradual transitions.

The lithology of the grab samples MF2017-2 and MF2017-3 was not inspected, since the Van Veen Grab does not allow storage of the sample with an intact stratigraphy.

4.3 Dating

Applying dating horizons onto sediment cores MF2017-1 and MF2017-2 provides a time resolution on variation in the biological, chemical and physical characteristics of the sediments. The dating relates variations in the sediment material throughout the sediment record to environmental change that occurred in the Ikjefjord and its surrounding area. Applying dating horizons onto the sediment record is furthermore required to indicate the sources of any pollution found in the sediment record.

The dating of the sediment cores was done using the method presented by Paetzel & Dale (2010). In addition to freshwater diatoms, this method uses the grainsize distribution (in percentage of sand, silt and clay of the total mineral grain fraction) in marine sediments of Western Norwegian fjord basins in relation to regional precipitation (cumulative in mm per year). Paetzel & Dale (2010) predict that similar freshwater diatom and/or grainsize-climate relations are likely to be found in other Western Norwegian fjord sediments. Langeng & Slinning (2018) confirm this prediction in ^{210}Pb-dated sediments of the Fjærlandsfjord, Western Norway.

Riverine discharge is the main source of sediment supply in temperate non-glaciated fjords with a restricted exchange of coastal water (Howe et al., 2010). Variation in the mineral fraction could thus indicates a change in the river discharge. The riverine discharge is related to precipitation. Sediments were dated by comparing the sand, silt and clay fractions (% of total mineral grains) of particulate matter throughout the sediment cores with the cumulative annual precipitation. Smear slide analyses of particulate matter provided the grainsize data.

The precipitation data originates from weather station Lavik, i.e. station number 56320 of the Norwegian Meteorological Institute, located 5km north of the Ikjefjord. The precipitation data of the period 1957-2017 is retrieved from the eKlima database. eKlima is a web portal of the DNMI that contains data from their meteorological weather stations all over Norway (Norwegian Meteorological Institute, 2018a). The specifications of weather station Lavik, including its location and recordings, are listed in Table 4.1.

A moving average is used to smoothen the grainsize graphs and the precipitation graph. This happens by calculating average values across a static number of successive data points. For example, in a 5-point moving average, each data point of the moving average graph represents an average of five successive data points. The mark of this average would occur at the position of each fifth data point in the graph. Using a moving average allows to flexibly adjust the relationship between the precipitation and the sediment record to changes in sedimentation rates.

It should be noted that inaccuracies might occur when trying to sample exactly 0.5 cm successive sediment material for a smear slide from soft (>85% water content), organic matter rich (~10% organic carbon) sediments (Paetzel 2018, *Personal communication*). This might lead to a deviation of up to several millimetres of the smear slide depth, compared to the real depth. This has to be taken into account when interpreting the exact position of single data point or peaks. To avoid this discussion, it is reasonable to interpret areas of similar trends rather than single data

points or peaks when comparing smear slide data with independent data sets, i.e. in this case precipitation data.

Meteorological station	Site reference	Latitude	Longitude	Elevation (m)	Recorded parameters	Operational since
Lavik	56320	61.1122°	5.5413°	31	Precipitation	01-07-1895

Table 4.1: The specifications of meteorological station Lavik, including its location and recordings (Norwegian Meteorological Institute, 2018b).

4.4 Smear slide analyses of particulate matter

The particulate mineral and organic matter content of the sediments relates to the transport conditions from their source towards the location of sedimentation (Chapter 2.2). Variation in the particulate matter content throughout a sediment record can therefore indicate environmental change.

Smear slides were made continuously down-core along 0.5cm segments of sediment cores MF2017-1 and MF2017-2. Three particulate matter ratios were analyzed in the smear slides: (a) the percentage distribution of mineral matter versus organic matter, (b) the percentage distribution of terrestrial organic matter versus marine organic matter, and (c) the percentage distribution of mineral grainsizes. The smear slides were analyzed using a Leitz Aristoplan light microscope at 40× magnification. The determinations were performed on three representative areas per smear slide, each with a size of ±0.072 mm^2. The average values of these areas were then calculated for each smear slide following the description of Rothwell (1989).

4.4.1 Smear slide preparation

The following steps describe the smear slide preparation of sediment cores MF2017-1 and MF2017-2. Steps 9-11 need to be performed in a fume hood cupboard. This is required to prevent health risks during the evaporation of toluene, which is the carcinogenic solvent of the mounting medium Naphrax® (Brunel Microscopes Ltd) used for mounting the smear slides.

Step 1. Label a microscope object glass and place it on a heat plate (~ 50°C) to let it pre-heat.

Step 2. Place sediment of a continuous segment 0.5 cm thickness of the sediment core on a microscope object glass.

Step 3. Add one or two drops of distilled water to the sample if the sample is dry. Use a toothpick to homogenize the sediment.

Step 4. Take a small amount of the homogenized sediment on the tip of a toothpick and place it onto a microscope cover glass.

Step 5. Add a drop of distilled water to the sample with a pipette and stir with the toothpick to disintegrate the particles in the sample.

Step 6. Add a drop of Kodak Photo Flo wetting agent with a pipette to remove the surface tension of the previously added water. This step is required to be able to smear out the sample.

Step 7. Use the entire length of the toothpick to smear out the sample evenly over the microscope cover glass. Do not cover an area of 0.5 cm at each side of

the microscope cover glass with any sample. This is to prevent the sample from coming in to contact with the hand that holds the sample, possible disturbing or even destroying the sample.

Step 8. Place the microscope cover glass on the heat plate (max 50°C) in a fume cupboard to evaporate the water in the sample. Avoid temperatures above 50°C to prevent the burning of organic matter during this step.

Step 9. Use a pipette to place a stripe of the mounting medium Naphrax over the entire length of the sample/cover glass.

Step 10. Drop the pre-heated labelled microscope object glass gently onto the cover glass. Quickly turn over the microscope slide, making sure that the microscope cover glass lies on top.

Step 11. Heat up the heat-plate to 100-120°C to evaporate the solvent. The bubbling of Naphrax indicates the start of the evaporation process of the solvent. When the Naphrax has almost stopped bubbling, the process of evaporation is completed.

Step 12. Remove the smear slide from the heat plate and place it at room temperature. Let the smear slide cool down to room temperature.

4.4.2 Organic matter determination

The particulate organic matter fraction can be subdivided into terrestrial organic matter and marine organic matter. Terrestrial organic matter originates from higher plants on land and is transported towards a fjord by riverine discharge and land runoff. The source of marine organic matter is primary production in the photic zone of the fjord or adjacent waterbodies (Howe et al., 2010). Variation in the terrestrial organic matter versus marine organic matter fraction (in %) can indicate changes in the organic matter sources, for example an increase or decrease of the primary productivity. Variation can furthermore indicate changes in the transport conditions from their source towards the location of sedimentation.

The terrestrial organic matter versus marine organic matter fraction was determined by estimating the volume of terrestrial organic matter of the entire organic matter fraction of the representative area. This ratio was then expressed in the percentage of the total area covered by particulate organic matter.

Terrestrial organic matter has a clear fibrous structure, i.e. clear edges and shapes, and a dark brown to black colour. Marine organic matter can be recognized by its light brown colour and fuzzy aggregates that have a lack of structure (Paetzel & Schrader, 1995). Appendix IB illustrates the organic matter determination.

4.4.3 Mineral matter determination

In general, riverine discharge is the main source of mineral matter in temperate non-glaciated fjords with a restricted exchange with coastal water, such as the Ikjefjord (Howe et al., 2010). As discussed in 2.2, the grainsize distribution of riverine discharge is related to the riverine flow speed (Hjulström, 1935). Variation in the relative abundancy of particulate mineral matter is thus possible related to changes in the riverine discharge.

Mineral matter versus organic matter

The mineral matter versus organic matter content was determined by estimating the volume of mineral matter of all particulate matter in the representative smear slide areas. This ratio was then expressed in percentages. Mineral matter has shapes with clear borders and a black (pyrite), translucent to grey (feldspar and quartz), green (biotite) or yellow colour (muscovite); see Rothwell (1989) for an extensive description of the smear slide analysis. Appendix IB illustrates the mineral matter determination.

Grainsize distribution (using the Udden-Wentworth Scale)

The ratio between sand, silt and clay was determined for all MF2017-1 and MF2017-2 smear slides. In addition, the silt sub-sizes of coarse silt, medium silt, fine silt and very fine silt in all MF2017-2 smear slides were determined. The ratios were determined by estimating the volume of each grainsize fraction against the fraction of the largest grain size within the representative smear slide area, using the Udden-Wentworth scale of grainsize distribution (Table 4.2). For example, the coarsest grain fraction within a representative smear slide area is coarse silt. The value of “one” is then assigned to the volume of the total number of coarse silt grains. As the coarse silt size is the largest, the value of “zero” is assigned to the sand fraction. The value of all the other fractions will be assigned relative to their volume compared with the coarse silt fraction. The average ratio of each smear slide was recalculated to percentages.

Table 4.2: Udden-Wentworth (1922) scale of grain size distribution and the corresponding units on the microscope measuring bar.

Mineral matter fraction	Grain size (µm)	Units on microscope measuring bar (1 unit = 4 µm)
Sand	62 – 2000	≥ 16
Coarse silt	31 – 62	8 - 16
Medium silt	16 – 31	4 – 8
Fine silt	8 – 16	2 – 4
Very fine silt	4 – 8	1 – 2
Clay	< 4	< 1

4.5 Geochemical analyses

The geochemistry of the total fraction of the sediment material relates to its source and to the transport conditions from the source(s) towards the Ikjefjord. Variation in the geochemistry of the bulk sediment material throughout the Ikjefjord sediment record can therefore indicate changes in the environment of the Ikjefjord. This thesis takes the gamma density, magnetic susceptibility, elemental composition and the magnetic coherence versus incoherence ratio of sediment core MF2017-2 into account. In addition, a high-resolution optical image and a high resolution X-radiograph were made.

The geochemical analyses are high-resolution relative determinations of the sediment composition, allowing a wider perspective of interpretation. These analyses have therefore been used in addition to the particulate matter analyses performed on smear slides. The geochemical analyses were performed at Earth Lab geological laboratories at the Department of Earth Science at the University of Bergen, Norway.

Sediment core MF2017-2 was prepared for the geochemistry analysis by slicing the core into halves with an electrical saw and smoothing its surface with a knife and a spatula.

4.5.1 Geochemical analyses with the GEOTEK Multi Sensor Core Logger (MSCL)

The gamma density and magnetic susceptibility of the sediments were measured with the GEOTEK Multi Sensor Core Logger (MSCL, Figure 4.2).

Mineral matter is denser than organic matter, the gamma density therefore relates to the mineral matter versus organic matter distribution. The MSCL measures the gamma density at a resolution of 0.2 cm, and therefore provides more detailed information about the particulate mineral matter versus particulate organic matter content than the smear slide analysis that were taken at a resolution of 0.5 cm.

The magnetic susceptibility is a parameter that depends on how easy particles are magnetized and the size of the particles (Dearing, 1999). Mineral matter is more easily magnetized than organic matter and has therefore a higher magnetic susceptibility (Haflidason 2017, *Personal communication*). Thus, the magnetic susceptibility can indicate the relative amount of mineral matter content in relation to the relative amount of organic matter content of a sample. Furthermore, magnetism is less strong in finer grained mineral matter (fine silt to clay) than in coarser grained mineral matter (medium silt to sand) due to the non-uniform distribution of the magnetic momentum in the smaller mineral grains (Weiss & Foëx, 1926). Thus, the magnetic susceptibility has also a potential for indicating changes in grain size.

The used MSCL procedure is as follows. The split core was placed at the right side of the gamma detector, with the bottom of the sediment core facing towards the core pusher (Figure 4.2). The belt driven pusher block then moved the sediment core past the gamma unit and the magnetic susceptibility point sensor. The computer section of the MSCL controls the pusher block and the sensors automatically.

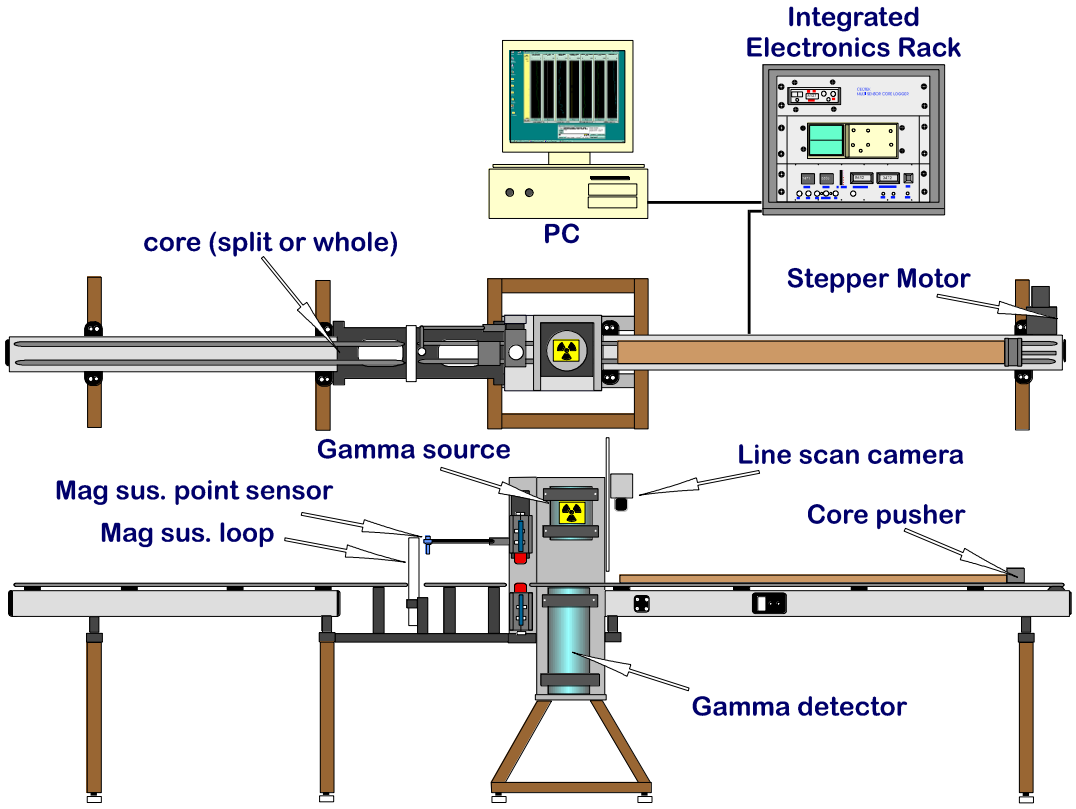

Figure 4.2: Illustration of the GEOTEK Multi Sensor Core Logger (MSCL) (Department of Earth Science UiB, 2017).

The gamma unit consist of a Cesium-137 (^{137}Cs) source and a sodium iodide detector. The Cesium-137 source emits a beam of gamma rays that passes through the sediment core. The sediment causes scattering of the emitted gamma radiation. The degree of scattering relates to the amount of electrons that the gamma radiation meets on its way through the sediment core. This value relates to the density of the sediment. The sodium iodide detector located underneath the sediment core measures the outgoing gamma radiation. The computer automatically compares the gamma radiation that passed through the sediment to this attenuation value for aluminium; and uses this data to calculate the gamma density of the sediment (Department of Earth Science UiB, 2017). Aluminium represents the natural mineral background radiation in rocks or sediment. Therefore, aluminium is used as a reference material (Haflidason 2017, *Personal communication*).

The computer section of the MSCL calculates the gamma density automatically, using the following formula of Evans (1965):

$$p = \frac{1}{\mu d} * In(I_0/I)$$

P= gamma density (g/cm^3)
μ= Compton mass attenuation coefficient of sediment (cm^2/g)
d= thickness of the sediment (cm)
I_0= Intensity of the gamma beam after passing through the sediment
I= Intensity of the detected gamma beam when no sediment core is present (this value is equal to the intensity of the gamma beam after passing through the core liner)

The Compton mass attenuation coefficient is a standard. Since not all sediments have the same electron composition, this causes a measuring uncertainty (Department of Earth Science UiB, 2017).

The magnetic susceptibility point sensor moves in and out of contact with the sediment when the sediment moves pass this sensor. The point sensor creates a magnetic field. Material with a magnetic susceptibility, i.e. material that can be magnetized, alters this magnetic field when it comes into contact. This signal is measured and expressed on the SI scale. The Barrington loop of the MSCL can also measure the magnetic susceptibility. However, this results in lower resolution data (Department of Earth Science UiB, 2017).

4.5.2 Geochemical analyses with the ITRAX- multi-functional X-ray core scanner

The relative elemental composition and the magnetic coherence versus incoherence ratio of the sediment core were determined with the ITRAX- multi-functional X-ray core scanner (XRF). The ITRAX- multi-functional X-ray core scanner also made a high-resolution optical image and a high resolution X-radiograph.

The relative elemental composition of sediments relates to their source area. The elemental composition can provide information about the geology and biological activity of their sources (Croudace et al., 2006).

The magnetic coherence and incoherence are the strength of two types of scattering caused by material when material is irradiated with X-ray radiation. The strength of magnetic incoherence is related to the thickness of the material. This type of scattering is stronger when material is thicker, giving a lower detected magnetic incoherence value. The magnetic coherence is not influenced by the thickness of material (Croudace et al., 2006). The magnetic coherence versus incoherence ratio is therefore higher when the sediment has a higher content of thick particulate matter, i.e. enhanced amounts of mineral matter in relation to organic matter, or larger grain sizes (coarser silt sizes and sand).

The optical imaging shows variations (layers) throughout a sediment record at a high resolution. These variations relate to the mineral matter and organic matter content of

the sediment core (Haflidason 2017, *Personal communication*). Darker colours indicates a larger organic matter content. The optical image can be used to relate characteristics indicated by various (geochemical) analyses to the colour of the sediments. One can use the optical image during the scanning process to decide which transects of the sediment core should be scanned.

The X-radiograph is a radiographic positive image. Thus, this image illustrates high-density areas dark and lower density areas lighter (Croudace et al., 2006). The density of the sediments relates to their mineral matter and organic matter content. The X-radiograph therefore illustrates the mineral versus organic matter distribution.

The ITRAX- multi-functional X-ray core scanning procedure was as follows. A layer of plastic foil was placed on the surface of the split sediment core to prevent the sediment core from getting dry. The sediment core was then placed on the designated place, with the top of the sediment core orientated to the right. A set of procedures followed to make sure that the settings of the equipment were appropriate. These procedures included analyses on several characteristics, while the sediment core was moving multiple times from left to right through the scanner. The optical imaging is one of these procedures. The scanning started when the procedures were completed. The sediment core went through the scanner twice. The first time an X-radiographic image was made. The XRF elemental data was acquired the second time (Croudace et al., 2006). Figure 4.3 illustrates the different components of the ITRAX-multi-functional X-ray core scanner.

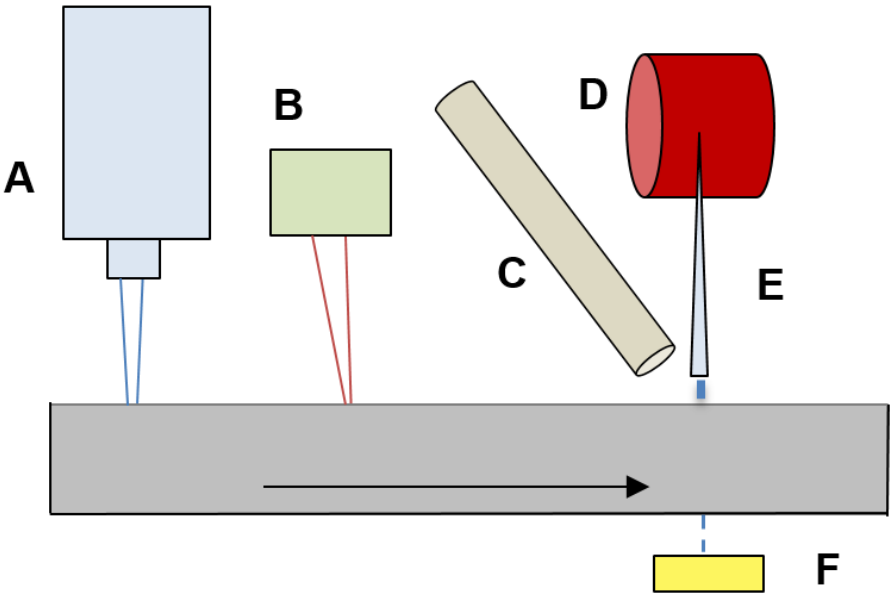

Figure 4.3: Illustration of the ITRAX core scanner showing the optical-line camera (A), laser triangulation system (B), motorized XRF Si-drift chamber detector (C), X-ray tube (D), flat-beam X-ray waveguide (E) and the X-ray line camera (F). The horizontal arrow shows the moving direction of the sediment core.

As described by Croudace et al. (2006), the function of the optical-line camera system (A) is to make an optical image of the sediment core with a resolution of 50 µm × 50 µm pixels. The laser triangulation system (B) measures the location of the sediment core surface. This data is used to keep the distance between the sediment core and the sample constant. The motorized XRF Si-drift chamber detector (C) sends out X-ray radiation. When this radiation hits an element, the element sends out electromagnetic radiation. The XRF detector detects the released radiation. The detected radiation relates to the elemental composition of the measured sediment. The XRF detector detects the coherence and incoherence of the radiation as well. The X-ray tube (D) generates X-ray beams and sends them through the flat-beam X-ray waveguide (E) towards the sediment core. The flat-beam X-ray waveguide concentrates the X-ray beams to an X-ray beam of 20 × 0.2 mm. The X-ray line camera (F) detects the intensity of the radiation that passed through the sediment core. The X-ray line camera transfers the received signals to an image, i.e. a radiographic positive X-radiograph, with a resolution of up to 20 µm × 20 µm pixels.

4.6 Pollution analyses

Quantitative determinations of trace metals, polychlorinated biphenyls (PCBs), polycyclic aromatic hydrocarbons (PAHs) and Tributyltin (TBT) were performed on three transects of the Ikjefjord sediment record. Analyzing these three transects makes it possible to indicate temporal and spatial variety in the presence of metals, PCBs, PAHs and TBT throughout the sediment record. Thereafter, the results were compared to the environmental quality standards for marine sediments to indicate pollution and the severity of any pollution.

4.6.1 Quantitative determination of pollutants

Eurofins Environment Testing Norway AS has conducted quantitative determinations of metals, PCBs, PAHs and TBT on three transects of the Ikjefjord sediment record. The analyzed transects are 0-2 cm and 10-12 cm in MF2017-2 and 0-10 cm in MF2017-3.

The determinations are performed according to Norwegian standard NS EN ISO 17294-2 (all trace metals excluding mercury), a modified version of Norwegian standard NS-EN ISO 17852:2008 (mercury), the Norwegian standard NS-EN 16167:2012 (PCBs), a modified version of Norwegian standard ISO 18287:2006 (PAHs) and Eurofins Internal Method 2085 (TBT). Table 4.3 describes the corresponding international standards of the Norwegian standards and provides the standard description.

Table 4.3: The standards applied in the quantitative determination of pollutants

Norwegian standard	Corresponding international standard	Standard description
NS EN ISO 17294-2	ISO 17294-2:2016	Water quality—Application of inductively coupled plasma mass spectrometry (ICP-MS) -- Part 2: Determination of selected elements including uranium isotopes
NS EN ISO 17852:2008	ISO 17852:2008	Water quality—Determination of mercury—Method using atomic fluorescence spectrometry
NS-EN 16167:2012	EN 16167:2012	Sludge, treated bio-waste and soil - Determination of polychlorinated biphenyls (PCB) by gas chromatography with mass selective detection (GC-MS) and gas chromatography with electron-capture detection (GC-ECD)
ISO 18287:2006	ISO 18287:2006	Soil quality—Determination of polycyclic aromatic hydrocarbons (PAH) -- Gas chromatographic method with mass spectrometric detection (GC-MS)

ISO 17294-2:2016 is a standard for the quantitative determination of elements in water, sludge and sediment using inductively coupled plasma mass spectrometry (ICP-MS) (International Organization for Standardization, 2016). Inductively Coupled Plasma Mass Spectrometry (ICP-MS) is a two-step determination in which an Inductively Coupled Plasma (ICP) source first converts elements to ions, after which mass spectrometry (MS) is applied to detect the ions (Wiley-VHC, 1998). Mass spectrometry measures the intensity of different mass/charge ratios of vaporized and ionized samples. The mass/charge ratio relates to specific ions. The intensity of the mass/charge ratio is proportional to the concentration of the ion. A magnetic field is applied to deflect the ions, a specific range of mass/charge ratios, and thus ions, can be detected in this way (Wiley-VHC, 1998).

ISO 17852:2008 specifies the quantitative determination of mercury in water using atomic fluorescence spectrometry (Standards Norway, 2008). In this method, electrons of mercury atoms present in the sample are excited to a higher state with a mercury lamp that emits light of a specific intensity (PS Analytical, 2015). When these electrons return to their previous energy level, the mercury atoms emit light. The emitted light relates to the concentration of mercury in the sample. A detector measures the light output (PS Analytical, 2015).

EN 16167:2012 is the European standard for the quantitative determination of seven PCBs (PCB28, PCB52, PCB101, PCB118, PCB138, PCB153 and PCB180) in sludge and treated bio-waste using gas chromatography followed by one of two detection techniques (Standards Norway, 2012). Gas chromatography (GC) is a technique that separates a sample based on vapour pressure and boiling point (Stauffer et al., 2008). In this method, one injects a solution of a sample into the injection port of the gas chromatographer. The injection port heats the solution. A carrier gas transports the vaporized sample towards a column in which a stable phase, i.e. a liquid, is present. In this column, the vaporized sample continuously switches between being dissolved in the stable phase and moving forward, carried by the carrier gas. A detector measures the output of the column and transfers it to an electronic signal (Stauffer et al., 2008). The PCBs are detected by either mass spectrometry or by electron-capture detection (ECD). Electron-capture detection is a detection method based on the affinity of a compound to take over electrons from its surrounding. When a compound takes over electrons from its surrounding, this causes a decline in the charge between two electrodes. This charge difference is then measured (Lovelock, 1958). The intensity of the electronic signal relates to the concentration of the compound. The identification of the compound is based on the time between injection of the sample in the gas chromatographer and the detection by electron-capture detection (Bianco et al., 2008).

Standard ISO 18287:2006 describes the quantitative determination of 16 PAHs (Naphthalene, Acenaphthylene, Acenaphthene, Fluorene, Phenanthrene, Anthracene, Fluoranthene, Pyrene, Benzo[a]anthracene, Chrysene, Benzo[b]fluoranthene, Benzo[k]fluoranthene, Benzo[a]pyrene, Indeno[1,2,3-cd]pyrene, Dibenzo[a,h]anthracene, Benzo[ghi]perylene) in soil using gas chromatography with mass spectrometry detection (International Organization for Standardization, 2006).

Eurofins Environment Testing Norway AS (Moss) uses their internal Method 2085 for the quantitative determination of Tributyltinn (TBT) – Sn. Thereafter, the Tributyltinn (TBT) – Sn results are used to calculate the TBT content.

4.6.2 Interpreting environmental quality

The results of the quantitative determinations were compared to the environmental quality standards for marine sediments formulated by the Norwegian Environment Agency (Miljødirektoratet, 2016). The Norwegian Environment Agency distinguishes five environmental quality reference classes, i.e. background, good, moderate, bad and very bad, for a variety of prioritized compounds (Table 4.4).

The upper limit of reference class 1 relates to the natural occurrence (background value) of the prioritized compounds in the environment. The upper limit of anthropogenic pollutants that do not occur in the environment naturally is zero. The upper limits of all other classes relate to risk and effect. Environmental quality classes III, IV and V indicate pollution. The Norwegian Environment Agency has used international systems for the formulation of environmental quality standards and risk assessment of chemicals in the EU to define the environmental quality classes (Miljødirektoratet, 2016).

Table 4.4: Classification system for water and sediment (Miljødirektoratet, 2016)
AA-QS: Ambient Air Quality Standards. PNEC: Predicted No Effect Concentration. MAC-QS: Maximum Allowable Concentration Quality Standard. $PNEC_{acute}$: Predicted No Effect Concentration with a factor applied to indicate the acute toxicity level. AF^{1}: Safety factor that takes into account the variation in sensitivity between organisms.

I Background	II Good	III Moderate	IV Bad	V Very bad
Background values	No toxic effects	Chronical effects with a long exposure time	Acute toxic effects with a short exposure time	Wide toxic effects
Upper limit: background	Upper limit: AA-QS, PNEC	Upper limit: MAC-QS, $PNEC_{acute}$	Upper limit: $PNEC_{acute}$ * AF^{1}	

5 Results

This chapter provides descriptions of the two sediment cores, and the results of sediment dating, smear slide analyses, geochemical analyses and pollution analyses.

5.1 Core description

Figure 5.1 illustrates sediment cores MF2017-1 and MF2017-2 using the Munsell® (1994) colour classification.

The sediment of core MF2017-1 has a very dark brown colour (7.5YR 2.5/2 and 10YR 2/2) from 31.5cm to 15.0 cm (Figure 5.1). The segment 15.0-13.5 cm is olive grey (5Y 4/2) and contains courser grains than the rest of sediment core MF2017-1. The segment 12.5-1.5 cm is very dark brown (10YR 2/2). The sediment is black coloured in segment 1.5-0.0cm. Shell fragments occur mainly below 27cm sediment depth.

The sediment of core MF2017-2 is black from 32.0cm to 11.5cm (7.5YR 2.5/1). The segment from 11.5cm up to 9.5cm is very dark greyish brown (2.5Y 3/2), and contains courser grains than the rest of sediment core MF2017-2. The sediment is very dark grey from 9.5cm up to 0.0cm (7.5YR 2/1 and 10YR 3/1). Shell fragments occur throughout the entire length of sediment core MF2017-2.

The stratigraphy of sediment cores MF2017-1 and MF2017-2 is undamaged. Both cores smell like hydrogen sulfide (H_2S), indicating the occurrence of anoxia throughout the sediments.

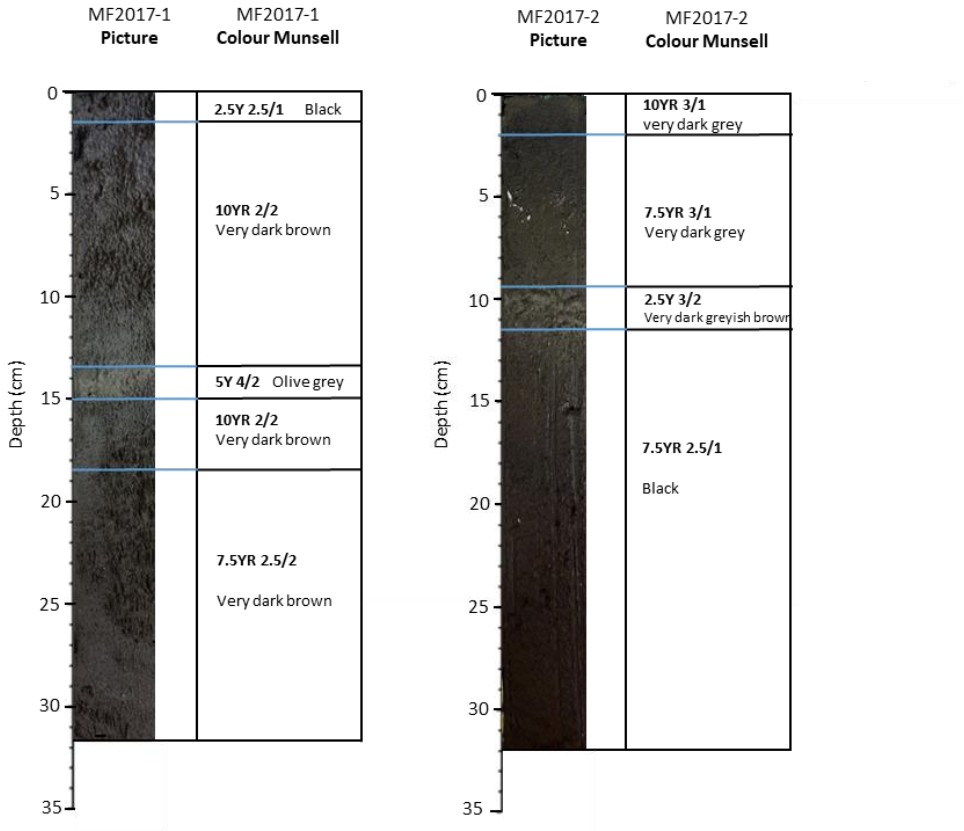

Figure 5.1: Description of sediment cores MF2017-1 and MF2017-2, using the Munsell® (1994) colour classification.

5.2 Dating

A relation is found between the sand fraction (62-2,000 µm) of sediment cores MF2017-1 and MF2017-2, and the precipitation (cumulative in mm/year) of weather station number 56320 located at Lavik, approximately 5km north of the Ikjefjord and closest to the sampling stations.

Figure 5.2 illustrates the sand-precipitation relationship of both sediment cores and the resulting dating. The moving average of the sand fraction (4-point moving average in MF2017-1 and 3-point moving average in MF2017-2), follows roughly the same trend and pattern down-core as the precipitation graph, expressed as a 5-point moving average. The relationship remains visible in all layers of the cores, suggesting that the sediment mostly accumulated continuously throughout the years of deposition, rather than spontaneously during events. The dating indicates higher sedimentation rates in MF2017-1 (0.47 cm/year) compared to MF2017-2 (0.44 cm/year) since 1960.

The dating horizons indicate that the olive grey (5Y 4/2) and the very dark greyish brown (2.5Y 3/2) coarser grained layers of sediment cores MF2017-1 and MF2017-2 started to deposit at some time between 1980 and 1990. This layer will later be referred to as the ‘marker’ layer.

It is difficult apply a dating upon the top layers of sediment cores MF2017-1 and MF2017-2 due to the high water content of top layer sediments (>95%) and the unconsolidated structure (Paetzel 2018, *Personal communication*). However, the sand and precipitation data indicates sedimentation of the top sediments during 2017, as expected due to the use of the Niemistö (1974) Gravity Corer.

The grab sample of MF2017-2 was not dated, as it is not possible to establish a detailed stratigraphy across a bulk grab sample. However, based on the dating of the core sample MF2017-2, the upper 0-2 cm of the MF2017-2 grab sample would have been deposited over the last 5 years and the sample at 10-12cm would have been deposited around 1995.

No time reference or sedimentation rate could be estimated for the grab sample of MF2017-3, as no sediment core (and thus no time reference) was available from the Outer Ikjefjord. However, the grab sample of MF2017-3 covers an average of 0-10cm surface sediment. At similar sedimentation rates as MF2017-1 (the core closest to the sample location and water depth of MF2017-3), this would represent a period of 20 years back in time, starting at 2017, i.e. the sediment surface.

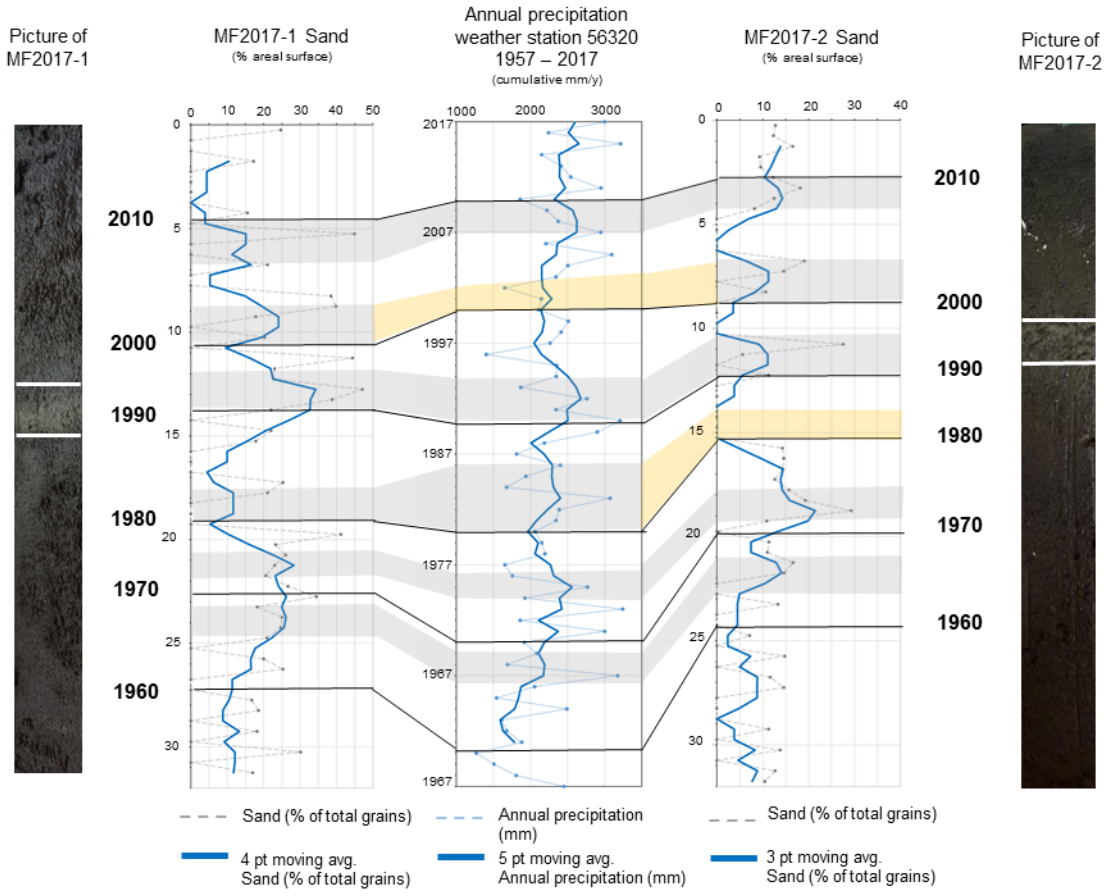

Figure 5.2: The dating of sediment cores MF2017-1 and MF2017-2 based on the sand-precipitation relationship. Grey translucent bars indicate similar patterns, yellow translucent boxes indicate patterns where the relatioship is less visible. Black lines correspond to the indicated decennia.

5.3 Smear slide analyses of particulate matter

5.3.1 Results sediment core MF2017-1

Figure 5.3 shows the total mineral matter versus total organic matter fraction (in %), the terrestrial organic matter versus marine organic matter fraction (in %), and the grain size distribution of sand, silt, and clay (in cumulative %), gathered by smear slide analyses of core MF2017-1. The dataset is presented against the sediment depth. A picture and an optical image (provided by the ITRAX- multi-functional X-ray core scanner) are presented besides the data set. The optical image shows colour variation throughout a sediment record at a high resolution, thus it more accurately indicates colour variation than the ordinary picture. However, the optical image does not show the colours that one can observe with the bare eye while the picture does. Appendix IIa provides individual parameter graphs.

As indicated by the linear trend line in Figure 5.3 mineral matter varies around 40% between 31.5cm and 23.0cm, absolute values range between 30% and 65%. Mineral matter decreases between 23.0cm (40%) and 15.0cm (30%) along a trend line. An increase follows, reaching a peak at 14.0 cm (57%). The peak is located within the layer of grey sediments. Mineral matter decreases along a trend line between 14.0cm (>50%) and 5.0cm (40%), with values of 30-67%. A steeper trend of decrease occurs between 5.0cm (40%) and 0.0cm (32%). Organic matter follows the opposite trend.

Terrestrial organic matter values vary around a trend line located at approximately 15% between 31.5cm and 22.0cm. Values range from 8.3% to 21.7%. Terrestrial organic matter decreases between 22.0cm (17%) and 16.5cm (13%). Terrestrial organic matter increases between 14.0cm (12%) and 0.0cm (15%). Marine organic matter follows the opposite trend.

The sand fraction increases along a trend line from 31.5cm (10%) to 19.5cm (25%). The sand fraction decreases from 13.5cm (25%) to 8.0cm (20%). This decrease starts within the marker layer. Between 8.0cm and 0.0cm the sand fraction varies between values of 45-0% with a relatively constant trend at 8%. Throughout sediment core MF2017-1 sand shows a variation of 0-47%. The clay fraction varies around a trend line located at 20% between 31.5cm and 14cm. The clay fraction shows a trend along 15% between 13.5cm and 7.5cm. Clay increases along a trend between 7.0cm (20%) and 0.0cm (30%).

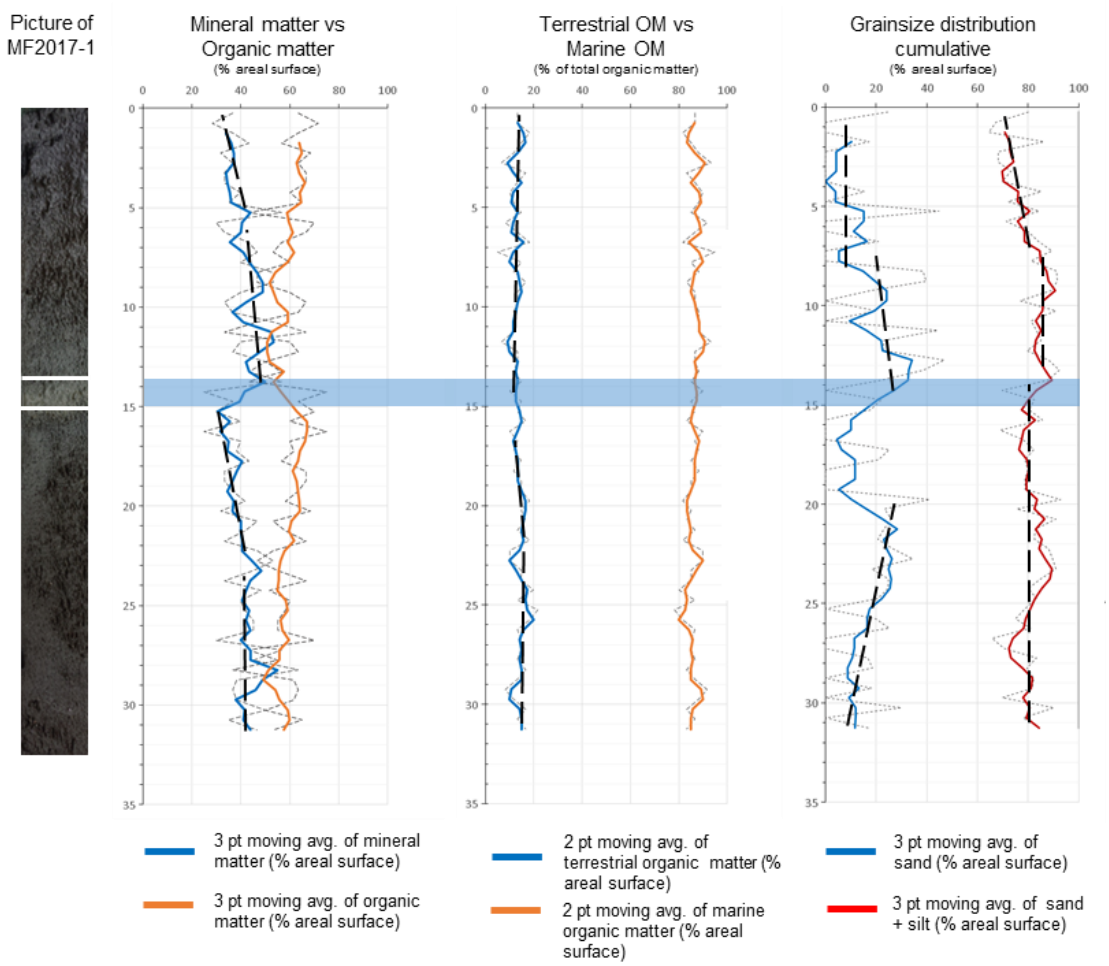

Figure 5.3: Results of smear slide analyses on sediment core MF2017-1, showing the total mineral matter vs organic matter content, the terrestrial organic matter vs marine organic matter content and the cumulative grainsize distribution of sand, silt and clay. The blue, translucent area indicates the position of the marker layer in the sediment.

5.3.2 Results sediment core MF2017-2

Figure 5.4 shows the total mineral matter versus total organic matter fraction (in %), the terrestrial organic matter versus marine organic matter fraction (in %), and the grain size distribution of sand, silt, and clay (in cumulative %), gathered by smear slide analyses of core MF2017-2. The dataset is presented against the sediment depth, besides a picture and an optical image. Appendix IIB provides all remaining results, i.e. the grain sizes of the different silt fractions (coarse silt, medium silt, fine silt, and very fine silt), and individual parameter graphs.

As indicated by the linear trend line in Figure 5.4 mineral matter decreases continuously between 32.0cm (40%) and 13.0cm (35%). Mineral matter reaches its maximum within the marker layer at 11cm (80%). Mineral matter decreases between 9.5cm (45%) and 4.0cm (<30%). Mineral matter increases between 4.0cm (35%) and 0.0cm (>40%). Organic matter follows the opposite trend.

Terrestrial organic matter shows values of 5-20% between 32.0cm and 14.0cm. Terrestrial organic matter is increased between 14.0cm and 9.0cm with a maximum of 27% at 12.0cm. Terrestrial matter decreases between 9.5 cm (15%) and 6.0cm (10%). Terrestrial matter increases between 6.0cm (7%) and 0.0cm (15%). Marine organic matter follows the opposite trend.

The sand fraction increases between 32.0cm (5%) and 18.0cm (15%). The clay fraction varies with 37% (11-48%), along an increasing trend line, between 18.0cm (17%) and 11.0cm (25%). The sand fraction decreases between 18.0cm (15%) and 13.5 cm (5%), which is followed by an increase up to 0.0 cm depth (>15%). The silt fraction is at its minimum of 47% at 11.0cm, thus within the marker layer.

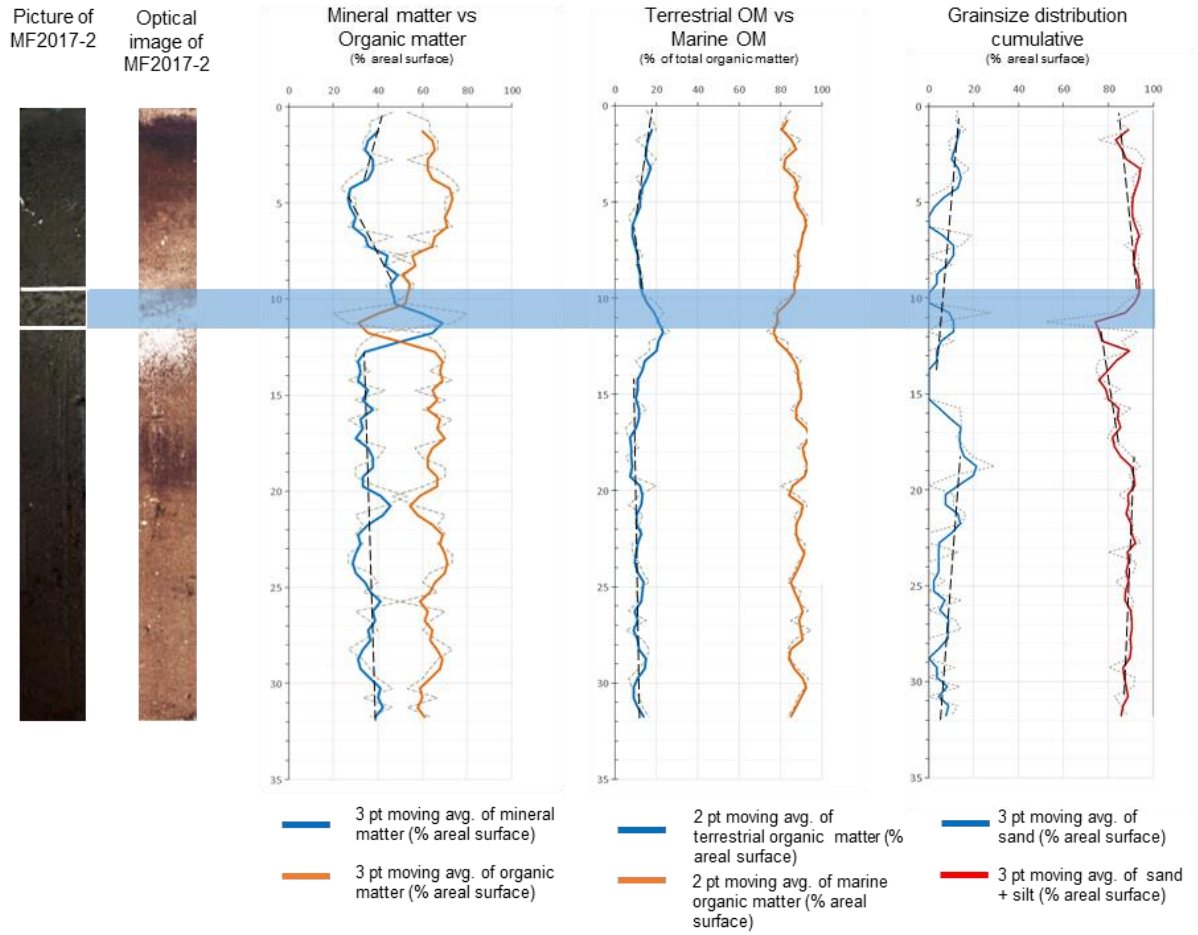

Figure 5.4: Results of smear slide analyses on sediment core MF2017-2, showing the total mineral matter vs organic matter content, the terrestrial organic matter vs marine organic matter content and the cumulative grainsize distribution of sand, silt and clay. The blue, translucent area indicates the position of the marker layer in the sediment.

5.4 Geochemical analyses of particulate matter

The geochemical analysis preformed with the GEOTEK Multi Sensor Core Logger, i.e. the gamma density and magnetic susceptibility analyses, have provided data of sediment core MF2017-2 segment 0.2-31.4 cm. It seems that the analyses of the upper 0.2cm and the lower 0.6cm of sediment core MF2017-2 have been affected by the sealant Oasis®. The geochemical analyses preformed with the ITRAX- multi-functional X-ray core scanner (XRF) have provided data of the entire sediment core.

Figures 5.5 and 5.6 show a selection of the data gathered by geochemical analyses. The dataset is presented against the sediment depth. The translucent boxes indicate the locations of 2 layers of grey coloured sediments. Appendix III provides individual parameter graphs.

Gamma density

The gamma density varies from 0.59 g/cm^3 to 0.94 g/cm^3 between 31.4cm and 12.5cm. The gamma density increases between 12.5cm (0.85 g/cm^3) and 11.2cm (1.61 g/cm^3). The maximum value of 1.61 g/cm^3 lies within the marker layer (Figure 5.5). The X-radiograph shows a dark colour between approximately 10.0cm and 12.5cm, and thus confirms higher densities. Therefore, the X-radiograph is provides a more precise impression of the thickness of the marker layer than an ordinary picture. The gamma density decreases between 9.0cm (0.80 g/cm^3) and 2.0cm (0.39 g/cm^3). Between 2.0cm and 0.2cm the gamma density increases from 0.39 g/cm^3 to 0.44 g/cm^3.

Magnetic susceptibility

The magnetic susceptibility has values of 0 to 40 × 10^{-5} between 31.4cm and 15.0cm. The magnetic susceptibility increases between 15.0cm (40 × 10^{-5}) and 10.6cm (527 × 10^{-5}). The peak value of 527 × 10^{-5} lies within the marker layer. The increase occurs mainly between 12.0cm and 10.6cm. Between 9.0cm and 1.2cm the magnetic susceptibility varies between 32 × 10^{-5} and 125 × 10^{-5}. The magnetic susceptibility increases between 1.2cm (50 × 10^{-5}) and 0.2cm (146 × 10^{-5}).

The magnetic coherence versus incoherence ratio

The magnetic coherence versus incoherence ratio varies from 0.200 to 0.227 between 32.0cm and 15.0cm. The magnetic coherence versus incoherence ratio increases between 15.0cm (0.210) and 10.9cm (0.308). Between 10.9cm and 2.0cm the magnetic coherence versus incoherence ratio decreases to 0.220. The magnetic coherence versus incoherence ratio increases between 2.0cm (0.220) and 0.2cm (0.275). Peak value 0.308 lies within the marker layer.

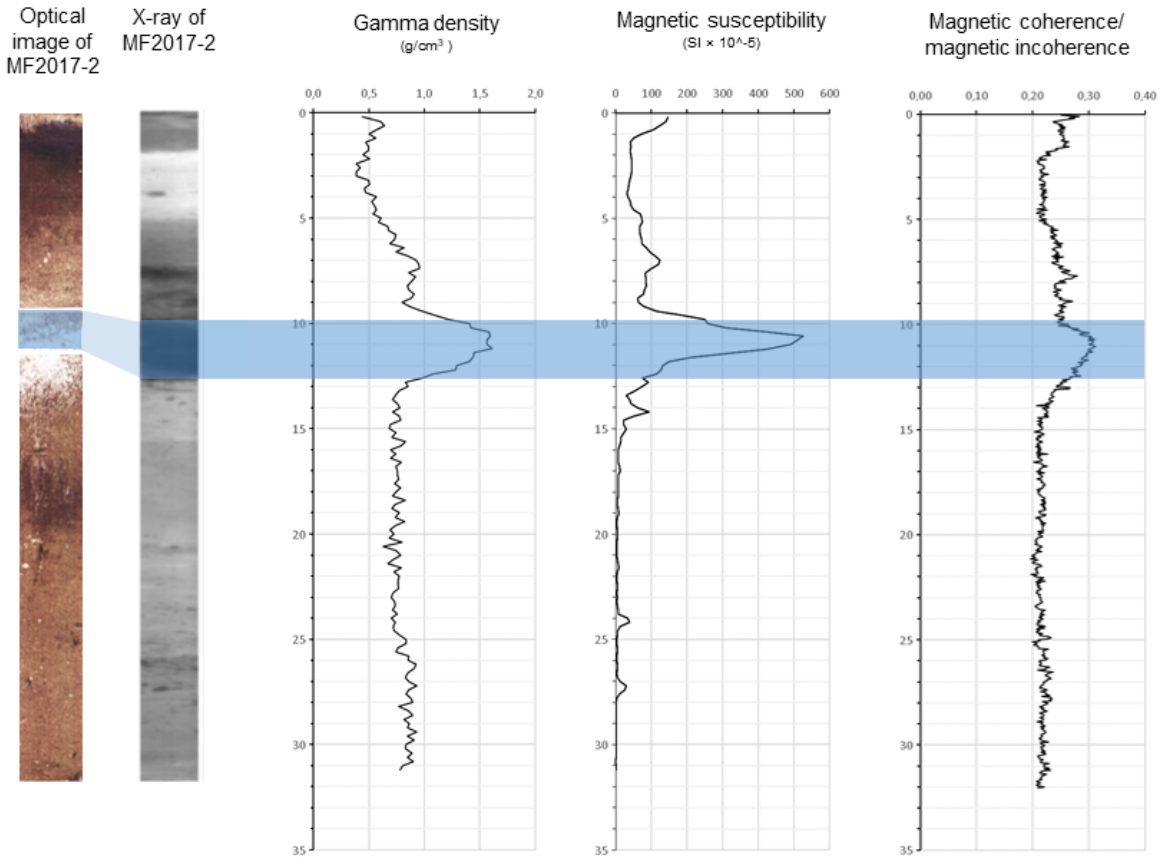

Figure 5.5: Results of geochemical analysis on sediment core MF2017-2 part 1, showing the gamma density, magnetic suceptibility and the magnetic coherence versus incoherence ratio next to an optical image and X-radiograph. The blue, translucent area indicates the position of the marker layer in the sediment after a precise indication by the X-radiograph.

Elemental composition

Figure 5.6 shows the XRF results of a selection of elements. This selection of elements is presented due to the relevance of these elements for further interpretations on mineralogy and the organic matter content. The elemental data is normalized against iron because iron is the most abundant element throughout the sediment record. Figure 5.6 shows the results of the iron analyses framed. Since iron varies, one should consider the iron values when interpreting the element/iron graphs. Iron varies strongest from 15.0cm up to 0.0cm.

Potassium against iron (K/Fe) varies from 0.03 (3% of Fe) to 0.05 (5% of Fe) between 32.0cm and 15.0cm. K/Fe increases between 15.0cm and 12.1cm with a peak value of 0.12 at 12.1cm. Between 12.1cm and 2.4cm values decrease to 0.03. The strongest decrease occurs from 12.1cm to 10.0cm. K/Fe increases between 2.4 cm (0.03) and 0.3 cm (0.06). Elements calcium (Ca) and silicon (Si) show, presented against iron, a similar trend. Si/Fe indicates this trend within a variation of 2% (equal to value 0.02) of the iron present.

Bromine against iron (Br/Fe) varies around 0.045 between 32.0cm and 28.0cm. Br/Fe increases between 28.0cm (0.040) and 21.3cm (0.062). Between 21.3cm and 19.8cm, Br/Fe decreases. Br/Fe increases between 19.8cm (0.048) and 15.6cm (0.063). A decrease to 0.011 at 11.3cm follows. Between 11.3cm and 4.2cm Br/Fe increases to 0.063. Br/Fe decreases between 4.2cm (0.063) and 0.02cm (0.019).

Values of residual sulphur against iron (S/Fe) vary between 0.0005 and 0.0047 throughout the sediment core. In general, the values of S/Fe, i.e. residual sulphur against iron, are higher above the layer of grey coloured sediment compared to below.

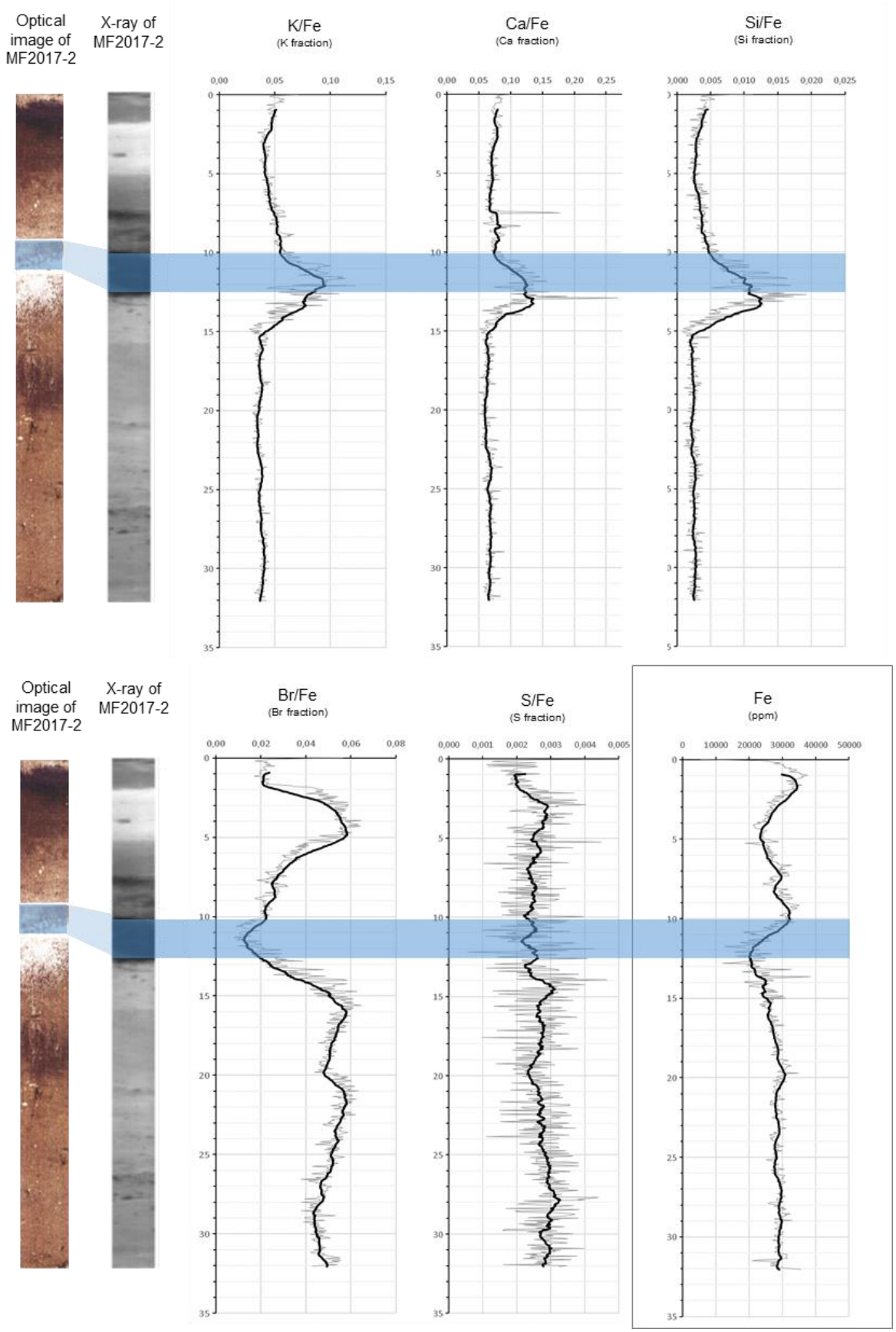

Figure 5.6: Results of geochemical analysis on sediment core MF2017-2 part 2, showing the results of a selection of elements next to an optical image and X-radiograph. The results are presented against iron with an moving average of 20 (equal to 1 cm). The blue, translucent area indicates the position of the marker layer in the sediment after a precise indication by the X-radiograph.

5.5 Pollution analyses

The pollution analyses indicate pollution by Zinc (Zn), several polycyclic aromatic hydrocarbons (PAHs) and Tributyltin (TBT) throughout the Ikjefjord sediment record. Table 5.1 provides the results of all pollutants of which pollution is indicated. The concentrations of the pollutants are expressed in the environmental quality reference classes for marine sediments formulated by the Norwegian Environment Agency. Appendix IVA provides the results of the quantitative determinations. Appendix IVB provides an overview of al results expressed in environmental quality reference classes.

Pollution by three PAHs, i.e. Indeno[1,2,3-cd]pyrene, Dibenzo[a,h]anthracene, Benzo[ghi]perylene, and TBT is indicated in transect 0-2 cm of sediment grab MF2017-2. No pollution is indicated in transect 10-12 cm of sediment grab MF2017-2. Pollution by Zinc (Zn), nine PAHs, i.e. Anthracene, Pyrene, Benzo[a]anthracene, Benzo[b]fluoranthene, Benzo[k]fluoranthene, Benzo[a]pyrene, Indeno[1,2,3-cd]pyrene, Dibenzo[a,h]anthracene, Benzo[ghi]perylene and TBT is indicated in MF2017-3 transect 0-10 cm.

Table 5.1: Results of pollution analyses. The concentrations of various pollutants throughout three transects of the Ikjefjord sediment record expressed in environmental quality reference classes. Reference classes III, IV and V indicate pollution with an increasing severity.

		MF2017-2 0 - 2 cm					MF2017-2 10 - 12 cm					MF2017-3 0 - 10 cm				
		Environmental quality classes for sediment					Environmental quality classes for sediment					Environmental quality classes for sediment				
Name of substance		I	II	III	IV	V	I	II	III	IV	V	I	II	III	IV	V
Zinc (Zn)																
Anthracene	PAH(16)															
Pyrene																
Benzo[a]anthracene																
Benzo[b]fluoranthene																
Benzo[k]fluoranthene																
Benzo[a]pyrene																
Indeno[1,2,3-cd]pyrene																
Dibenzo[a,h]anthracene																
Benzo[ghi]perylene																
Tributyltin																

Grey: Measured value lies below detection limit, value can be within several environmental quality classes

6 Discussion

This chapter provides a discussion on the results of the sediment dating. Furthermore, a comparison is made between the two sediment cores, variation in the particulate mineral and organic matter content is linked to documented environmental change and the results of the pollution analyses are discussed.

6.1 Dating

The dating of sediment indicates higher linear sedimentation rates of 0.47 cm/year in MF2017-1 compared to 0.44 cm/year in MF2017-2 over the past 57 years, i.e. since 1960. These rates sound reasonable compared to sedimentation rates determined in similar settings in other anoxic tributary fjords of the Sognefjord, e.g. the Barsnesfjord (ca. 0.5 cm/year, Paetzel & Dale, 2010).

The relationship between precipitation and grain size (Paetzel & Dale 2010) is generally somewhat biased as small changes in precipitation might already affect a different grain size to become favorably eroded. The riverine flow speed is a factor that influences the grain size distribution during riverine discharge (Hjulström, 1935). Variations in precipitation would thus influence the strength of the riverine discharge and consequently alter the grainsize distribution in the resulting sediment layer. Thus, an independent dating record should be used to confirm the grain size relationship. In this case, the sediment cores have been additionally dated based on the relationship between precipitation and the freshwater diatom content (Koek & van Doorn 2018). Paetzel & Dale (2010) established this method together with the grainsize versus precipitation relationship in the Barsnesfjord and Sogndalsfjord, Western Norway.

It should be noted, that a radiometric dating method (^{210}Pb, ^{137}Cs, or similar) could be used with advantage to confirm this parameter relationship dating. However, sediments first need to settle over a significant amount of time (+/- 1.5 years) after their retrieval, before these methods can be applied. The grainsize versus precipitation dating, as well as the freshwater diatom versus precipitation dating are a valid first approach to estimate time lines of sedimentation in Western Norwegian fjord sediments (Paetzel & Dale 2010).

Both sediment cores contain a layer of grey colored sediments that started to deposit at some time after 1980. Sediment core MF2017-2 contains a second layer of grey colored sediments in top segment between 0.5 and 0.0 cm. This segment was deposited close to 2017.

6.2 Comparison of the core records

In general, sediment parameters show an overall changing pattern in both cores above the marker layer, i.e. after 1980. In general, core MF2017-2 shows stronger variations and signals than core MF2017-1. This observation can be explained by the counter-clockwise moving surface currents in the Ikjefjord. This flow is the result of the deflection from water masses to the right of the wind direction in the northern hemisphere as described by Ekman (1905). Therefore, the river discharge originating from the Storelva and Snjogilet (Figure 6.1) would mainly follow the counter-

clockwise moving direction of the surface water current, influencing mostly the sediments of location MF2017-2. Furthermore, the suspended matter originating from the Øystrebøelva would have to travel against this counter-clockwise moving direction of the surface water current (Figure 6.1). The water discharge from the Øystrebøelva would gradually be forced from a westward moving direction into the northward moving direction of this surface current. Some of the suspended matter originating from the Øystrebøelva might thus deposit at the closer location of MF2017-2 before it is bended and transported northward (Figure 6.1). Only little of this suspended matter would reach the more central location of core MF2017-1 (Figure 6.1).

If this is correct, one would expect higher sedimentation rates at the shallow location MF2017-2 compared to the deeper location MF2017-1. This is not the case, as mainly the coarser sediment fraction coming from the Øystrebøelva might settle at MF2017-2 while the finer and the organic fraction is transported northward with the counter-clockwise moving water current. On the other hand, suspended matter reaching the calmer central part of the Inner Ikjefjord basin would be able to settle at location MF2017-1, leading to enhanced sedimentation rates.

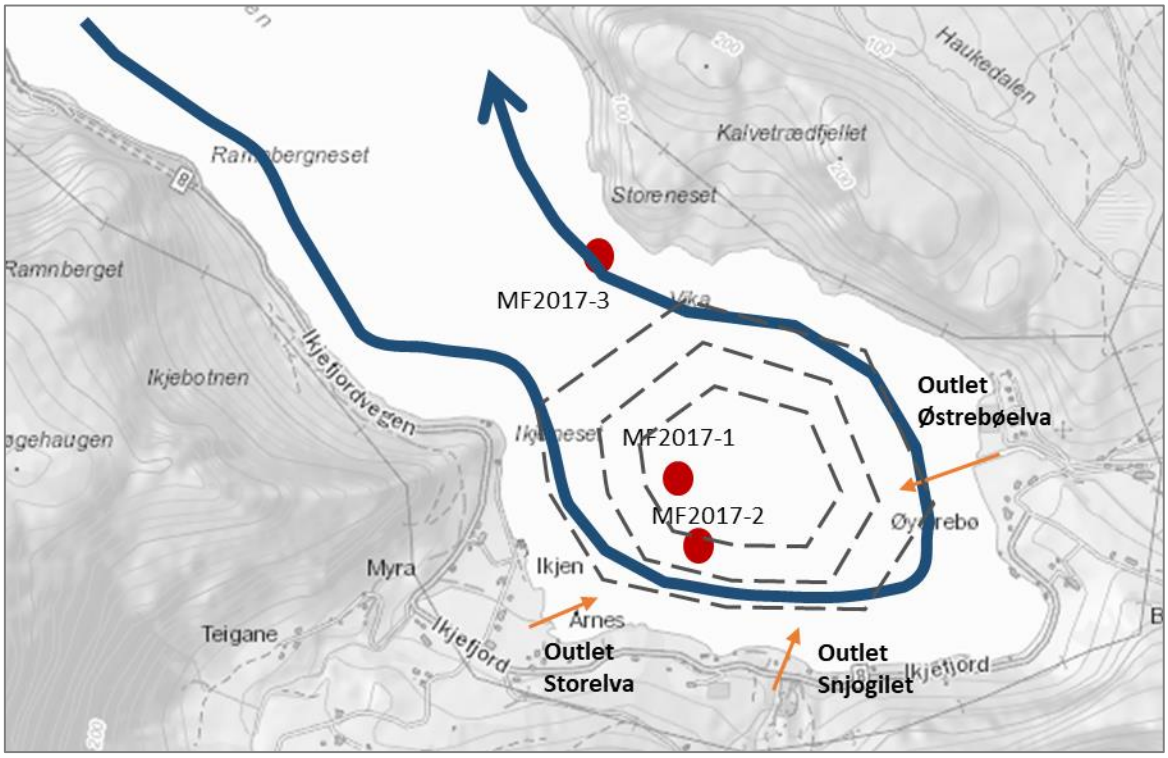

Figure 6.1: Surface current of the Ikjefjord, indicating sample locations (red dots) and river outlets (orange arrows). Background map: Norges vassdrags- og energidirektorat (2018b).

6.3 Relating variation in the particulate mineral and organic matter content to documented environmental change

The major changes in the sediments can be recognized in MF2017-1 and 2017-2, although they are more pronounced in MF2017-2, of the reasons mentioned above. In addition, the geochemical record only exists of core MF2017-2. Thus, interpretation of environmental change will mostly be illustrated using the results of core MF2017-2.

According to the dating, the deposition of the marker layer occurred around the middle of the 1980s. This fits well with the overflow event in the Øystrebøelva of 1983 that coloured the fjord water white for several days according to Massnes (2017, *personal communication*). With this time marker, the sediment deposition can be divided in the time before and after this event, i.e. before and after 1983. Particularly, the time after 1983 is of interest, as Massnes (2017, *personal communication*) states that the river valley of the Øystrebøelva was secured with the elevation of the riverbanks after the 1983 event. The artificial elevation of the riverbanks is also visible in aerial pictures of the area from 1973 and 1992; see Figure 6.2 for a comparison of these photographs.

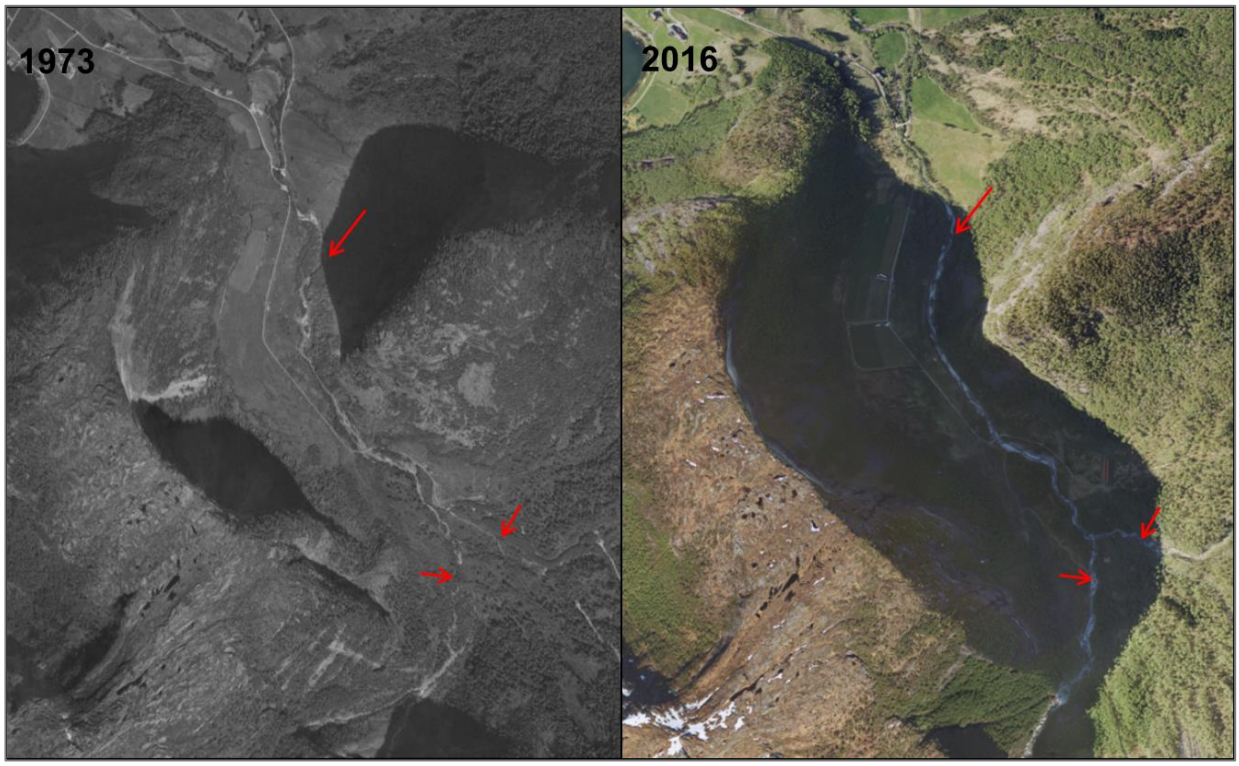

Figure 6.2: Areal pictures of the Øystrebøelva before the elevation of the riverbanks in 1973 (left picture) and after the elevation of the riverbanks in 2016 (right picture) (NorgeiBilder, 2018), red arrows indicate main chainges.

The evolution of the particulate mineral matter

Figure 6.3 illustrates a higher magnetic susceptibility and higher Si/Fe ratios after the event of 1983. This might indicate that the mineral matter had a different mineral composition, and thus a different source. This sounds reasonable as the material used for the elevation of the river banks most likely originated from elsewhere (Massnes 2017, *personal communication*). The change in source material could also be confirmed by a similar development of the K/Fe and Ca/Fe ratios (Figure 5.6), indicating different feldspar compositions.

The mineral matter curve seems to gradually decrease after 1983, allowing the conclusion that the river discharge is tending towards a new equilibrium, where gradually less of the rock material and rock dust from the building activity enters the fjord. Both the grainsizes and the mineral matter seem gradually to go back to the conditions before the 1983 event during the later years, although the source material seems to have changed. Similar discharge and recovery from river building activity has been observed in the Aurlandsfjord sediments due to the rebuilding of the river banks after the century flood of 2014 (Bortheim Mulelid et al., 2017; Midttømme et al., 2017).

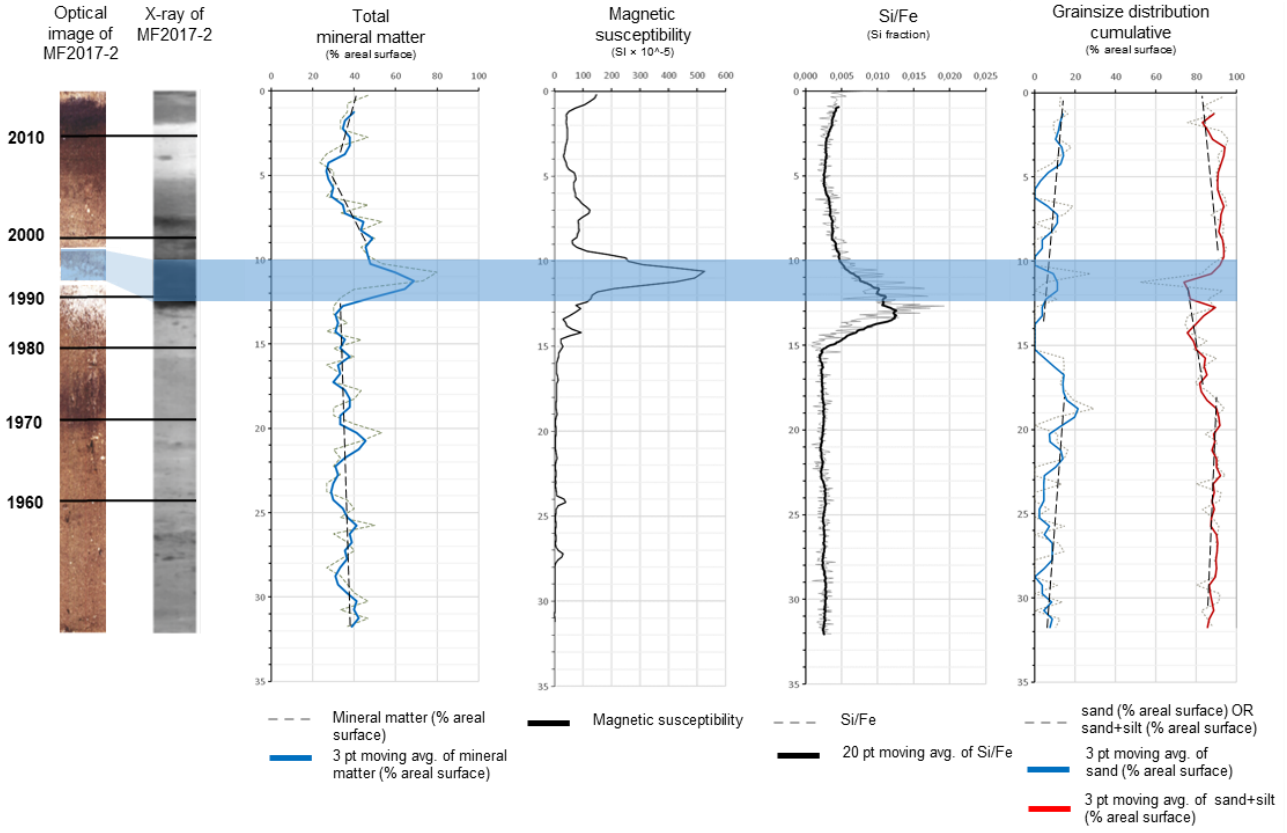

Figure 6.3: Summary of the results of particulate mineral matter parameters besides the dating. The blue, translucent box indicates the marker layer as shown by the X-radiograph.

The evolution of the particulate organic matter

Figure 6.4 illustrates that the terrestrial organic matter level decreases after 1983. This might indicate that the artificial elevation of the Øystrebøelva riverbank caused a temporarily lower presence of vegetation along the Øystrebøelva. During later years the terrestrial organic matter increases, a new equilibrium of the terrestrial organic matter discharge might be formed after ecological succession.

Bromine (Br) is an indicator of the organic matter content in sediments (Croudace et al, 2006). Both the organic matter fraction and the Br/Fe ratios develop after 1983 and go gradually back to the pre-1983 levels afterwards. Br/Fe indicates lower values across the upper 2cm of MF2017-2, suggesting either a new, recent event or decreasing supply of organic matter. This issue cannot be solved in this thesis due to the little amount of sediment material and thus little information.

Sediments contain less residual sulphur after 1983, meaning that more sulphur was bound to gasses like H_2S (Jørgensen, 1977). This suggests a higher degree of anoxia after 1983. The increasing anoxia is not confirmed by a parallel increase of the marine organic fraction (Figure 6.4), as would be expected (Syvitski et al., 1987). Similar changes have been observed in anoxic sediments of the Nærøyfjord, a more eastward located tributary fjord along the Sognefjord (Dybo et al., 2016). A possible explanation might be the overall oxygen decrease in the bottom waters of the Sognefjord since the 1960s/1970s (Dale 2017, *personal communication*). The issue of decreasing oxygen concentrations is in more detail discussed for the Inner Ikjefjord by Koek & Van Doorn (2018).

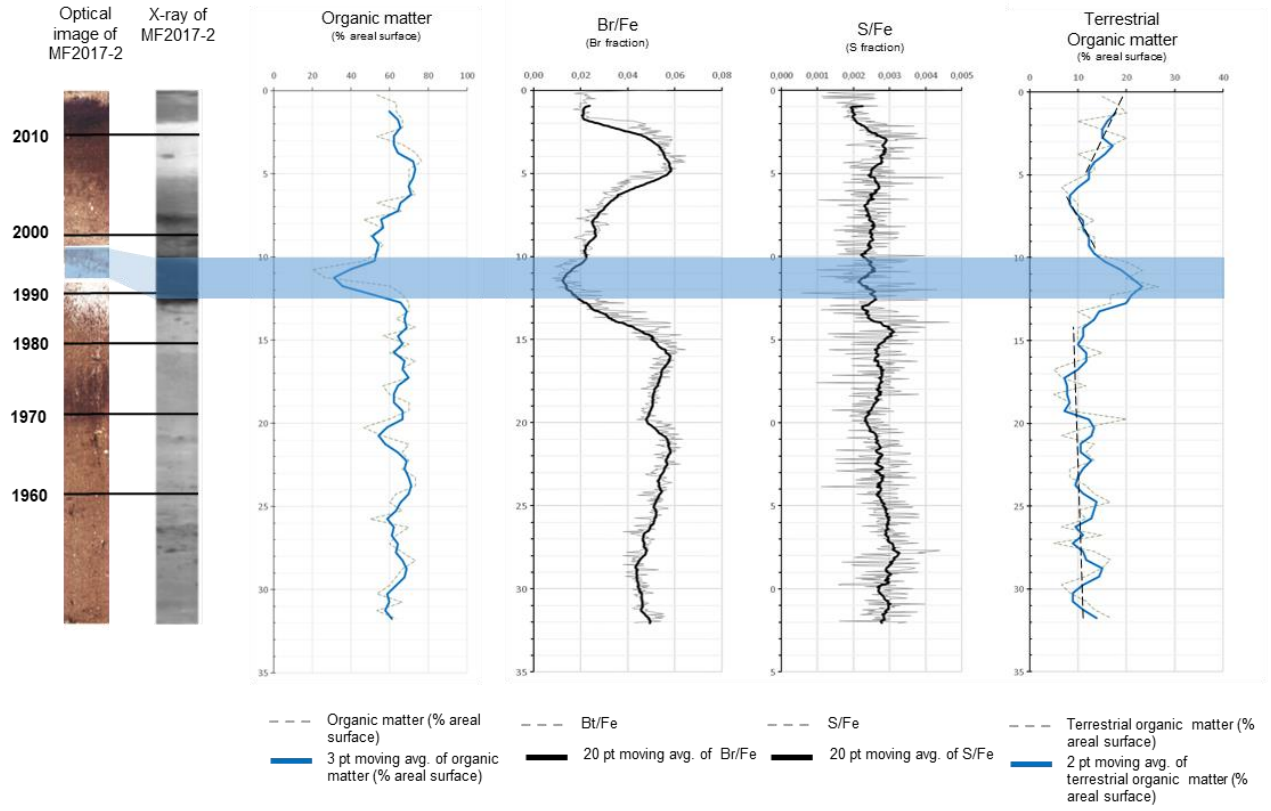

Figure 6.4: Summary of the results of particulate organic matter parameters besides the dating. The blue, translucent box indicates the marker layer as shown by the X-radiograph.

6.4 Pollution

Pollution by Zinc (Zn), Tributyltin (TBT) and several polycyclic aromatic hydrocarbons (PAHs) is indicated in sediments that started to deposit in 1997.

Zinc

Car traffic is a potential source of the indicated pollution by zinc. Bækken (1993) states that the extensive use of spikes on car winter tires damages the road surface considerable. This might release zinc and other environmental hazardous compounds.

Pollution by Zinc is not indicated in sediments of MF2017-2 grab sample segment 10-12 cm. These sediments were deposited around 1995. A plausible explanation could be the fact that the marker layer in sediment core MF2017-2 occurs exactly at the same position of 10-12 cm sediment depth as the non-polluted sediment. Pollution in fjord sediment is often adsorbed to smaller grainsizes (fine silt and clay) and organic matter (Salomons et al., 1988). Both fractions are low during the deposition of the marker layer, suggesting that polluting material would be captured less in the sediment during the time of the deposition of the marker layer. MF2017-3 suggests that the pollution also occurs in the deeper sediment layers.

Tributyltin

The only known potential source of Tributyltin in the Ikjefjord is boat traffic on the Sognefjord and Ikjefjord. Tributyltin was used in anti-fouling paints on ships between the 1960s and 2003. There is a total ban on ships with an antifouling layer containing TBT in Norwegian waters since 2008 (The European Maritime Safety Agency, 2017).

Pollution by TBT has been indicated in sediments deposited over the previous 5 years (MF2017-2 segment 0-2 cm). The occurrence of TBT in sediments deposited more than 4 years after the ban of ships with an anti-fouling layer that contains accessible TBT from the waters of all member states of the United Nations in 2008 can be explained by long retention times of TBT in the water column of the Sognefjord and the Ikjefjord before sedimentation.

TBT was most likely not indicted in MF2017-2 grab sample segment 10-12 cm due to the low fractions of organic matter and small grainsizes, as described above.

Polycyclic aromatic hydrocarbons

Pollution by PAHs Anthracene, Pyrene, Benzo[a]anthracene, Benzo[b]fluoranthene, Benzo[k]fluoranthene, Benzo[a]pyrene, Indeno[1,2,3-cd]pyrene, Dibenzo[a,h]anthracene and Benzo[ghi]perylene is indicated in sediments that started to deposit in 1997.

The oil refinery of Statoil Refining ASA at Mongstad, located 72km to the South-West of the Ikjefjord, went into operation in 1975. Any PAHs released from this facility can travel towards the Ikjefjord by means of wind and end up in the Ikjefjord by either water exchange with adjacent waterbodies, such as the Sognefjord, or by direct atmospheric deposition. Other potential sources of the indicated PAHs are car traffic and boat traffic due to incomplete combustion of fossil fuels. Car traffic is in addition a potential source of the indicated PAHs due the extensive use of spikes on car winter tires (Bækken, 1993).

Pollution by PAHs was most likely not indicted in MF2017-2 grab sample segment 10-12 cm due to the low fractions of organic matter and small grainsizes, as described above.

7 Conclusion

Ikjefjord sediments have been dated based on a sand-precipitation relationship suggesting that the sediments of the two sediment cores deposited with a linear sedimentation rate of 0,47 cm/year and 0,44 cm/year since 1960.

The main changing pattern of the particulate mineral matter fraction occurs after 1980. The variations are more pronounced in sediments deposited at the transition where the outflowing water from the Øystrebøelva meets the counter-clockwise moving waters of the Ikjefjord surface water current. The signals are less pronounced in the calmer central part of the Ikjefjord.

The changing pattern in sedimentation after 1980 is related to the overflow event in the river Øystrebøelva of 1983. Differences in the particulate matter content of sediments deposited before 1983 compared to sediments deposited after 1983 is presumably related to the riverbank elevation of the Øystrebøelva shortly after the overflow event of 1983.

Pollution by Zinc (Zn), Tributyltin (TBT) and several polycyclic aromatic hydrocarbons (PAHs) is indicated in surface sediments down to 10cm sediment depth. Further research is required to conclude about the occurrence of pollution in deeper sediments deposited.

Boat traffic on the Sognefjord and the Ikjefjord between the 1960s and 2008 is assumed the plausible general source of pollution by TBT. Pollution by zinc might relate to the release of road dust as a consequence of the extensive use of spikes on car winter tires on the Norwegian road surface. Potential sources of pollution by PAHs are the oil refinery of Statoil refining ASA at Mongstad, car traffic and boat traffic.

Final concluding remark

The Sogn og Fjordane River Basin District states that due to the lack of data about the ecological and chemical state of the Ikjefjord, there is a risk that the environmental goals of the EU Water Framework Directive will not be reached before the deadline of 2021 (Norges vassdrags- og energidirektorat, 2018a). This thesis has provided data on the chemical state of the Ikjefjord, based on sediment analyses. This data indicates that the pollution state of the Ikjefjord is more alarming than previously argued, and thus brings up the risk that environmental goals might not be reached before 2021.

Similar conditions might occur in other tributary fjords of the Sognefjord, leaving a challenge for the regional environmental authorities of the County Governor (Fylkesmannen i Sogn og Fjordane).

8 Reference list

Bianco, G., Novario, G., Bochicchio, D., Anzilotta, G., Palma, A., & Cataldi, T. R. (2008, August). Polychlorinated biphenyls in contaminated soil samples evaluated by HC-ECD with dual-column and GC-HRMS. *Chemosphere, 73*(1), 104-112.

BKK AS. (2017 , August). Water level and overflow data of Stølsvatnet.

BKK AS. (2018 , January 25). *Matre river systems and the adjacent river systems*. Retrieved from www.bkk.no: https://www.bkk.no/en/hydropower/matre-river-systems

Bortheim Mulelid, O. S., Olaisen , V., & Strømme, k. (2017). *Avsetinger fra historiske hendelser i Indre Aurlandsfjord, Vest-Norge, over de siste 40 år. Del II. De geokjemiske signalene.* Western Norway University of Applied Sciences, Sogndal.

Bækken, T. (1993). *Miljøvirkninger av vegtrafikkens asfalt og dekkslitasje.* The Nowegian Institute for Water Research (NIVA).

Croudace, I. W., Rindby, A., & Rothwell, R. G. (2006). ITRAX: description and evaluation of a new multi-function X-ray core scanner. *New Techniques in Sediment core Analysis*, 51-63.

Dale, T. (2017, August-December). Personal communication. (M. van Rossum, Interviewer)

Dearing , J. (1999). *Environmental Magnetic Susceptibility, Using the Bartington MS2 system.* Kenilworth, England: Chi publishing.

Department of Earth Science UiB. (2017). *2017_English version_Laboratory _methods.* Bergen.

Dybo, M. H., Sundheim, A. L., & Søgnesand, A. M. (2016). *Analyse av resente sedimentkjerner i den anoksiske Nærøyfjorden, Vest-Norge.* Western Norway University of Applied Sciences, Sogndal.

Ekman, V. W. (1905, May 10). On the Influence of the Earth`s Rotation on Ocean-Currents. *Arkiv för Mathematik, Astronomi och Fysik, 2*(11), 1-53.

Ese, K. (2005). *Sørsidevegen i Høyanger*. Retrieved February 12, 2018, from https://www.fylkesarkivet.no/: https://leksikon.fylkesarkivet.no/article/22ab0919-95d0-491c-b25c-721ac961bcfa/

Evans, H. B. (1965). GRAPE - a device for continious determination of material density and porosity. *Society of professionall well log analysts, logging 6th annual symposium.* Dallas, Texas.

Haflidason, H. (2017, November 23). Personal communication. (M. van Rossum, Interviewer) Bergen.

Hjulström, F. (1935). Studies of the morphological activity of rivers as illustrated by the River Fyris. *Bulletin of the Geological Institute of Uppsala*(25), 221-527.

Howe, J. A., Austin, W. E., Forwick, M., Paetzel, M., Harland, R., & Cage, A. G. (2010). Fjord systems and archives: a review. *Fjord systems and Archives*, 5-15.

Inall, M. E., & Gillebrand, P. A. (2010). The physics of mid-latitude fjords: a review. *Fjord Systems and Archives. Geological Society, London, Special Publications, 344*, 16-33.

Institute of Marine Research . (2014, April 25). Fjords - water exchange and currents. Retrieved May 18, 2018, from https://www.imr.no/temasider/kyst_og_fjord/fjorder_vannutskiftning_og_strom/en

International Organization for Standardization. (2006, January). *ISO 18287:2006*. Retrieved April 30, 2018, from www.iso.org: https://www.iso.org/standard/33387.html

International Organization for Standardization. (2016, July). *ISO 17294-2:2016*. Retrieved April 30, 2018, from www.iso.org: https://www.iso.org/standard/62962.html

Jørgensen , B. B. (1977). The sulfur cycle of a coastal marine sediment (Limfjorden, Denmark). *Limnology and Oceanography, 5*(22), 814-832.

Kartverket. (2018, January 25). *Ikjefjordsbrua*. Retrieved from http://www.seeiendom.no/: http://www.seeiendom.no/

Koek, A., & van Doorn, M. (2018). *Investigating environmental change in the micro-organism distribution of anoxic Ikjefjord sediments since the 1960s, Western Norway.* Western Norway University of Applied Sciences, Sogndal.

Kvernheim, A. L., Brevik, M. E., Næs, K., Oug, E., Klungsøyr, J., Knutzen, J., . . . Goksøyr, A. (1992). *Organochlorines and PAHs in the marine environment: State of the art and research needs.* Oslo: Royal Norwegian Council for Scientific and Industrial Research.

Langeng, T., & Slinning, A. (2018). *A 400 year historical sediment record from the Fjærlandsfjord, Western Norway.* Western Norway University of Applied Sciences, Sogndal.

Lovelock, J. E. (1958). A sensitive detector for gas chromatography. *Journal of Chromatography*, 35-46.

Massnes, A. (2017, August 29). Personal communication. (M. van Rossum, Interviewer)

Meskanen, E. (2017). *Ikjefjord sampling August 2017.* Ikjefjord, Høyanger.

Midttømme, M., Thiem, E. R., & Haga, O. N. (2017). *Avsetninger fra historiske hendelser i Indre Aurlandsfjord, Vest-Norge, over de siste 40 år. Del I. De sedimentologiske signalene.* Western Norway University of Applied Sciences, Sogndal.

Miljødirektoratet. (2016). *Grenseverdier for klassifisering av vann, sediment og biota.* Trondheim: Miljødirektoratet.

Munsell®. (1994). *Soil color charts* (Revised Edition ed.). New York: GretagMacbeth.

Nesse, W. D. (2012). *Introduction to mineralogy* (second edition ed.). New York: Oxford University Press.

Niemistö, L. (1974). A gravity corer for studies of soft sediments. *Merentutkimuslait. Julk/Havforskningsinstituttets Skrifter 238*, 33-38.

NorgeiBilder. (n.d.). Retrieved May 20, 2018, from http://norgeibilder.no/

Norges geologiske undersøkelse. (2018, May 10). *Berggrunn N250.* Retrieved from http://www.ngu.no/: http://geo.ngu.no/kart/minkommune/?kommunenr=1416

Norges vassdrags- og energidirektorat. (2018a, January 16). *Ikjefjorden*. Retrieved from vann-nett.no: https://vann-nett.no/portal/#/waterbody/0280020300-C

Norges vassdrags- og energidirektorat. (2018b, January 24). *Sognefjorden*. Retrieved from www.vann-nett.no: https://vann-nett.no/portal/#/waterbody/0280020100-1-C

Norwegian Meteorological Institute. (2018a). *eKlima*. Retrieved from www.sharki.oslo.dnmi.no: http://sharki.oslo.dnmi.no/portal/page?_pageid=73,39035,73_39049&_dad=portal&_schema=PORTAL

Norwegian Meteorological Institute. (2018b). *Stations with Kml*. Retrieved May 8, 2018, from http://eklima.met.no: http://eklima.met.no/Help/Stations/toDay/all/en_stations.html

Norwegian Ministry of Climate and Environment. (2014). *Norway's Sixth National Communication under the Framework Convention on Climate Change.*

Paetzel, M. (2017a, October 18). Results of echosounder measurements.

Paetzel, M. (2017b). *Flood protection Øystrebøelva.* Ikjefjord.

Paetzel, M., & Dale, T. (2010). Climate proxies for recent fjord sediments in the inner Sognefjord region, western Norway. *Fjord Systems and Archives*, 271-288.

Paetzel, M., & Schrader, H. (1995). Sewage history in the anoxic sediments of the fjord Nordåsvannet, Western Norway: (2) the sources of the sedimented organic matter fraction. *Norsk Geologisk Tidsskrift*, 146-155.

PS Analytical. (2015). *Atomic fluorescence spectrometry (AFS).* Retrieved May 1, 2018, from www.psanalytical.com: https://www.psanalytical.com/information/afs.html

Puşcaş, C. M., Stremțan, C. C., & Kristály, F. (2010). Hjulström diagram with dashed line showing the flow velocity calculated in ScallopEx. *Past surface conditions and speleogenesis as inferred from cave sediments in the Great Cave of Salitrari Mountain (SW Romania).* Universitatis Babeş-Bolyai.

Rothwell, R. G. (1989). *Minerals and mineraloids in marine sediments - An optical identification guide.* Elsevier Science Publishers Ltd.

Salomons, W., Bayne, B. L., Duursma, E. K., & Förstner, U. (1988). *Pollution on the North Sea - An assessment.* New York: Springer verlag.

Smol, J. P. (1992). Paleolimnology: an important tool for effective ecosystem management. *Journal of Aquatic Ecosystem Health*, 49-58.

Solbakken, R., Henriksen, K., Reitan, K. I., Arff, J., Ellingsen, I. H., Hindar, K., . . . Johnsen, B. O. (2011). *Innsamling og sammenstilling av relevant kunnskap om Sognefjorden.* Trondheim.

Standards Norway. (2008, May 1). *NS-EN ISO 17852:2008.* Retrieved April 30, 2018, from www.standard.no: https://www.standard.no/no/Nettbutikk/produktkatalogen/Produktpresentasjon/?ProductID=330060

Standards Norway. (2012, November 1). *NS-EN 16167:2012*. Retrieved April 30, 2018, from www.standard.no: http://www.standard.no/no/Nettbutikk/produktkatalogen/Produktpresentasjon/?ProductID=595838

Statoil ASA. (2018a, January 30). *How to find us in Norway*. Retrieved from www.statoil.com: https://www.statoil.com/en/where-we-are/norway/how-to-find-us-in-norway.html

Statoil ASA. (2018b, January 30). *Mongstad production facility*. Retrieved from www.statoil.com: https://www.statoil.com/en/what-we-do/terminals-and-refineries.html#

Stauffer, E., Dolan, J. A., & Newman, R. (2008). *Fire Debris Analysis.* Elsevier Inc.

Syvitski, J. P., Burell, D. C., & Skei, J. M. (1987). *Fjords Processes and Products.* New York: Springer-Verlag.

The European Maritime Safety Agency. (2017). *Anti-Fouling Systems*. Retrieved from www.emsa.europa.eu: http://www.emsa.europa.eu/implementation-tasks/environment/anti-fouling-systems.html

Van Veen, J. (1933, July 7). Onderzoek naar het zandtransport van rivieren. *De Ingenieur B. Bouw- en waterbouwkunde 11, 48*(27), 151-159.

Vannportalen. (2015a, January 17). *Vassområde*. Retrieved from www.vannportalen.no: http://www.vannportalen.no/vannregioner/sogn--og-fjordane/vassomrade/

Vannportalen. (2015b). *Klassifisering av miljøtilstand i vann.* Trondheim.

Weiss, P., & Foëx, G. (1926). Le magnétisme. *Librairie Armand Collin, Section de physique*, 215.

Wiley-VHC. (1998). *Inductively Coupled Plasma Mass Spectrometry edited by Akbar Montaser.* Washington.

Appendices

Appendix I: Method descriptions

- A: Equipment for sample retrievement
- B: Microscope picture and result smear slide analysis

Appendix II: Results smear slide analyses of particulate matter

- A: Sediment core MF2017-1
- B: Sediment core MF2017-2

Appendix III: Results geochemical analyses of particulate matter

- A: The magnetic coherence versus incoherence ratio, magnetic susceptibility, gamma density
- B: Elemental composition

Appendix IV: Results of pollution analyses

- A: Quantitative determinations
- B: Quantitative determinations expressed in environmental quality reference classes

Appendix I: Method descriptions

A: Equipment for sediment retrievement

Figure Ia: Niemistö (1974) Gravity Corer (Meskanen, 2017)

Figure Ib: Van Veen Grab sampler (Meskanen, 2017)

B: Microscope picture and result smear slide analysis

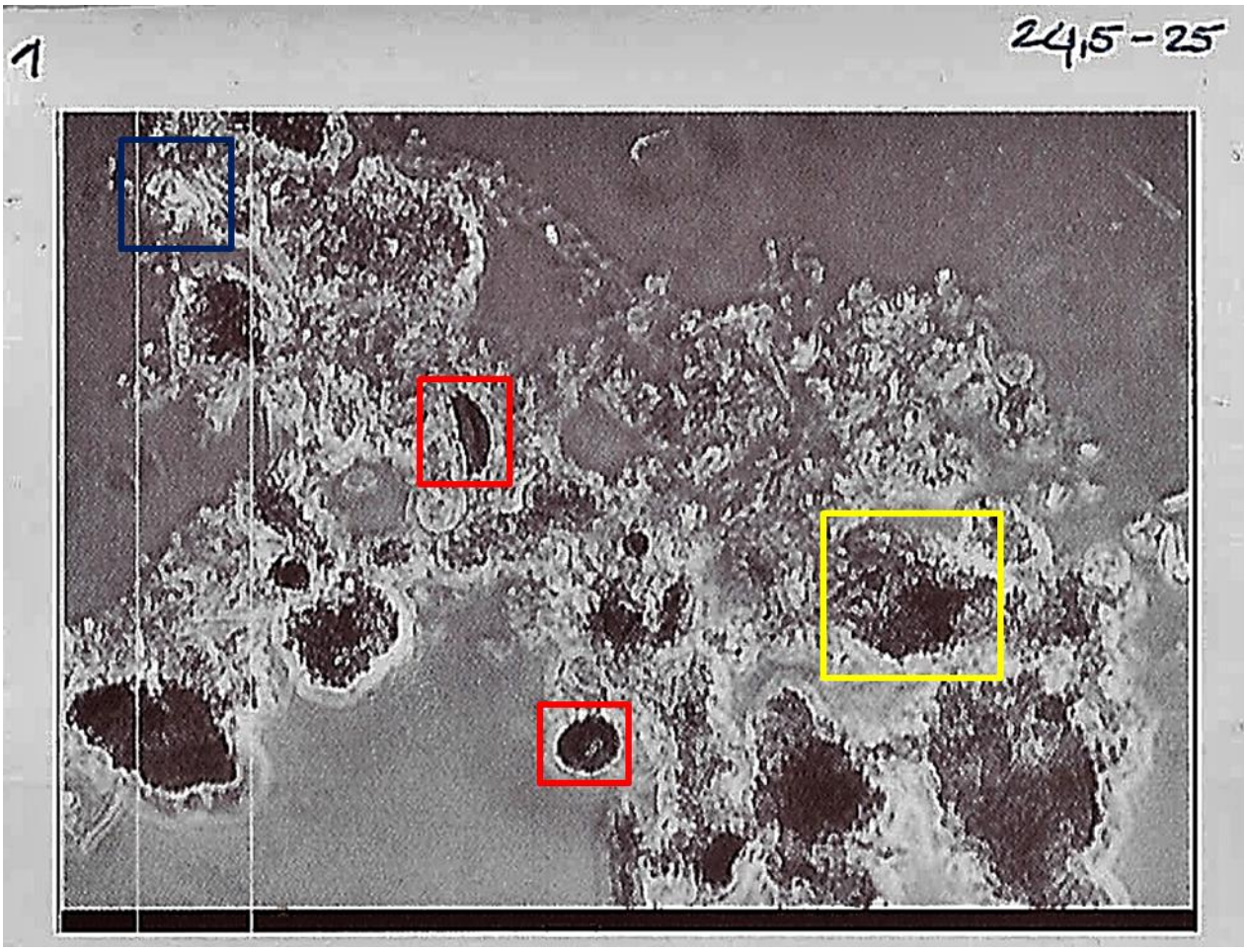

Figure Ic: Microscope view (bright-field microscopy) of sediment core MF2017-2 segment 24-24.5 cm area 3, showing mineral matter (in blue square), terrestrial organic matter (in the red square) and marine organic matter (in the yellow square).

Table Id: Raw data of the smear slide analysis, i.e the percentage distribution of mineral matter versus organic matter (in blue), the percentage distribution of terrestrial organic matter versus marine organic matter (in green), and the ratio of mineral grainsizes (in orange), performed on sediment core MF2017-2 segment 24 – 24.5 cm area 3

Slide	Area	min : org	ter : mar	Sand	Course silt	Medium silt	Fine silt	Very fine silt	Clay
24 – 24.5	3	30 : 70	20 : 80	0	0	0	1	2	2

Appendix II: Results smear slide analyses of particulate matter

A: Sediment core MF2017-1

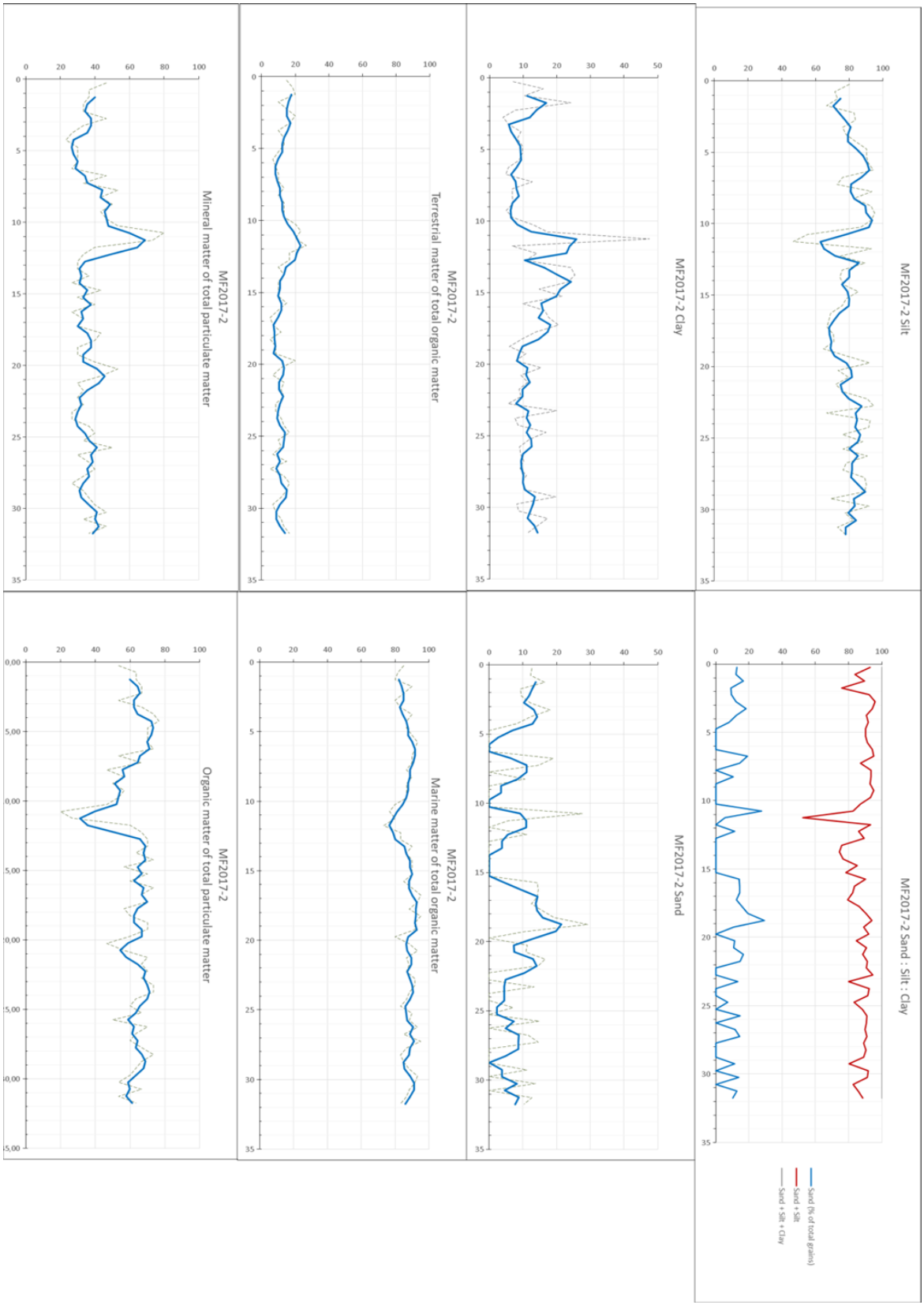

B: Sediment core MF2017-2

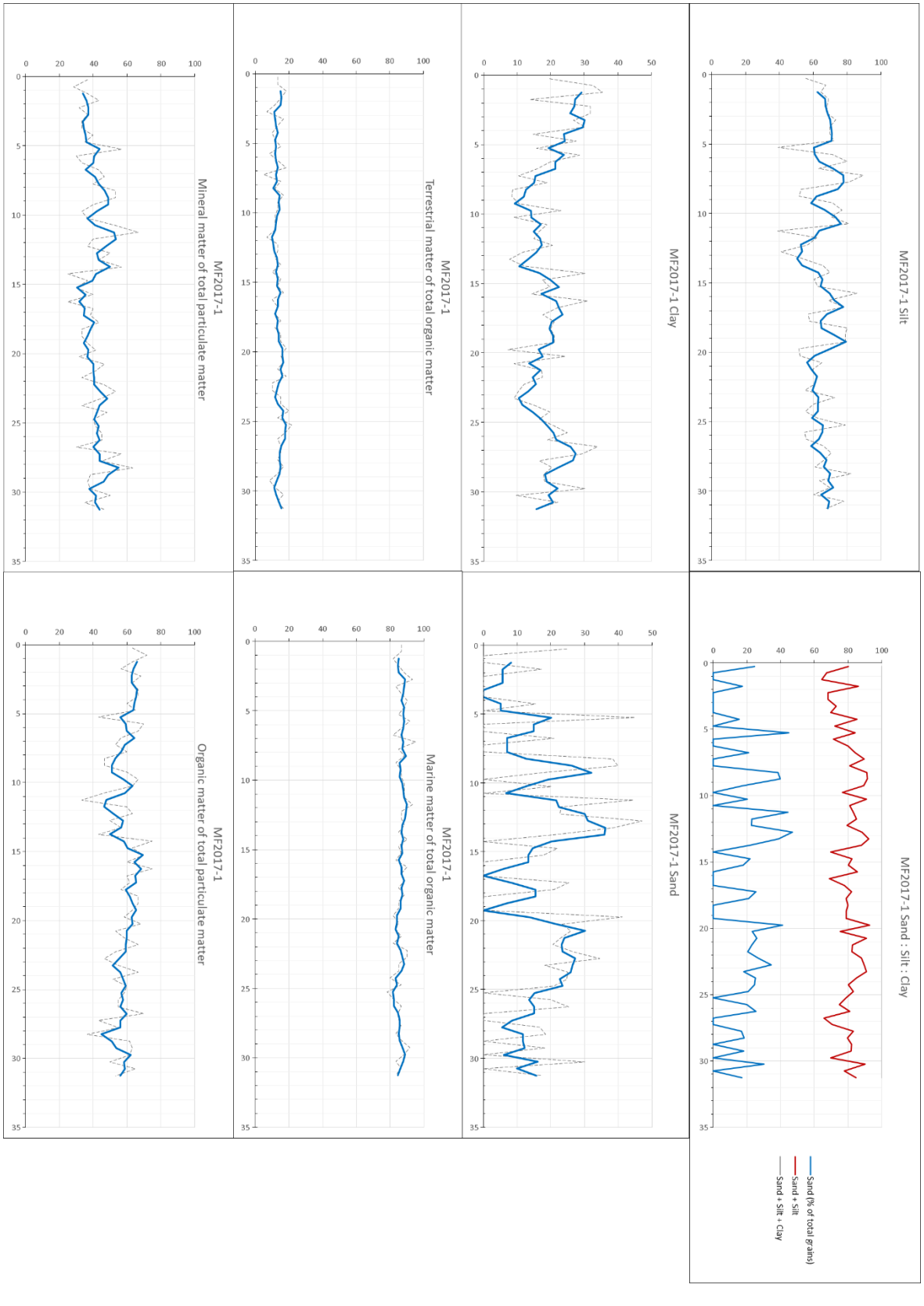

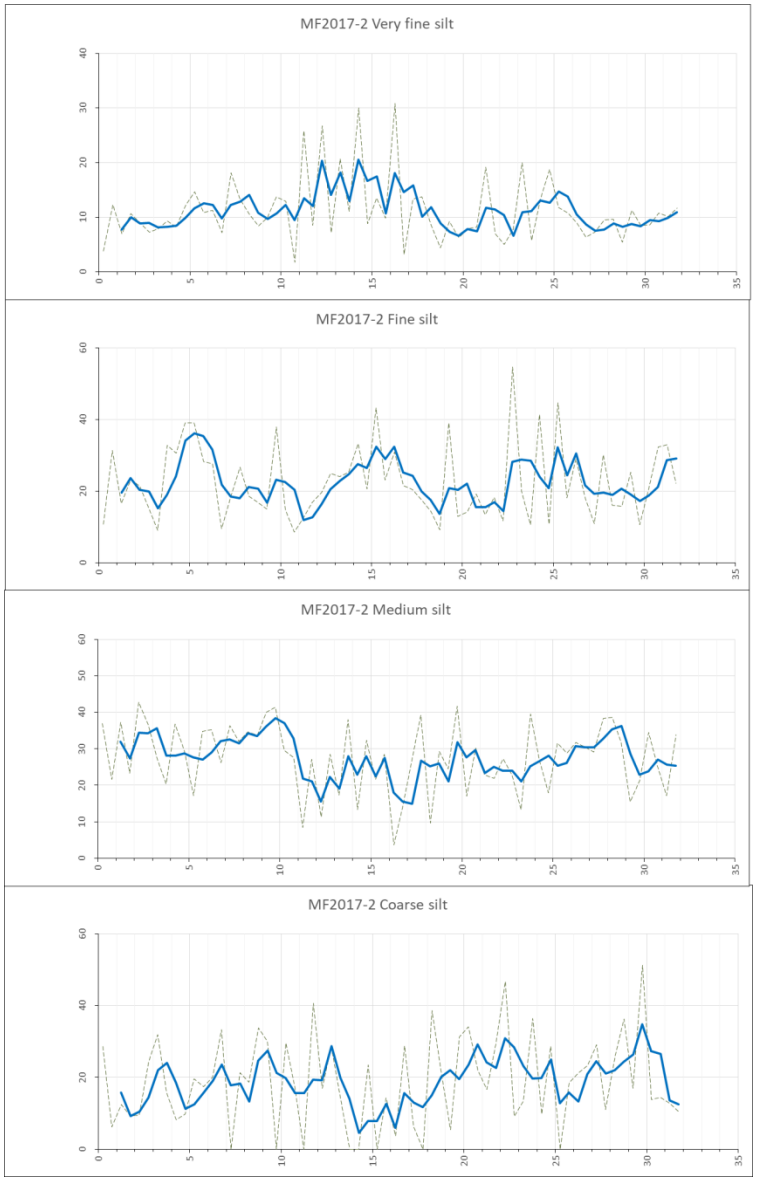
MF2017-2 Very fine silt
MF2017-2 Fine silt
MF2017-2 Medium silt
MF2017-2 Coarse silt

Appendix III: Geochemical analyses of particulate matter

A: Magnetic coherence versus incoherence ratio, magnetic susceptibility, gamma density

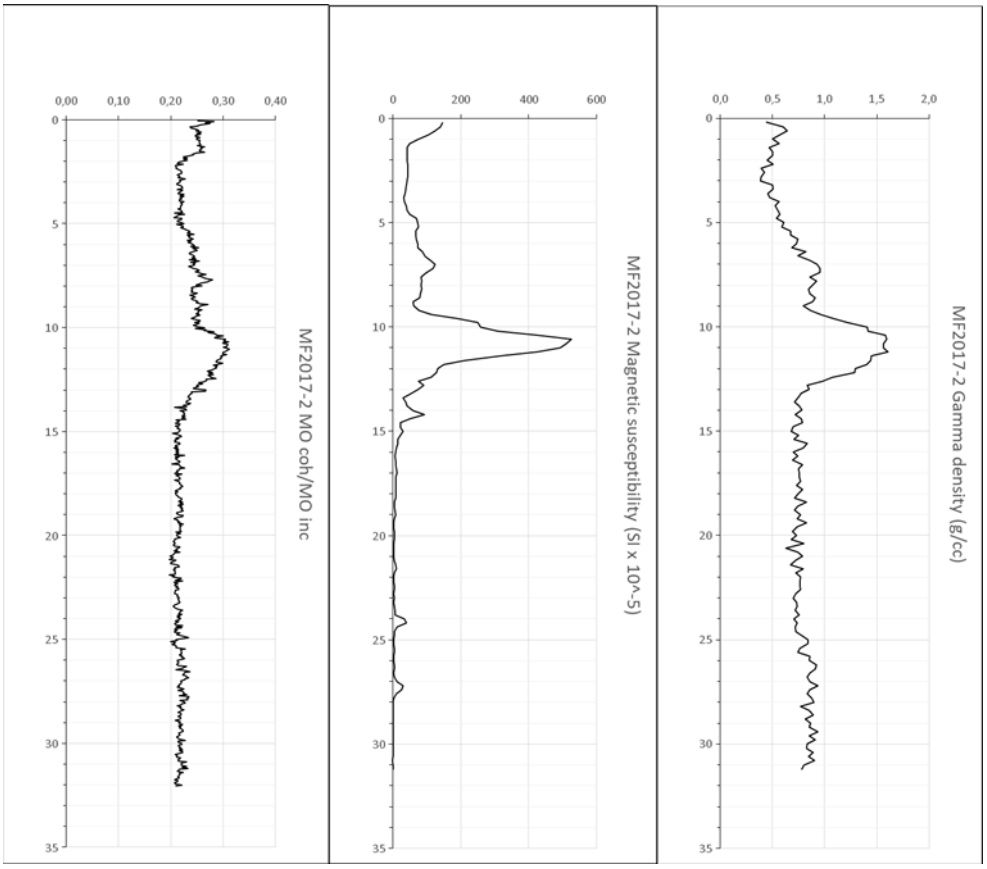

B: Elemental composition

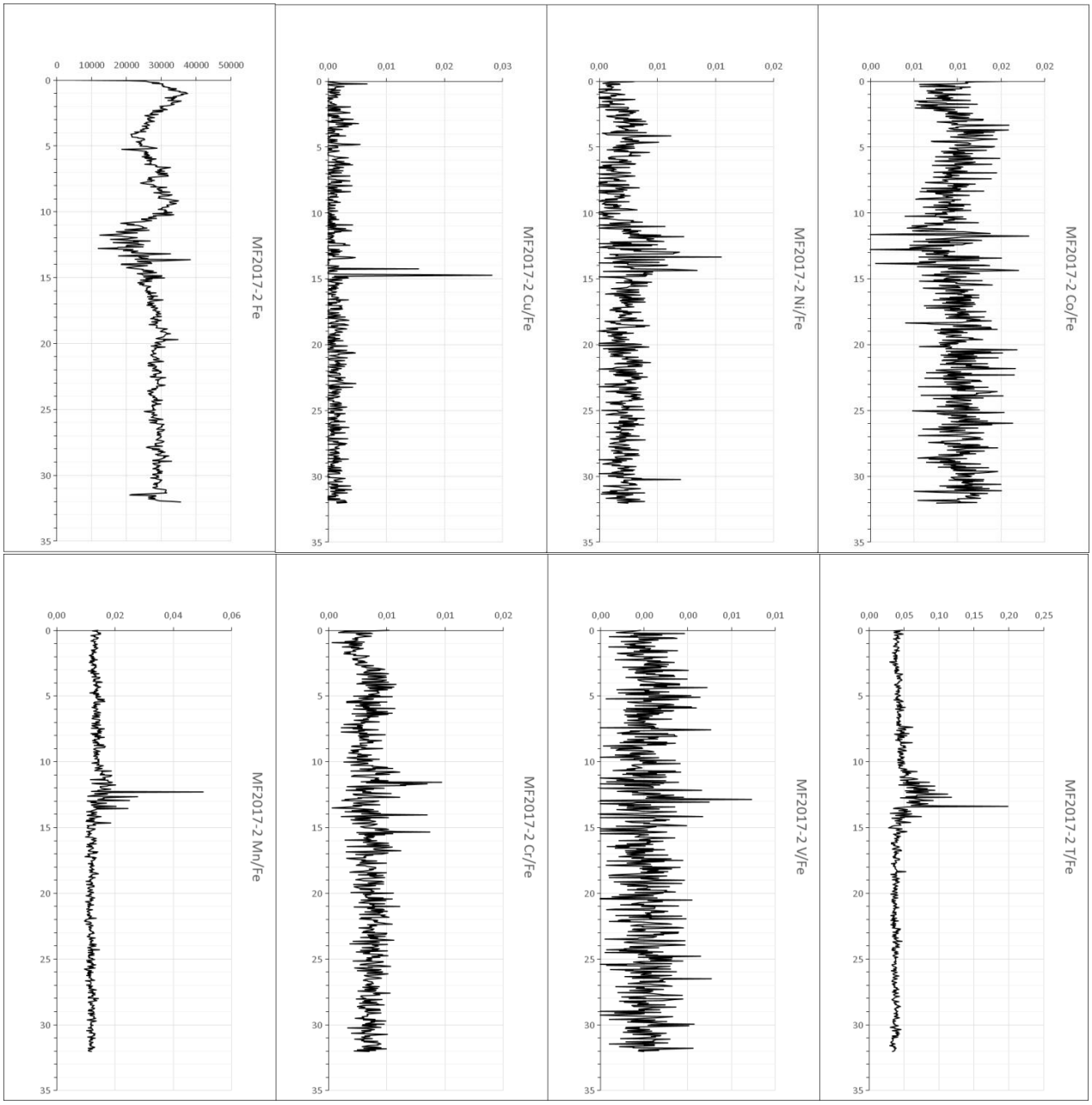

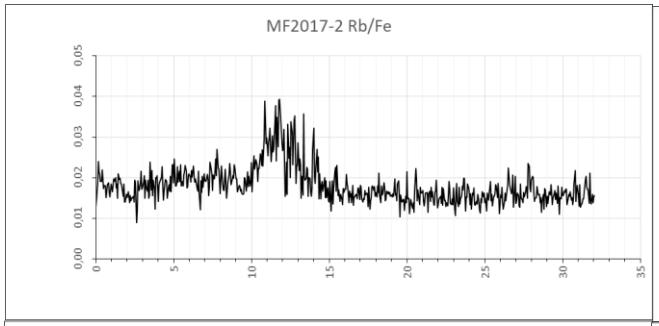
MF2017-2 Rb/Fe
0,00
0,01
0,02
0,03
0,04
0,05
0
5
10
15
20
25
30
35

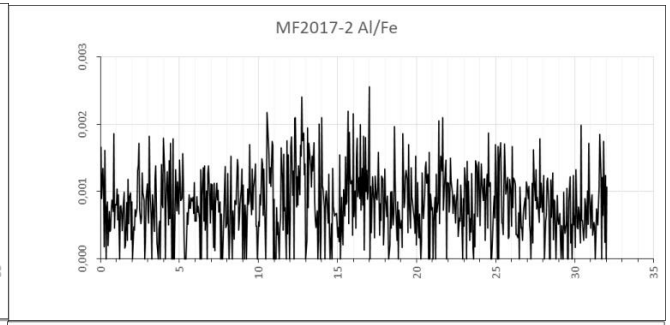
MF2017-2 Al/Fe
0,000
0,001
0,002
0,003
0
5
10
15
20
25
30
35

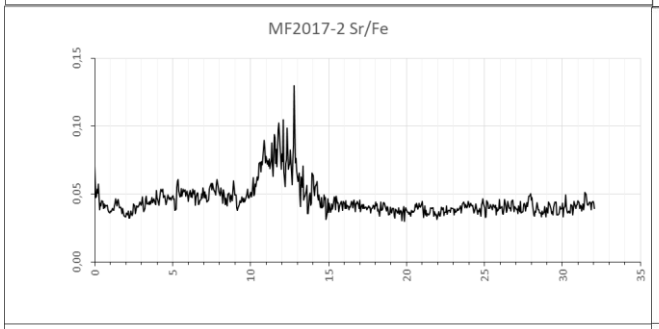
MF2017-2 Sr/Fe
0,00
0,05
0,10
0,15
0
5
10
15
20
25
30
35

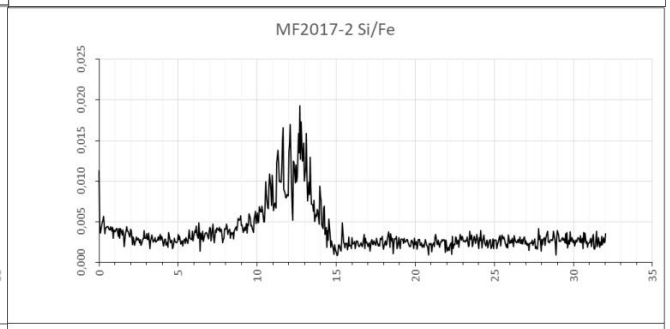
MF2017-2 Si/Fe
0,000
0,005
0,010
0,015
0,020
0,025
0
5
10
15
20
25
30
35

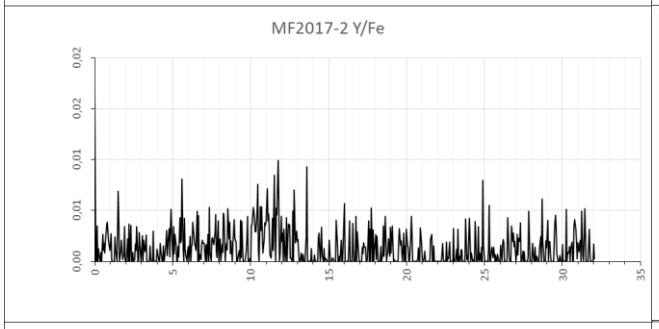
MF2017-2 Y/Fe
0,00
0,01
0,01
0,02
0,02
0
5
10
15
20
25
30
35

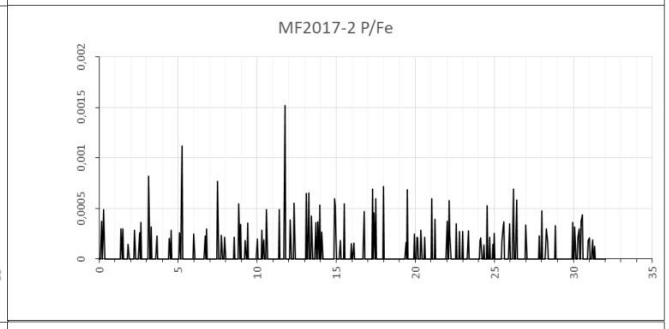
MF2017-2 P/Fe
0
0,0005
0,001
0,0015
0,002
0
5
10
15
20
25
30
35

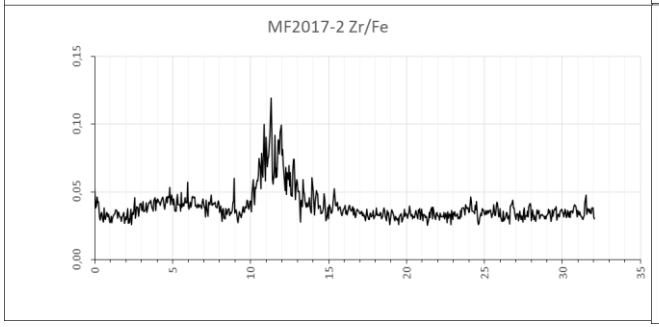
MF2017-2 Zr/Fe
0,00
0,05
0,10
0,15
0
5
10
15
20
25
30
35

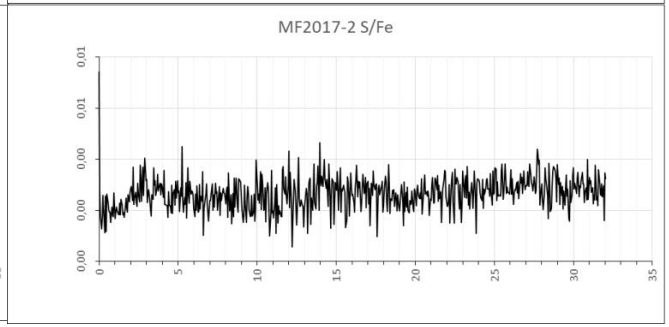
MF2017-2 S/Fe
0,00
0,00
0,00
0,01
0,01
0
5
10
15
20
25
30
35

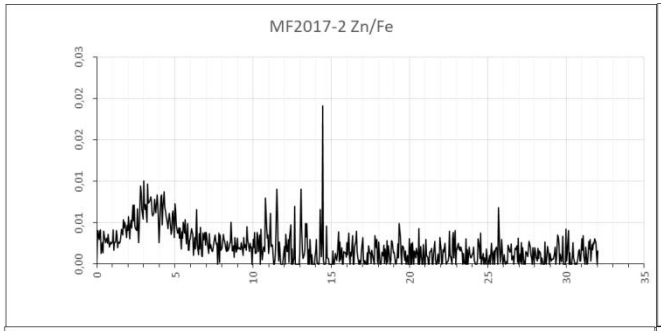
MF2017-2 Zn/Fe

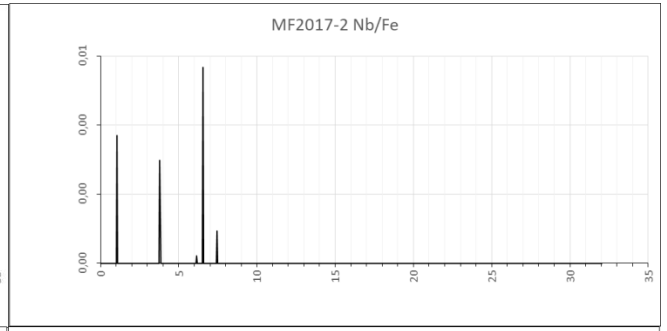
MF2017-2 Nb/Fe

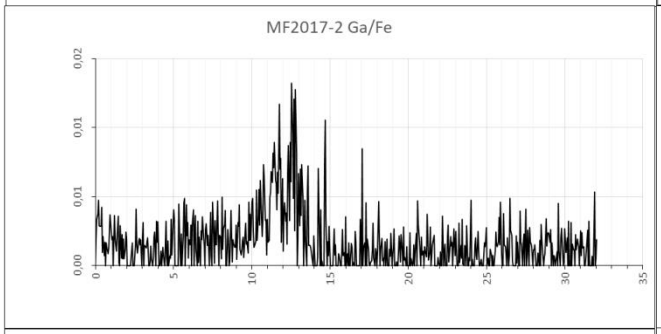
MF2017-2 Ga/Fe

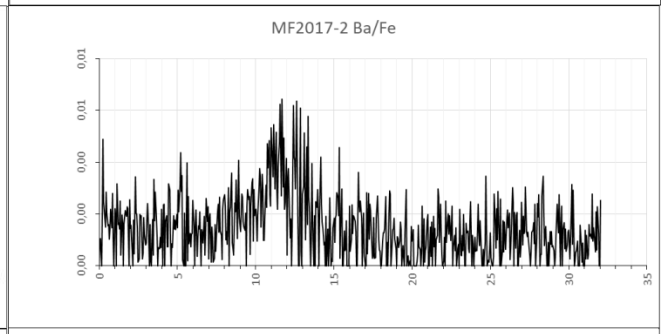
MF2017-2 Ba/Fe

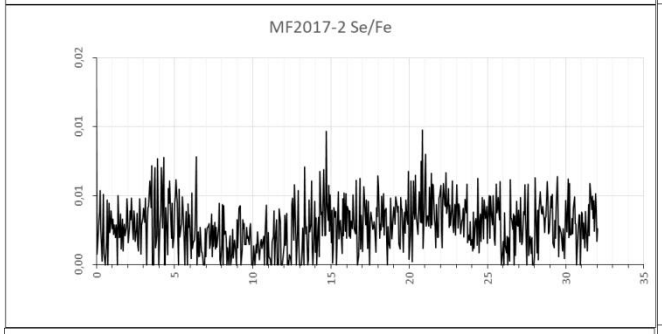
MF2017-2 Se/Fe

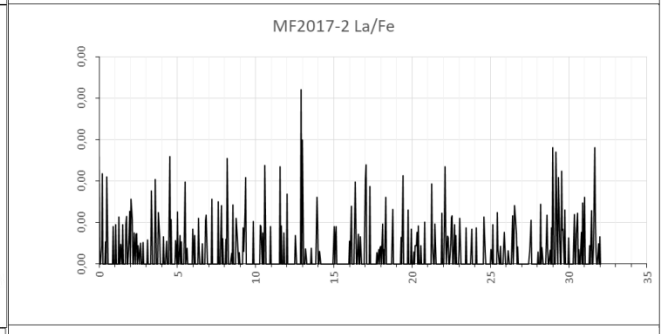
MF2017-2 La/Fe

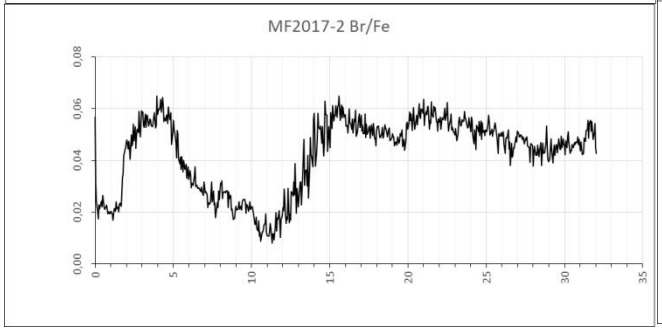
MF2017-2 Br/Fe

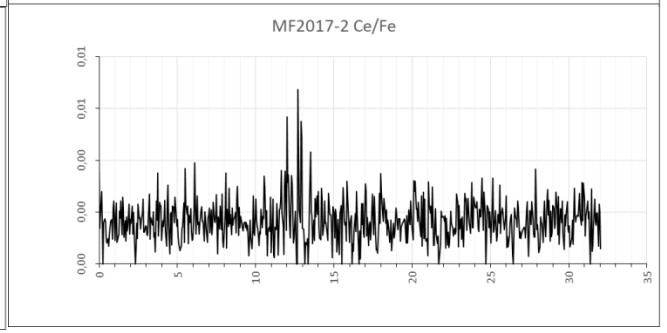
MF2017-2 Ce/Fe

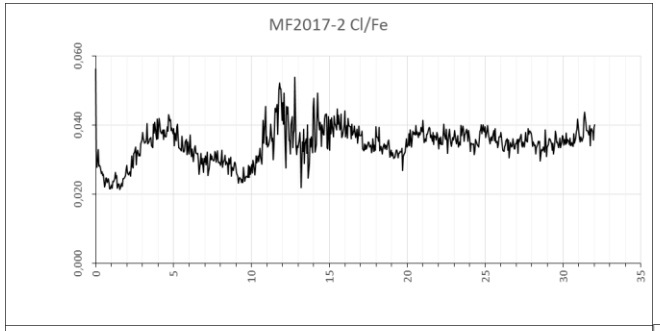
MF2017-2 Cl/Fe
0,060
0,040
0,020
0,000
0
5
10
15
20
25
30
35

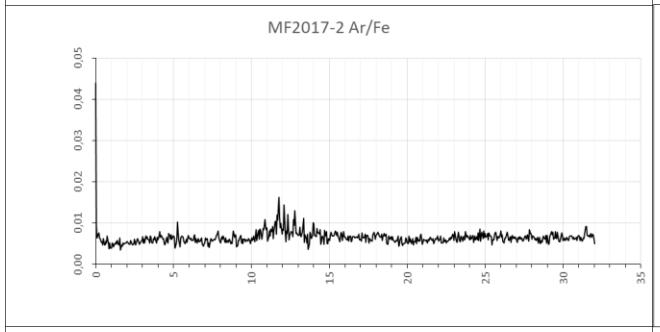
MF2017-2 Ar/Fe
0,05
0,04
0,03
0,02
0,01
0,00
0
5
10
15
20
25
30
35

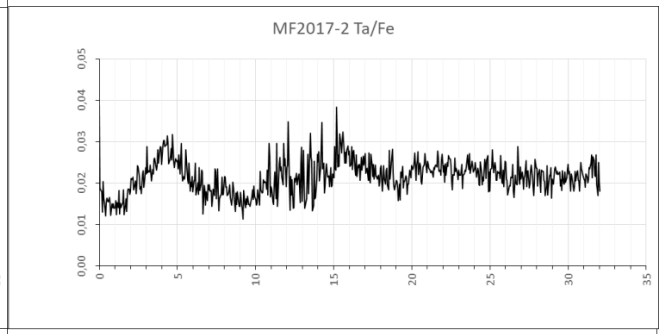
MF2017-2 Ta/Fe
0,05
0,04
0,03
0,02
0,01
0,00
0
5
10
15
20
25
30
35

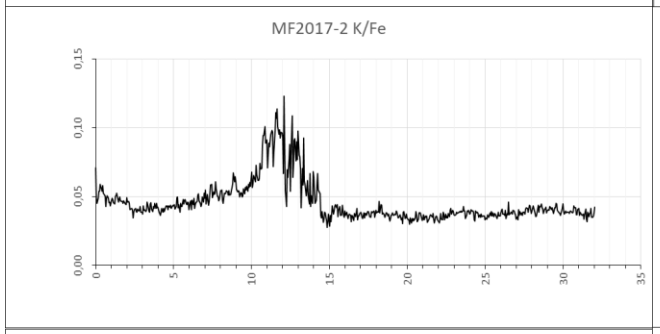
MF2017-2 K/Fe
0,15
0,10
0,05
0,00
0
5
10
15
20
25
30
35

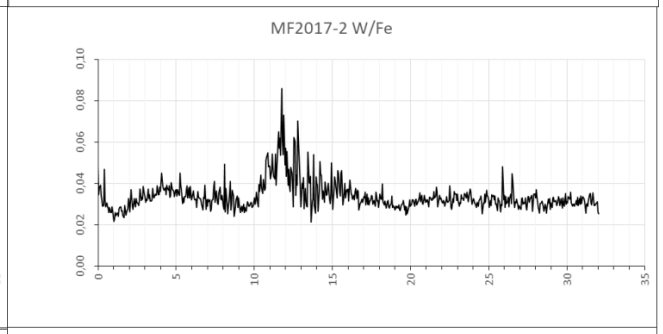
MF2017-2 W/Fe
0,10
0,08
0,06
0,04
0,02
0,00
0
5
10
15
20
25
30
35

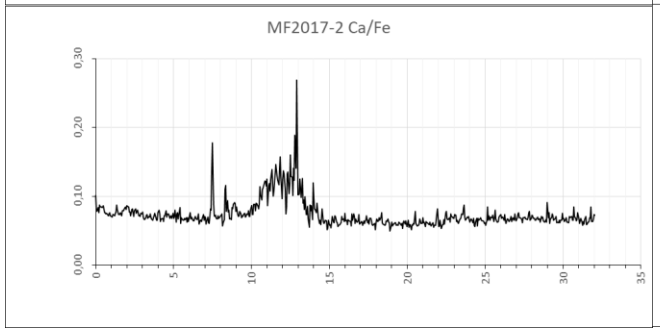
MF2017-2 Ca/Fe
0,30
0,20
0,10
0,00
0
5
10
15
20
25
30
35

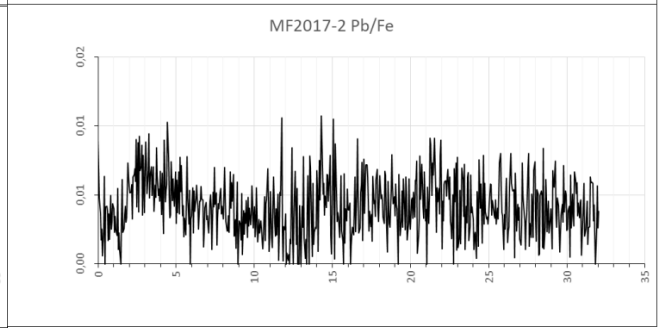
MF2017-2 Pb/Fe
0,02
0,01
0,01
0,00
0
5
10
15
20
25
30
35

Appendix IV: Results of pollution analyses

A: Quantitative determinations

- MF2017-2 0-2 cm
- MF2017-2 10-12 cm
- MF2017-3 0-10 cm

Eurofins Environment Testing Norway
AS (Moss)
F. reg. 965 141 618 MVA
Mølleåkken 50
NO-1538 Moss

Tlf: +47 69 00 52 00
Fax: +47 69 27 23 40

Høgskulen i Sogn og Fjordane
And. for ing. og naturfag
Røyrgt. 6
6856 SOGNDAL
Attn: Torbjørn Dale

AR-17-MM-020068-01

EUNOMO-00175199

Prøvemottak: 31.08.2017
Temperatur:
Analyseperiode: 31.08.2017-13.09.2017
Referanse: Sedimentprøver

ANALYSERAPPORT

Prøvenr.:	439-2017-08310177	Prøvetakingsdato:	29.08.2017
Prøvetype:	Sedimenter	Prøvetaker:	Oppdragsgiver
Prøvemerking:	0-2 cm	Analysestartdato:	31.08.2017

	Analyse	Resultat	Enhet	LOQ	MU	Metode
c)	Arsen (As)	13	mg/kg TS	0.5	30%	NS EN ISO 17294-2
c)	Bly (Pb)	41	mg/kg TS	0.5	40%	NS EN ISO 17294-2
c)	Kadmium (Cd)	0.78	mg/kg TS	0.01	25%	NS EN ISO 17294-2
c)	Kobber (Cu)	24	mg/kg TS	0.5	30%	NS EN ISO 17294-2
c)	Krom (Cr)	18	mg/kg TS	0.5	30%	NS EN ISO 17294-2
c)	Kvikksølv (Hg)	0.041	mg/kg TS	0.001	20%	028311mod/EN ISO17852mod
c)	Nikkel (Ni)	14	mg/kg TS	0.5	30%	NS EN ISO 17294-2
c)	Sink (Zn)	100	mg/kg TS	2	30%	NS EN ISO 17294-2
c)	**PCB(7)**					
c)	PCB 28	< 0.00050	mg/kg TS	0.0005		EN 16167
c)	PCB 52	< 0.00050	mg/kg TS	0.0005		EN 16167
c)	PCB 101	< 0.00050	mg/kg TS	0.0005		EN 16167
c)	PCB 118	< 0.00050	mg/kg TS	0.0005		EN 16167
c)	PCB 153	< 0.00050	mg/kg TS	0.0005		EN 16167
c)	PCB 138	< 0.00050	mg/kg TS	0.0005		EN 16167
c)	PCB 180	< 0.00050	mg/kg TS	0.0005		EN 16167
c)	Sum 7 PCB	nd				EN 16167
c)	**PAH(16)**					
c)	Naftalen	< 0.010	mg/kg TS	0.01		ISO 18287, mod.
c)	Acenaftylen	< 0.010	mg/kg TS	0.01		ISO 18287, mod.
c)	Acenaften	< 0.010	mg/kg TS	0.01		ISO 18287, mod.
c)	Fluoren	< 0.010	mg/kg TS	0.01		ISO 18287, mod.
c)	Fenantren	0.021	mg/kg TS	0.01	25%	ISO 18287, mod.
c)	Antracen	< 0.010	mg/kg TS	0.01		ISO 18287, mod.
c)	Fluoranten	0.071	mg/kg TS	0.01	25%	ISO 18287, mod.
c)	Pyren	0.057	mg/kg TS	0.01	25%	ISO 18287, mod.
c)	Benzo[a]antracen	0.041	mg/kg TS	0.01	25%	ISO 18287, mod.
c)	Krysen/Trifenylen	0.024	mg/kg TS	0.01	25%	ISO 18287, mod.
c)	Benzo[b]fluoranten	0.27	mg/kg TS	0.01	25%	ISO 18287, mod.

Tegnforklaring:
* Ikke omfattet av akkrediteringen LOQ: Kvantifiseringsgrense MU: Måleusikkerhet
< Mindre enn > Større enn nd: Ikke påvist. Bakteriologiske resultater angitt som <1,<50 e.l. betyr 'ikke påvist'.

eurofins

c)	Benzo[k]fluoranten	0.055 mg/kg TS	0.01	30%	ISO 18287, mod.
c)	Benzo[a]pyren	0.087 mg/kg TS	0.01	25%	ISO 18287, mod.
c)	Indeno[1,2,3-cd]pyren	0.14 mg/kg TS	0.01	25%	ISO 18287, mod.
c)	Dibenzo[a,h]antracen	0.030 mg/kg TS	0.01	30%	ISO 18287, mod.
c)	Benzo[ghi]perylen	0.13 mg/kg TS	0.01	25%	ISO 18287, mod.
c)	Sum PAH(16) EPA	0.93 mg/kg TS			ISO 18287, mod.
a)	Tributyltinn (TBT)	12 µg/kg tv	2.4	40%	Kalkulering
a)	Tributyltinn (TBT) - Sn	4.9 µg/kg TS	1	40%	Internal Method 2085
b)	**Kornstørrelse <2µm**				
b)	Kornstørrelse <2 µm	2.0 % TS	1		Internal Method 6
b)	**Kornstørrelse <63µm**				
b)	Kornstørrelse < 63 µm	68.3 % TS	0.1		Internal Method 6
	TOC kalkulert				
	Totalt organisk karbon kalkulert	8.1 % TS		12%	Intern metode
c)	Total tørrstoff glødetap	14.2 % TS	0.1	10%	EN 12879
c)	THC >C5-C8	< 5.0 mg/kg TS	5		EPA 5021
c)	**THC >C8-C35**				
c)	THC >C8-C10	<10 mg/kg TS	5		ISO 16703 mod
c)	THC >C10-C12	<10 mg/kg TS	5		ISO 16703 mod
c)	THC >C12-C16	<10 mg/kg TS	5		ISO 16703 mod
c)	THC >C16-C35	<40 mg/kg TS	20		ISO 16703 mod
c)	Sum THC (>C5-C35)	N.D.			Kalkulering
c)	**Tørrstoff**				
c)	Total tørrstoff	23.4 %	0.1	10%	EN 12880

Merknader:
THC: Forhøyet LOQ pga lav TS.

eurofins

Prøvenr.:	439-2017-08310178	Prøvetakingsdato:	29.08.2017
Prøvetype:	Sedimenter	Prøvetaker:	Oppdragsgiver
Prøvemerking:	10-12 cm	Analysestartdato:	31.08.2017

	Analyse	Resultat	Enhet	LOQ	MU	Metode
c)	Arsen (As)	13	mg/kg TS	0.5	30%	NS EN ISO 17294-2
c)	Bly (Pb)	15	mg/kg TS	0.5	40%	NS EN ISO 17294-2
c)	Kadmium (Cd)	0.44	mg/kg TS	0.01	25%	NS EN ISO 17294-2
c)	Kobber (Cu)	11	mg/kg TS	0.5	30%	NS EN ISO 17294-2
c)	Krom (Cr)	13	mg/kg TS	0.5	30%	NS EN ISO 17294-2
c)	Kvikksølv (Hg)	0.013	mg/kg TS	0.001	20%	028311mod/EN ISO17852mod
c)	Nikkel (Ni)	9.7	mg/kg TS	0.5	30%	NS EN ISO 17294-2
c)	Sink (Zn)	51	mg/kg TS	2	30%	NS EN ISO 17294-2
c)	**PCB(7)**					
c)	PCB 28	< 0.00050	mg/kg TS	0.0005		EN 16167
c)	PCB 52	< 0.00050	mg/kg TS	0.0005		EN 16167
c)	PCB 101	< 0.00050	mg/kg TS	0.0005		EN 16167
c)	PCB 118	< 0.00050	mg/kg TS	0.0005		EN 16167
c)	PCB 153	< 0.00050	mg/kg TS	0.0005		EN 16167
c)	PCB 138	< 0.00050	mg/kg TS	0.0005		EN 16167
c)	PCB 180	< 0.00050	mg/kg TS	0.0005		EN 16167
c)	Sum 7 PCB	nd				EN 16167
c)	**PAH(16)**					
c)	Naftalen	< 0.010	mg/kg TS	0.01		ISO 18287, mod.
c)	Acenaftylen	< 0.010	mg/kg TS	0.01		ISO 18287, mod.
c)	Acenaften	< 0.010	mg/kg TS	0.01		ISO 18287, mod.
c)	Fluoren	< 0.010	mg/kg TS	0.01		ISO 18287, mod.
c)	Fenantren	< 0.010	mg/kg TS	0.01		ISO 18287, mod.
c)	Antracen	< 0.010	mg/kg TS	0.01		ISO 18287, mod.
c)	Fluoranten	0.017	mg/kg TS	0.01	25%	ISO 18287, mod.
c)	Pyren	0.026	mg/kg TS	0.01	25%	ISO 18287, mod.
c)	Benzo[a]antracen	0.011	mg/kg TS	0.01	25%	ISO 18287, mod.
c)	Krysen/Trifenylen	< 0.010	mg/kg TS	0.01		ISO 18287, mod.
c)	Benzo[b]fluoranten	0.036	mg/kg TS	0.01	25%	ISO 18287, mod.
c)	Benzo[k]fluoranten	0.015	mg/kg TS	0.01	30%	ISO 18287, mod.
c)	Benzo[e]pyren	0.022	mg/kg TS	0.01	25%	ISO 18287, mod.
c)	Indeno[1,2,3-cd]pyren	0.056	mg/kg TS	0.01	25%	ISO 18287, mod.
c)	Dibenzo[a,h]antracen	< 0.010	mg/kg TS	0.01		ISO 18287, mod.
c)	Benzo[ghi]perylen	0.048	mg/kg TS	0.01	25%	ISO 18287, mod.
c)	Sum PAH(16) EPA	0.28	mg/kg TS			ISO 18287, mod.
a)	Tributyltinn (TBT)	< 2.4	µg/kg tv	2.4		Kalkulering
a)	Tributyltinn (TBT) - Sn	< 1	µg/kg TS	1		Internal Method 2065
b)	**Kornstørrelse <2µm**					
b)	Kornstørrelse <2 µm	1.9	% TS	1		Internal Method 6
b)	**Kornstørrelse <63µm**					

Tegnforklaring:
* Ikke omfattet av akkrediteringen LOQ: Kvantifiseringsgrense MU: Måleusikkerhet
< Mindre enn >: Større enn nd: Ikke påvist. Bakteriologiske resultater angitt som <1,<50 e.l. betyr 'ikke påvist'.

Opplysninger om måleusikkerhet og konfidensintervall fås ved henvendelse til laboratoriet.
Rapporten må ikke gjengis, unntatt i sin helhet, uten laboratoriets skriftlige godkjennelse. Resultatene gjelder kun for de(n) undersøkte prøven(e).

eurofins

b)	Kornstørrelse < 63 µm	63.1	% TS	0.1		Internal Method 6
	TOC kalkulert					
	Totalt organisk karbon kalkulert	5.9	% TS		12%	Intern metode
c)	Total tørrstoff glødetap	10.3	% TS	0.1	10%	EN 12879
c)	THC >C5-C8	< 5.0	mg/kg TS	5		EPA 5021
c)	**THC >C8-C35**					
c)	THC >C8-C10	<5.0	mg/kg TS	5		ISO 16703 mod
c)	THC >C10-C12	<5.0	mg/kg TS	5		ISO 16703 mod
c)	THC >C12-C16	<5.0	mg/kg TS	5		ISO 16703 mod
c)	THC >C16-C35	<20	mg/kg TS	20		ISO 16703 mod
c)	Sum THC (>C5-C35)	N.D.				Kalkulering
c)	**Tørrstoff**					
c)	Total tørrstoff	40.2	%	0.1	10%	EN 12880

Utførende laboratorium/ Underleverandør:

a) Eurofins Environment A/S (Vejen), Ladelundvej 85, DK-6600, Vejen DS EN ISO/IEC 17025 DANAK 168,
b) Eurofins Analyses pour l'Environnement France (S1), 5, rue d'Otterswiller, F-67700, Saverne DS EN ISO/IEC 17025 DANAK 168,
c) Eurofins Environment Sweden AB (Lidköping), Box 887, Sjöhagsg. 3, SE-53119, Lidköping ISO/IEC 17025 2005 SWEDAC 1125,

Moss 13.09.2017

Stig Tjomsland

ASM/Bachelor Kjemi

Tegnforklaring:

* Ikke omfattet av akkrediteringen LOQ: Kvantifiseringsgrense MU Måleusikkerhet
< Mindre enn > Større enn nd: Ikke påvist. Bakteriologiske resultater angitt som <1,<50 o.l. betyr "ikke påvist".

Opplysninger om måleusikkerhet og konfidensintervall fås ved henvendelse til laboratoriet.
Rapporten må ikke gjengis, unntatt i sin helhet, uten laboratoriets skriftlige godkjennelse. Resultatene gjelder kun for de(n) undersøkte prøven(e).

Eurofins Environment Testing Norway AS (Moss)
F. reg. 965 141 618 MVA
Møllebakken 50
NO-1538 Moss

Tlf: +47 69 00 52 00
Fax: +47 69 27 23 40

Høgskulen i Sogn og Fjordane
And. for ing. og naturfag
Røyrgt. 6
6856 SOGNDAL
Attn: Torbjørn Dale

AR-17-MM-024974-01

EUNOMO-00179708

Prøvemottak: 20.10.2017
Temperatur:
Analyseperiode: 20.10.2017-03.11.2017
Referanse: 242405NO Dale, Sedimentprøve

ANALYSERAPPORT

Prøvenr.:	**439-2017-10200109**	Prøvetakingsdato:	18.10.2017
Prøvetype:	Sedimenter	Prøvetaker:	Torbjørn Dale
Prøvemerking:	Unummerert	Analysestartdato:	20.10.2017

	Analyse	Resultat	Enhet	LOQ	MU	Metode
c)	Arsen (As)	17	mg/kg TS	0.5	30%	NS EN ISO 17294-2
c)	Bly (Pb)	63	mg/kg TS	0.5	40%	NS EN ISO 17294-2
c)	Kadmium (Cd)	1.3	mg/kg TS	0.01	25%	NS EN ISO 17294-2
c)	Kobber (Cu)	35	mg/kg TS	0.5	30%	NS EN ISO 17294-2
c)	Krom (Cr)	30	mg/kg TS	0.5	30%	NS EN ISO 17294-2
c)	Kvikksølv (Hg)	0.047	mg/kg TS	0.001	20%	028311mod/EN ISO17852mod
c)	Nikkel (Ni)	22	mg/kg TS	0.5	30%	NS EN ISO 17294-2
c)	Sink (Zn)	140	mg/kg TS	2	30%	NS EN ISO 17294-2
c)	**PCB(7)**					
c)	PCB 28	< 0.00050	mg/kg TS	0.0005		EN 16167
c)	PCB 52	< 0.00050	mg/kg TS	0.0005		EN 16167
c)	PCB 101	< 0.00050	mg/kg TS	0.0005		EN 16167
c)	PCB 118	< 0.00050	mg/kg TS	0.0005		EN 16167
c)	PCB 153	< 0.00050	mg/kg TS	0.0005		EN 16167
c)	PCB 138	< 0.00050	mg/kg TS	0.0005		EN 16167
c)	PCB 180	< 0.00050	mg/kg TS	0.0005		EN 16167
c)	Sum 7 PCB	nd				EN 16167
c)	**PAH(16)**					
c)	Naftalen	< 0.010	mg/kg TS	0.01		ISO 18287, mod.
c)	Acenaftylen	< 0.010	mg/kg TS	0.01		ISO 18287, mod.
c)	Acenaften	< 0.010	mg/kg TS	0.01		ISO 18287, mod.
c)	Fluoren	< 0.010	mg/kg TS	0.01		ISO 18287, mod.
c)	Fenantren	0.052	mg/kg TS	0.01	25%	ISO 18287, mod.
c)	Antracen	0.011	mg/kg TS	0.01	25%	ISO 18287, mod.
c)	Fluoranten	0.16	mg/kg TS	0.01	25%	ISO 18287, mod.
c)	Pyren	0.14	mg/kg TS	0.01	25%	ISO 18287, mod.
c)	Benzo[a]antracen	0.096	mg/kg TS	0.01	25%	ISO 18287, mod.
c)	Krysen/Trifenylen	0.047	mg/kg TS	0.01	25%	ISO 18287, mod.
c)	Benzo[b]fluoranten	0.72	mg/kg TS	0.01	25%	ISO 18287, mod.

Tegnforklaring:
* Ikke omfattet av akkrediteringen LOQ: Kvantifiseringsgrense MU: Måleusikkerhet
<: Mindre enn >: Større enn nd: Ikke påvist. Bakteriologiske resultater angitt som <1,<50 e.l. betyr 'ikke påvist'.

Opplysninger om måleusikkerhet og konfidensintervall fås ved henvendelse til laboratoriet.
 Resultatene gjelder kun for de(n) undersøkte prøven(e).

c)	Benzo[k]fluoranten	0.19	mg/kg TS	0.01	30%	ISO 18287, mod.
c)	Benzo[a]pyren	0.19	mg/kg TS	0.01	25%	ISO 18287, mod.
c)	Indeno[1,2,3-cd]pyren	0.42	mg/kg TS	0.01	25%	ISO 18287, mod.
c)	Dibenzo[a,h]antracen	0.069	mg/kg TS	0.01	30%	ISO 18287, mod.
c)	Benzo[ghi]perylen	0.48	mg/kg TS	0.01	25%	ISO 18287, mod.
c)	Sum PAH(16) EPA	2.6	mg/kg TS			ISO 18287, mod.
a)	Tributyltinn (TBT)	24	µg/kg tv	2.4	40%	Kalkulering
a)	Tributyltinn (TBT) - Sn	10	µg/kg TS	1	40%	Internal Method 2085
b)	**Kornstørrelse <2µm**					
b)	Kornstørrelse <2 µm	2.3	% TS	1		Internal Method 6
b)	**Kornstørrelse <63µm**					
b)	Kornstørrelse < 63 µm	75.4	% TS	0.1		Internal Method 6
	TOC kalkulert					
	Totalt organisk karbon kalkulert	10.4	% TS		12%	Intern metode
c)	Total tørrstoff glødetap	18.2	% TS	0.1	10%	EN 12879
c)	THC >C5-C8	< 5.0	mg/kg TS	5		EPA 5021
c)	**THC >C8-C35**					
c)	THC >C8-C10	<10	mg/kg TS	5		ISO 16703 mod
c)	THC >C10-C12	<10	mg/kg TS	5		ISO 16703 mod
c)	THC >C12-C16	<10	mg/kg TS	5		ISO 16703 mod
c)	THC >C16-C35	<40	mg/kg TS	20		ISO 16703 mod
c)	Sum THC (>C5-C35)	N.D.				Kalkulering
c)	**Tørrstoff**					
c)	Total tørrstoff	20.7	%	0.1	10%	EN 12880

Utførende laboratorium/ Underleverandør:

a) Eurofins Environment A/S (Vejen), Ladelundvej 85, DK-6600, Vejen DS EN ISO/IEC 17025 DANAK 168,
b) Eurofins Analyses pour l'Environnement France (S1), 5, rue d'Otterswiller, F-67700, Saverne DS EN ISO/IEC 17025 DANAK 168,
c) Eurofins Environment Sweden AB (Lidköping), Box 887, Sjöhagsg. 3, SE-53119, Lidköping ISO/IEC 17025:2005 SWEDAC 1125,

Moss 03.11.2017

Kjetil Sjaastad

Kjetil Sjaastad

Kjemitekniker

Tegnforklaring:

* Ikke omfattet av akkrediteringen LOQ: Kvantifiseringsgrense MU: Måleusikkerhet

<: Mindre enn >: Større enn nd: Ikke påvist. Bakteriologiske resultater angitt som <1,<50 e.l. betyr 'ikke påvist'.

Opplysninger om måleusikkerhet og konfidensintervall fås ved henvendelse til laboratoriet.

B: Quantitative determinations expressed in environmental quality reference classes

		MF2017-2 0 - 2 cm					MF2017-2 10 - 12 cm					MF2017-3 0 - 10 cm				
		Environmental quality classes for sediment					Environmental quality classes for sediment					Environmental quality classes for sediment				
Name of substance		I	II	III	IV	V	I	II	III	IV	V	I	II	III	IV	V
Arsenic (As)																
Lead (Pb)																
Cadmium (Cd)																
Copper (Cu)																
Chromium (Cr)																
Mercury (Hg)																
Nickel (Ni)																
Zinc (Zn)																
Sum 7 PCB*																
Naphthalene	PAH(16)															
Acenaphthylene																
Acenaphthene																
Fluorene																
Phenanthrene																
Anthracene																
Fluoranthene																
Pyrene																
Benzo[a]anthracene																
Chrysene/Triphenylene**																
Benzo[b]fluoranthene																
Benzo[k]fluoranthene																
Benzo[a]pyrene																
Indeno[1,2,3-cd]pyrene																
Dibenzo[a,h]anthracene																
Benzo[ghi]perylene																
Sum PAH(16) EPA***																
Tributyltin																

*Sum 7 PCB is the calculated sum of PCB 28, PCB52, PCB 101, PCB 118, PCB 138 and PCB 180

**The Norwegian Environment Agency has not formulated environmental classes Chrysene/Triphenylene, Chrysene/Triphenylene has been compared with the environmental classes for Chrysene

***The Norwegian Environment Agency has not formulated environmental classes for Sum PAH(16) EPA

Grey: Measured value lies below detection limit, value can be within several environmental quality classes

I Background	II Good	III Moderate	IV Bad	V Very bad
Background values	No toxic effects	Chronical effects with a long exposure time	Acute toxic effects with a short exposure time	Wide toxic effects
Upper limit: background	Upper limit: AA-QS, PNEC	Upper limit: MAC-QS, $PNEC_{acute}$	Upper limit: $PNEC_{acute}$ * AF^{1}	

Table VIa: Classification system for water and sediment (Miljødirektoratet, 2016)

AA-QS: Ambient Air Quality Standards. PNEC: Predicted No Effect Concentration. MAC-QS: Maximum Allowable Concentration Quality Standard. $PNEC_{acute}$: Predicted No Effect Concentration with a factor applied to indicate the acute toxicity level. AF^{1}: Safety factor that takes into account the variation in sensitivity between organisms.